Université de Montréal

Caractérisation et utilisation de polymères en brosse pour la lubrification des tissus et des dispositifs médicaux

Par

Duy Anh Pham

Faculté de Pharmacie

Mémoire présenté en vue de l'obtention du grade de maîtrise (M.Sc.) en Sciences Pharmaceutiques, option Technologie Pharmaceutique

Août 2023

Université de Montréal

Faculté de Pharmacie

Ce mémoire intitulé

Caractérisation et utilisation de polymères en brosse pour la lubrification des tissus et des dispositifs médicaux

Présenté par

Duy Anh Pham

A été évalué par un jury composé des personnes suivantes

François-Xavier Lacasse

Président-rapporteur

Xavier Banquy

Directeur de recherche

Suzanne Giasson

Membre du jury

REMERCIEMENTS

Ces 2 ans en maîtrise m'ont fourni une formation et des expériences importantes ayant permis le développement de mes connaissances scientifiques et de mes compétences. Avant tout, je voudrais adresser mes remerciements aux personnes citées ci-dessous qui m'ont aidé dans différents aspects de ma maîtrise.

Tout d'abord, je voudrais remercier mon directeur Xavier Banquy. M'embauchant quand j'étais en France en 2021, vous m'avez confié ce projet très intéressant avec lequel j'ai appris beaucoup de choses, ainsi que collaboré avec les chercheurs compétents de votre laboratoire. Malgré mes difficultés en début de maîtrise, vous m'avez fait confiance tout au long de mon projet. Votre patience est un des éléments importants qui me donnent la motivation pour compléter mon projet.

Ensuite, je voudrais remercier mon comité de parrainage comprenant Monsieur François-Xavier Lacasse et Monsieur Marc Lavertu. Malgré nos courtes rencontres, vos conseils relatifs au projet, au choix du stage et à la gestion efficace du travail ont été importants pour la progression de mon projet.

Je voudrais aussi remercier Madame Sylvie Marleau, Madame Andrée Mathieu, Monsieur Lenickson Desert et les membres administratifs de la faculté de Pharmacie pour leur soutien dans mon processus d'admission et mes procédures d'inscription.

Merci à Line Séguy pour la tonne d'aide que tu m'as donné dans les corrections des idées et grammaticales pour tous mes dossiers importants. Pour moi, ton support est incomparable. Merci à Chang-Sheng Wang pour tes idées et tes conseils pendant notre collaboration. Merci à tous les

membres du groupe de recherche du directeur Xavier Banquy pour les bons moments ensemble. Je suis tellement chanceux de pouvoir travailler avec vous durant mes années d'étude.

Enfin, je voudrais remercier les membres du jury d'évaluation, incluant Monsieur François-Xavier Lacasse, Madame Suzanne Giasson et Monsieur Xavier Banquy. Merci d'avoir pris votre temps précieux pour lire et évaluer mon mémoire.

Cordialement.

Duy Anh Pham

RESUME

La friction entre les surfaces mobiles de l'organisme peut être un problème difficile à résoudre, notamment dans les pathologies dégénératives comme l'arthrose ou la sécheresse oculaire. Malgré le développement de nombreux produits pharmaceutiques, les matériaux actuellement utilisés pour protéger les tissus blessés et les dispositifs biomédicaux contre l'usure par frottement sont encore limités dans leurs performances. Il existe un besoin urgent de matériaux injectables capables de protéger ces tissus et dispositifs afin de prolonger leur durée de vie et de traiter efficacement des maladies dégénératives.

Parmi les innovations de la dernière décennie, les polymères à structure dite « en brosse » (BBs) se sont révélés prometteurs pour amoindrir les problèmes de friction et d'usure. Inspirés de l'architecture spécifique du protéoglycane 4, l'un des principaux composants lubrifiants du cartilage, les macromolécules BBs sont constituées d'un squelette linéaire et de chaînes latérales formant une brosse dense pouvant maintenir de l'eau sous une pression élevée. Les différentes structures des BBs, selon le squelette et leurs chaînes latérales, conduisent à plusieurs caractéristiques morphologiques et propriétés tribologiques intéressantes dans l'ingénierie tissulaire. Bien que leurs propriétés lubrifiantes aient été prouvées dans plusieurs études, les BBs n'ont à ce jour que peu d'applications. D'une part, la corrélation entre leur structure et leurs propriétés physicochimiques n'est pas encore clairement établie. D'autre part, il manque encore des études relatives à l'efficacité des BBs sur de vrais tissus.

Pour pallier ce problème, notre projet vise à caractériser les propriétés physicochimiques et tribologiques des BBs sur différents types de surfaces en fonction de leur structure. La longueur du squelette, la densité de greffage et l'addition du groupe d'ancrage sont les 3 variables

principales étudiées dans ce projet. La lubrification ainsi que d'autres propriétés importantes des BBs ont été évaluées sur les surfaces molles des cartilages, des yeux et des lentilles en contact. Les tests tribologiques ont été menés en utilisant un appareil à force de surface (SFA) via l'association du protocole classique et avancé qui l'adapte aux surfaces testées. A côté de la tribologie, l'affinité cinétique, la toxicité, les propriétés antisalissure et anti-inflammatoire des BBs sur les interfaces ont aussi été étudiées dans ce projet via les techniques de LigandTracer et de microscope fluorescent.

Mots clés : lubrification, friction, polymère en brosse, bio-affinité, appareil à force de surface.

ABSTRACT

Friction between the body's moving surfaces can be a difficult problem to solve, particularly in degenerative pathologies such as osteoarthritis or dry eye. Despite the development of numerous pharmaceutical products, the materials currently used to protect injured tissues and biomedical devices against frictional wear are still limited in their performance. There is an urgent need for injectable materials capable of protecting these tissues and devices in order to extend their life and effectively treat degenerative diseases.

Among the innovations of the last decade, polymers with a so-called "brush structure" (BBs) have shown promise in reducing friction and wear problems. Inspired by the specific architecture of proteoglycan 4, one of the main lubricating components of cartilage, BBs macromolecules consist of a linear backbone and side chains forming a dense brush capable of holding water under high pressure. The different structures of BBs, depending on the backbone and their side chains, lead to several morphological features and tribological properties of interest in tissue engineering. Although their lubricating properties have been proven in several studies, BBs have few applications to date. On the one hand, the correlation between their structure and physicochemical properties has not yet been clearly established. On the other hand, studies on the effectiveness of BBs on real tissues are still lacking.

To overcome this problem, our project aims to characterize the physicochemical and tribological properties of BBs on different types of surfaces, depending on their structure. Backbone length, graft density and anchoring group are the 3 main variables studied in this project. Lubrication and other important properties of BBs were evaluated on the soft surfaces of cartilages, eyes and contact lenses. Tribological testing was carried out using a Surface Force Apparatus (SFA) via a combination of the classic and advanced protocol, adapting it to the surfaces tested. Alongside

tribology, the kinetic affinity, toxicity, anti-fouling and anti-inflammatory properties of BBs on interfaces were also studied in this project via LigandTracer and fluorescent microscopy techniques.

Key words: lubrication, friction, bottlebrush polymer, bio-affinity, surface force apparatus.

Table des matières

Liste des figures

Chapitre 3

Chapitre 4

Liste des schémas

Chapitre 3

Chapitre 4

Liste des tableaux

Chapitre 3

Liste des abréviations

^{1}H NMR	Proton nuclear magnetic resonance
ACL	Anterior cruciate ligament
AFM	Microscopie à force atomique
AINS	Anti-inflammatoires non stéroïdiens
ATRP	Atom transfer radical polymerization
BBs	Polymères en brosse
Case-ABC	Chondroitinase ABC
CDD	Charge-coupled device
CsA	Ciclosporine A
DCM	Dichloromethane
DF	Densité de greffage
DMEM	Dulbecco's modified Eagle's medium
DPBS	Dulbecco's phosphate-buffered saline
ELISA	Enzyme-linked immunosorbent assay
FBS	Fetal bovine serum
FDA	Food and Drug Administration Américaine
FECO	Fringes of equal chromatic order
GPC	Gel permeation chromatography
HA	Acide hyaluronique
HEMA	Hydroxyethyl methacrylate

MBI	Multiple beam interferometry
MBs	Macromolecular bottlebrushes
Me_6TREN	Tris(2-dimethylaminoethyl) amine
MMP	Matrix metalloproteinases
MSEA	2-(methylsulfinyl)ethyl acrylate
PBiBEM	Poly(2-bromoisobutyryloxyethyl methacrylate)
PEG	Polyethylene glycol
PMPC	Poly(2-methacryloyloxyethyl phosphorylcholine
PMSEA	Poly(2-(méthylsulfinyl)acrylate d'éthyle
RAFT	Reversible addition−fragmentation chain transfer
RBF	Round-bottom flask
RI	Refractive index
SEC	Size exclusion chromatography
SFA	Appareil à force de surface
TEM	Microscopie électronique en transmission
TPMA	Tris(2-pyridylmethyl) amine

CHAPITRE 1 : INTRODUCTION GENERALE

1.1) Contexte scientifique :

a) Définition de la bio-lubrification

Créé au milieu du XVIe siècle, le mot « friction » (ou « frottement ») est défini comme « la résistance qu'une surface ou un objet rencontre lorsqu'il se déplace sur une autre surface ou un autre objet ».[1] Il existe de nombreuses manifestations de la friction dans notre vie. En effet, il est difficile d'imaginer un processus, que ce soit dans la nature ou dans l'industrie, qui soit entièrement exempt de friction. Dans notre corps, la bio-friction peut être définie comme le frottement appliqué aux systèmes biologiques des jointures synoviales, du poumon, des parois thoraciques et des surfaces oculaires.[2] La friction est généralement faible dans des conditions normales grâce aux systèmes lubrifiants créés dans notre corps. Pourtant, dans des conditions anormales et pathologiques, elle devient élevée à cause de la déficience de ces systèmes lubrifiants.

b) Maladies à cause de la friction

Dans le système des articulations mobiles (ou diarthrose), le liquide synovial joue un rôle crucial de lubrification entre les surfaces où les cartilages articulaires sont considérés comme surfaces d'appui et les os comme matériaux de soutien.[3] Dans l'état normal, ce coussin de cartilage articulaire avec l'aide du liquide synovial présente un coefficient de frottement aussi bas que 0.002 pour assurer les mouvements quotidiens tout au long de la vie d'une personne.[2] Pourtant, dans plusieurs cas, les changements de propriétés chimiques du cartilage, les lésions liées au vieillissement ou aux accidents entraînent la dégradation du liquide synovial qui provoque une augmentation de la friction entre les cartilages. Cela peut conduire finalement à une maladie

appelée « l'arthrose ».[4] Le cartilage d'une articulation arthrosique commence à se dégrader et l'os sous-jacent se modifie. Avec le temps, les fragments de dégradation du cartilage sont phagocytés par des cellules (telles que les macrophages et les fibroblastes synoviaux) qui enflamment la synoviale et détériorent la lubrification.[5] De cette manière, une boucle de rétroaction se forme sous l'effet du renforcement mutuel de l'augmentation de la friction et de la sécrétion d'enzymes de dégradation, entraînant une destruction totale du cartilage articulaire.[6, 7] L'arthrose est l'une des affections chroniques les plus courantes, qui a un impact non seulement sur la douleur et la fonction physique, mais aussi sur de nombreux autres aspects, notamment la santé mentale, le sommeil, la participation au travail et même la mortalité.[8] Selon les chercheurs, la prévalence de l'arthrose est passée de 247,51 millions en 1990 à 527,81 millions en 2019, ce qui fait de l'arthrose une maladie mondiale grave définie par l'*Osteoarthritis Research Society International* en 2016.[9] Elle se manifeste le plus souvent dans les mains, les hanches et les genoux. Il est donc important de prévenir la maladie à un stade précoce, notamment en considérant le rôle de la lubrification du liquide synovial et du cartilage.

Une autre surface qui nécessite la lubrification est la surface oculaire. L'aspect externe de l'œil comprend la surface oculaire (cornée, conjonctive et film lacrymal) et l'annexe oculaire (paupières, système lacrymal, orbite, et muscles et nerfs qui s'y rattachent).[10] La cornée possède une structure transparente en forme de dôme, d'une épaisseur de 500 μm, qui constitue la partie centrale externe de l'œil.[11] Nourrie par le film lacrymal, la cornée fournit le principal pouvoir de réfraction de l'œil, courbant les rayons lumineux pour mettre au point les images sur la rétine. Le film lacrymal est aussi en charge de la lubrification de la surface oculaire. Le film lacrymal se compose de trois couches : lipidique, aqueuse et muqueuse.[12] Chez une personne saine, ce composant muqueux fournit un revêtement lacrymal uniforme et glissant, minimisant la friction et protégeant la cornée

pendant le clignement des yeux. Lorsqu'une couche du film lacrymal est déficiente, son instabilité irrite la surface oculaire et évolue vers les symptômes classiques de la sécheresse oculaire, une affection qui touche des millions de personnes à nos jours.[13] La sécheresse oculaire par carence aqueuse se caractérise par une diminution de la sécrétion de larmes par les glandes lacrymales, tandis que la sécheresse oculaire par évaporation résulte d'une évaporation accrue du liquide lacrymal à la surface de l'œil. Les symptômes comprennent des brûlures, des picotements, des rougeurs et des larmoiements de l'œil.[14] Les raisons du dysfonctionnement de la lubrification oculaire sont nombreuses : les changements hormonaux, les maladies auto-immunes, l'inflammation des glandes des paupières ou les maladies oculaires allergiques.[15] En particulier, lors du port de lentilles de contact, la lentille interagit directement avec le film lacrymal et affecte l'étalement de la couche lipidique du film lacrymal, la stabilité du film lacrymal et l'évaporation du film lacrymal, ce qui contribue souvent à la sécheresse des yeux .[16] Au cours d'une journée, nous clignons des yeux plus de 11 500 fois.[17] Pour les personnes souffrant de sécheresse oculaire, chaque clignement peut être irritant, voire douloureux. La prévalence de la sécheresse oculaire dans la population varie de 5 % à 34 % selon les pays et augmente linéairement avec l'âge.[18]

1.2) Etat de l’art :

a) Actuelles thérapies pour l’arthrose

Contrairement à d'autres formes d'arthrite pour lesquelles de grandes avancées ont été réalisées ces dernières années, les progrès sont beaucoup plus lents dans le cas de l'arthrose.[19]

Actuellement, **les médicaments** se concentrent sur la diminution des symptômes de la maladie. Bien que plusieurs médicaments soient disponibles, il n'existe pas encore de médicaments capables d'inverser totalement la progression de l'arthrose et certains médicaments peuvent avoir des effets secondaires indésirables.[20]

Le paracétamol, les anti-inflammatoires non stéroïdiens (AINS) et le tramadol sont prescrits à de nombreux patients souffrant légèrement d'arthrose pour soulager leurs symptômes.[21] Pour les personnes qui ne tolèrent pas les AINS ou d'autres traitements, l'antidépresseur chlorhydrate de duloxétine (Cymbalta®) approuvé par la Food and Drug Administration Américaine (FDA) en 2010 est utilisé pour traiter les douleurs liées à l'arthrose.[22] Pourtant, ces traitements pharmacologiques ne soulagent que temporairement la douleur, alors que la maladie est chronique et que la cause de la pathologie doit être traitée.

Les méthodes de médecine régénérative deviennent de plus en plus populaires et l’une de ces méthodes est l’injection de cellules souches mésenchymateuses.[23] Cependant, son efficacité reste toujours controversée. Les chercheurs ont conclu que la confiance dans la sécurité de la thérapie par cellules souches mésenchymateuses pour l'arthrose du genou est modérée, mais que la confiance dans les résultats d'efficacité est faible en raison des limites des preuves actuelles.[20, 22]

Etant introduite à la fin du XIXe siècle, la viscosupplémentation est une des méthodes les plus intéressées aux dernières années. Dans ce traitement, un liquide gélifié à base d’acide hyaluronique

(HA) est injecté entre les articulations dans le but de restaurer la viscoélasticité physiologique du liquide synovial. La viscosupplémentation a été utilisée pour la première fois en Europe et en Asie, et a été approuvée par FDA en 1997.[24] Théoriquement, les personnes souffrant d'arthrose ont une concentration d'acide hyaluronique inférieure à la normale dans leurs articulations. Ainsi, l'ajout de la viscosupplémentation à l'articulation arthritique est supposé de faciliter le mouvement et réduise la douleur. Au cours des 10 dernières années, plusieurs produits visant au viscosupplementation ont été développés comme HYLAN G-F-20, GELSYN-3 DUROLANE.[25] Toutefois, leurs efficacités sur les patients ne sont pas concluantes et contradictoires. Alors que certaines études ont déterminé l'amélioration significative de la douleur après l'injection du viscosupplément, d'autres ont conclu que la viscosupplementation n'est pas considérablement efficace au-delà de l'effet placebo.[26, 27]

En phase terminale d'arthrose de la hanche ou du genou, le remplacement de l'articulation (aussi appelé arthroplastie) est une option thérapeutique inévitable. Comme pour toute intervention chirurgicale, l'arthroplastie présente des risques de complications comme l'apparence de caillots sanguins, des infections ou la lésion des nerfs autour de l'articulation remplacée.[28] En outre, dès le remplacement de l'articulation, les patients subissent une nouvelle source de friction venant du frottement entre les surfaces de la prothèse et l'os sous-jacent. Les prothèses articulaires nécessitent d'être remplacées après avoir subi le frottement chaque jour durant 15 à 25 ans, ou moins.[29, 30]

Avec les limites et les effets secondaires des traitement actuels, il est donc très important de faire la lumière sur la remarquable lubrification du cartilage et sur la corrélation entre la lubrification et la régénération du cartilage, dans le but d'améliorer la compréhension de l'arthrose et d'encourager le développement d'approches visant à l'atténuer, voire à la traiter.

b) Actuelles thérapies pour la sécheresse oculaire

Aujourd'hui, les traitements populaires de la sécheresse oculaire comprennent les larmes artificielles, les compresses chaudes et l'hygiène des paupières dans les cas légers.[31] Pour les patients présentant des signes d'inflammation oculaire ou un déficit modéré d'humeur aqueuse, la ciclosporine A (CsA) est utilisée comme médicament anti-inflammatoire.[32] Après avoir reçu l'approbation de la FDA pour la sécheresse oculaire en 2003, la CsA a été utilisée régulièrement en clinique au cours des 15 dernières années.[33] De nombreuses études ont montré que les patients traités par CsA présentaient une amélioration symptomatique et des scores inférieurs à l'indice de la maladie.[34, 35] Cependant, les différents effets secondaires de la CsA ont touché plusieurs utilisateurs comme la sensation de corps étrangers, le prurit et les troubles visuels. En particulier, la sensation de brulure oculaire constitue la raison la plus fréquente d'interruption du traitement (17% des patients).[36] En juillet 2016, le lifitegrast 5% est devenu le deuxième médicament anti-inflammatoire oculaire topique approuvé par la FDA.[37] Les études ont confirmé l'effet thérapeutique du lifitegrast 5 % sur l'amélioration des symptômes de la sécheresse oculaire.[37, 38] Cependant, comme la CsA, il existe encore des effets secondaires, notamment une irritation ou une douleur au niveau du site d'instillation, une réduction de l'acuité visuelle et une dysgueusie (altération du goût).[39, 40]

L'utilisation des lubrifiants est actuellement la thérapie la plus utilisée pour la sècheresse oculaire.[41] Une variété de composants lubrifiants a été ajoutée à la larme artificielle vendue dans le commerce, par ex. HA, cellulose éthers, carbomère, polyéthylène glycol.[42, 43] L'objectif de leur utilisation est d'augmenter l'humidité et d'améliorer la lubrification de la surface oculaire. Toutefois, les récentes larmes artificielles présentent des limites évidentes. Comme le film lacrymal sain est formé par la structure de tri-couche complexe alors que les larmes artificielles

sont délivrées par intermittence, les larmes artificielles ne peuvent pas encore entièrement remplacer à celui de la larme naturelle.[13] Une autre limite vient de leur courte durée au contact avec la surface oculaire, alors que l'utilisation répétée de collyres peut entraîner des effets secondaires sur la surface oculaire et sur le processus pathologique global de la sécheresse oculaire.[44, 45]

Malgré le nombre considérable d'efforts thérapeutiques pour la sécheresse oculaire, de nombreux patients en état grave ne voient pas encore une amélioration claire. De plus, la capacité et la stabilité de la lubrification des produits actuels peuvent encore être améliorés. Il est donc essentiel de bien comprendre et de réparer complètement le système lubrifiant dysfonctionnel oculaire des patients.

c) Le rôle des bio-macromolécules dans le mécanisme de lubrification à l'interface biologique glissante

Les bio-macromolécules jouent un rôle crucial dans la protection des interfaces de l'organisme humain contre le frottement, notamment durant les mouvements des articulations. Leur rôle consiste à créer des conditions rhéologiques et tribologiques optimales en s'adsorbant sur les surfaces biologiques pour former une fine couche d'hydratation garantissant la lubrification entre elles.[46] La plupart des films servant à lubrifier des surfaces humaines sont formés par des bio-macromolécules comme les mucines,[47] les phospholipides,[48] ou l'acide hyaluronique.[49]

Dans les surfaces oculaires, les mucines sont considérées comme des composants essentiels du processus de lubrification. Possédant une structure en « goupillon », ce sont de grandes molécules linéaires capables de s'attacher facilement à la surface des tissus ou des organes pour les hydrater et en favoriser la lubrification.[50] Dans le cas des surfaces cartilagineuses, le liquide synovial entre

elles contient une autre protéine : la lubricine, ou glycoprotéine 4. Composée de protéines et d'oligosaccharides en proportions à peu près égales, la lubricine présente une structure très similaire à celle des mucines, mais de plus petite taille.[51] La lubricine est reconnue comme l'un des principaux protagonistes de la lubrification du cartilage articulaire grâce à sa capacité à réduire la friction.[52]

Pourtant, les mucines, comme la lubricine, n'agissent pas seules dans le processus de bio-lubrification. En effet, les études récentes ont montré le rôle d'interactions synergiques complexes entre ces glycoprotéines et d'autres macromolécules comme les phospholipides ou l'acide hyaluronique.[53, 54] Par exemple, la couche d'hydratation de mucines accompagnée des phospholipides, présente entre la cornée et la paupière, nous permet de cligner des yeux 20 000 à 30 000 fois par jour sans ressentir aucune douleur due à la friction.[55, 56] Au cours d'une course ou d'un saut, le liquide synovial, où la lubricine et l'acide hyaluronique agissent en synergie, maintient un faible coefficient de friction sur le cartilage articulaire, même sous d'énormes charges externes.

Dans le cas du syndrome des yeux secs ou de l'arthrose, l'insuffisance de la quantité ou la détérioration de la qualité de ces macromolécules biologiques entraînent l'augmentation de la friction et l'usure des surfaces biologiques. Depuis les années 1930, d'intenses efforts de recherche ont été déployés pour décrypter leur mécanisme de lubrification pour le traitement des maladies. Pourtant, malgré quelques effets positifs, la plupart d'entre eux ne performent pas suffisamment pour éliminer l'inflammation et se dégradent trop vite dans un environnement physiologique.[57, 58] Il en est de même pour les patients ayant les yeux secs et utilisant souvent des lentilles qui doivent déposer des larmes artificielles chaque jour.[16]

Il est donc urgent de bien comprendre le mécanisme de lubrification des bio-macromolécules naturelles et de mettre au point des innovations synthétiques permettant le développement de nouveaux traitements. Ce projet a pour objectif de synthétiser des biolubrifiants multifonctionnels avec des performances de lubrification synchrones ainsi que des effets anti-inflammatoires.

CHAPITRE 2 : OBJECTIFS DE LA RECHERCHE ET COHÉRENCE DES ARTICLES

2.1) Identification du problème

Les polymères en brosse (BBs), également appelés « brosses moléculaires », ont été conçus et synthétisés au cours des dernières décennies.[59, 60] Il s'agit d'une classe spéciale de copolymères dans lesquels les chaînes latérales sont densement greffées, *via* une liaison covalente sur un squelette polymérique principal. Cette architecture moléculaire possèdent trois caractéristiques uniques que les polymères à chaîne linéaire ne peuvent pas avoir : une forte concentration de chaînes latérales ; un squelette étiré en raison de la répulsion stérique entre les chaînes latérales ; une occupation spatiale uniforme en raison de l'enchevêtrement des chaînes et de la conformation flexible de chaque molécule.[61] Depuis la première synthèse des polymères en brosse, le développement de techniques synthétiques avancées permet le contrôle de plus en plus précis de leurs différents paramètres architecturaux. Les polymères en brosse ont été appliqués dans divers domaines, allant des cristaux photoniques aux systèmes d'administration de médicaments, en passant par la synthèse de nouveaux nanomatériaux.[62-64]

Dans ce contexte scientifique, on se concentre sur la capacité de lubrification et de protection des polymères en brosse sur différentes surfaces. Inspirés par la structure de la lubricine et des mucines, qui jouent un rôle crucial dans la lubrification des articulations,[65, 66] les polymères en brosse sont probablement de futurs candidats-médicaments pour remplacer les bio-macromolécules lubrifiantes déficientes chez les patients souffrant d'arthrose ou de sécheresse oculaire. Plusieurs études ont montré que les propriétés de lubrification des BBs peuvent être étudiées *via* les techniques de mesure directe de la force comme l'appareil à force de surface (*Surface Force Apparatus,* SFA) [65, 67] ou la microscopie à force atomique (*Atomic Force*

Microscopy, AFM).[68, 69] Ils ont formé des systèmes de lubrification très efficaces sur les surfaces de mica et de silice en ajustant la structure des BBs,[69] la conformation de leur couche [70] et la force d'adsorption moléculaire.[71] Ces excellentes performances de lubrification sont prometteuses et d'un grand intérêt général, notamment pour soulager les douleurs arthritiques et oculaires.

Pourtant, les questions relatives à l'impact de la structure interne des polymères en brosse (leur densité de greffage ou leur groupe d'ancrage), à leurs interactions avec les surfaces molles et les tissus et aux mécanismes de synergie intermoléculaire dans le système de lubrification restent encore inexplorées. Notre projet vise donc à établir une corrélation précise entre les caractéristiques architecturales des BBs et leurs propriétés physiques, tribologiques et rhéologiques. En outre, notre approche consiste à caractériser l'interaction de ces polymères avec les interfaces biologiques, puis la synergie entre les polymères et l'acide hyaluronique existant dans les articulations. En explorant la corrélation entre l'architecture des BBs et leur capacité d'adhésion et de lubrification, ce projet a pour but de développer des matériaux brosses puissants affichant des coefficients de frottement extrêmement bas et une protection élevée contre l'usure des surfaces.

2.2) Objectifs généraux

Deux objectifs principaux ont été déterminés pour la caractérisation des polymères en brosse :

a. Effet de la densité de greffage et du squelette sur l'épaisseur du film polymérique, la lubrification et la prévention de l'usure des surfaces contre le frottement sous différentes pressions.

b. Effet du groupe d'ancrage sur l'affinité de l'adsorption, la stabilité de protection, les propriétés antisalissures et anti-inflammatoires de la couche polymérique absorbée sur les surfaces biologiques et biomédicales.

2.3) Cohérence des articles

Le premier article, intitulé "Synthesis and Characterization of Biocompatible Sulfoxide-Containing Molecular Bottlebrushes", publié dans ACS Applied Polymer Material (2022), détermine l'impact de la densité de greffage sur la lubrification du polymère en brosse.[72] Les polymères étudiés sont des brosses macromoléculaires et hydrosolubles contenant des chaînes latérales de poly(2-(méthylsulfinyl)acrylate d'éthyle) (PMSEA) avec des densités de greffage variant de 30 à 100%. L'appareil à force de surface a été utilisé pour mesurer l'épaisseur et la lubrification des polymères en brosses PMSEA sur mica. Les résultats des études de tribologie et de toxicité ont montré que ces polymères peuvent protéger la surface sans endommager les cellules et que l'épaisseur du film polymérique sur la surface est corrélée avec la densité de greffage.

Le deuxième article, intitulé "A bioinspired Bottlebrush polymer mitigates frictional wear of bioinspired and medical device surfaces", est prêt à soumettre. Il présente les performances lubrifiantes d'un polymère tri-bloc synthétisé avec un bloc central ayant une structure en brosse et deux parties latérales greffées fournissant une forte adhérence aux surfaces molles. L'importance du groupe d'ancrage dans la structure du polymère a été soulignée dans la partie de l'adsorption, de la stabilité de la couche polymérique sur les surfaces molles et de la synergie du polymère avec l'acide hyaluronique. Alors que le mica a été utilisé dans le premier article, des cartilages de poulets, des yeux de lapins et des lentilles de contact ont été utilisées comme surfaces cibles dans le deuxième.

CHAPITRE 3 : PREMIER ARTICLE

SYNTHESIS AND CHARACTERIZATION OF BIOCOMPATIBLE SULFOXIDE-CONTAINING MOLECULAR BOTTLEBRUSHES

ACS Applied Polymer Materials **2022**, *4* (11), 8564-8573.

Mateusz Olszewski[a†], Duy Anh Pham[b†], Sara González Bolívar[b], Jean Michel Rabanel[b], Michael Martinez[a], Krzysztof Matyjaszewski [a]*, Xavier Banquy[b,c,d]*

[a]*Department of Chemistry, Carnegie Mellon University, Pittsburgh, PA 15213, USA.*

[b]*Faculty of Pharmacy, Université de Montréal, Montréal, Québec H3C 3J7, Canada*

[c]*Department of Chemistry, Faculty of Art and Science, Université de Montréal, Montréal, Québec H3C 3J7, Canada*

[d]*Institute of Biomedical engineering, Faculty of Medicine, Université de Montréal, Montréal, Québec H3C 3J7, Canada*

[†]**These authors contributed equally to this work**

Corresponding authors: xavier.banquy@umontreal.ca; km3b@andrew.cmu.edu

Abstract

Macromolecular bottlebrushes (MBs) are emerging as an attractive polymer architecture for biomedical applications. Herein, synthesis and characterization of sulfoxide-containing water-soluble MBs with poly(2-(methylsulfinyl)ethyl acrylate) (PMSEA) side chains with varying grafting densities are reported. Highly hydrophilic PMSEA side chains were prepared by

grafting_from poly(2-bromoisobutyryloxyethyl methacrylate) (PBiBEM) using photoATRP with either CuBr2/TPMA (tris(2- pyridylmethyl)amine), CuBr2/TPMA*3 (tris([(4-methoxy-2,5-di_methyl)-2-pyridyl]methyl)amine), or CuBr2/Me6TREN (tris(2- dimethylaminoethyl)amine), which were photochemically reduced to the appropriate amount of activators CuBr/ligand to start atom transfer radical polymerization (ATRP). Kinetic experiments showed that the polymerization was the fastest using CuBr2/Me6TREN at 6-fold excess of ligand to Cu. Additionally, the increase of ligand concentration resulted in a faster reaction with CuBr2/Me6TREN. A series of PMSEA MBs with grafting densities of 30%, 50%, and 100% was synthesized. The PMSEA MBs exhibited tunable hydrodynamic lubrication properties and low cytotoxicity against different types of cells. PMSEA MBs reveal rheological properties characteristic for nonentangled polymer melts. Densely grafted PMSEA MBs showed a nonlinear relationship between the coefficient of friction and the applied force.

KEYWORDS: molecular bottlebrushes, controlled radical polymerization, lubrication, thin films, sulfoxides

3.1 Introduction

Molecular bottlebrushes (MBs) consist of densely grafted side chains along a polymeric backbone. Steric repulsion between the side chains stretches out the backbone, resulting in the MB taking up a rodlike conformation. MBs exhibit a tunable structure, high resistance to compression, and low viscosity in solution due to a lack of entanglement.[73, 74] The three main approaches to synthesis of MBs are grafting-from, grafting-through, and grafting-onto. In grafting-from, side chains are polymerized from initiation sites along a premade polymer backbone. Grafting-through is based on polymerization of macromonomers. In grafting-onto, premade side chains are attached to a

functionalized backbone via selective coupling techniques, including “click”, Diels−Alder chemistry, or disulfide coupling. The effective side chain grafting density depends on the chosen approach. The grafting-through approach ensures a side chain on every repeat unit. However, steric repulsion between large side chains is a significant factor, and preparation of MBs with long side chains is challenging. Due to steric effects, grafting density is usually the lowest using the grafting-onto approach. Grafting-from provides high grafting density, with a high density of functional groups that can be used for additional functionalization.[61] Because MB length, thickness, and rigidity can be easily tuned, they found use in a wide range of biomedical applications.[75] MBs can serve as effective carriers of therapeutic cargo,[76-78] scaffolds for injectable hydrogels,[79-81] effective lubricants,[67, 69, 70] and antifouling agents.[79, 82, 83] Currently, polyethylene glycol (PEG) and its derivative (meth)acrylates are the polymers of choice in biomedical applications due to their biocompatibility and “stealth” properties.[84] However, the recent rise in anti-PEG antibody results in higher than ever motivation to find alternative polymers.[85] Therefore, development of new types of hydrophilic and biocompatible polymers is needed. Synthetic hydrophilic polymers recently used in MBs for biomedical research include zwitterionic polymers, polyelectrolytes,[68] polyethylenimine,[86] and poly(dimethylaminoethyl)- methacrylate.[87] We previously reported the preparation of MBs with poly(2-methacryloyloxyethyl phosphorylcholine) (PMPC) side chains.[65] Monoblock, diblock, and triblock MBs with PMPC brush block and cationic segments had excellent lubrication performance with or without surface modification.[67, 88] PMPC MBs showed nontoxic and antifouling behavior.[62, 89] There is a growing interest in biocompatible and hydrophilic polymers containing sulfoxide groups, either in the main chain or as pendant groups. Attachment of sulfoxide groups to a polymer aims to overcome the cytotoxicity of small molecules while taking advantage of the unique interactions of sulfoxides with water.[90] Sulfoxide-containing

polymers demonstrated potential as antifouling films,[91] agents for nucleotide delivery,[92] and nanogels for skin penetration.[93] Poly(2-(methylsulfinyl)ethyl acrylate) (PMSEA) is an example of a sulfoxide-containing polyacrylate. It was first synthesized by free radical polymerization,[94] reversible addition−fragmentation chain transfer (RAFT) polymerization,[91] and atom transfer radical polymerization (ATRP).[95-98] PMSEA is highly hydrophilic, exhibits superior low-fouling behavior, and carries low immunogenic risk.[96] Recently, PMSEA with complex architecture was reported, including polymer stars,[96] surface brushes,[91] and bioconjugates.[98] Herein, we report the first hydrophilic and biocompatible MBs with PMSEA side chains with the aim to evaluate their lubricating and cytotoxic properties. The bottlebrush architecture was chosen due to tunable structure (length, thickness, and rigidity), low compressibility, and low viscosity in solution, which are excellent attributes for lubricating materials. Copolymers with either methyl methacrylate or butyl methacrylate were synthesized to control the density of initiation sites in the polymer backbones and therefore the density of pendant chains. MBs were synthesized via the photoATRP technique from a Poly(2-bromoisobutyryloxyethyl methacrylate) (PBiBEM) backbone. Side chains were incorporated using grafting-from of MSEA (**Figure 3.1**). Three catalysts were employed: CuBr2/tris(2-pyridylmethyl)amine (CuBr2/ TPMA), CuBr2/tris([(4-methoxy-2,5-dimethyl)-2-pyridyl]- methyl)amine (CuBr2/TPMA*3), and CuBr2/tris(2-dimethylaminoethyl)amine (Me6TREN), which were photo_chemically reduced to the appropriate amount of activators CuBr/ligand to start ATRP. These three catalysts were chosen because of large differences in activity. CuBr2/TPMA*3 is 1500 times more active than CuBr2/TPMA and 100× more active than CuBr2/Me6TREN. PMSEA MBs were synthesized with varying densities of grafted side chains. The impacts of grafting density and side chain lengths of PMSEA MBs on their lubrication properties, rheological behavior, and cytotoxicity were also investigated.

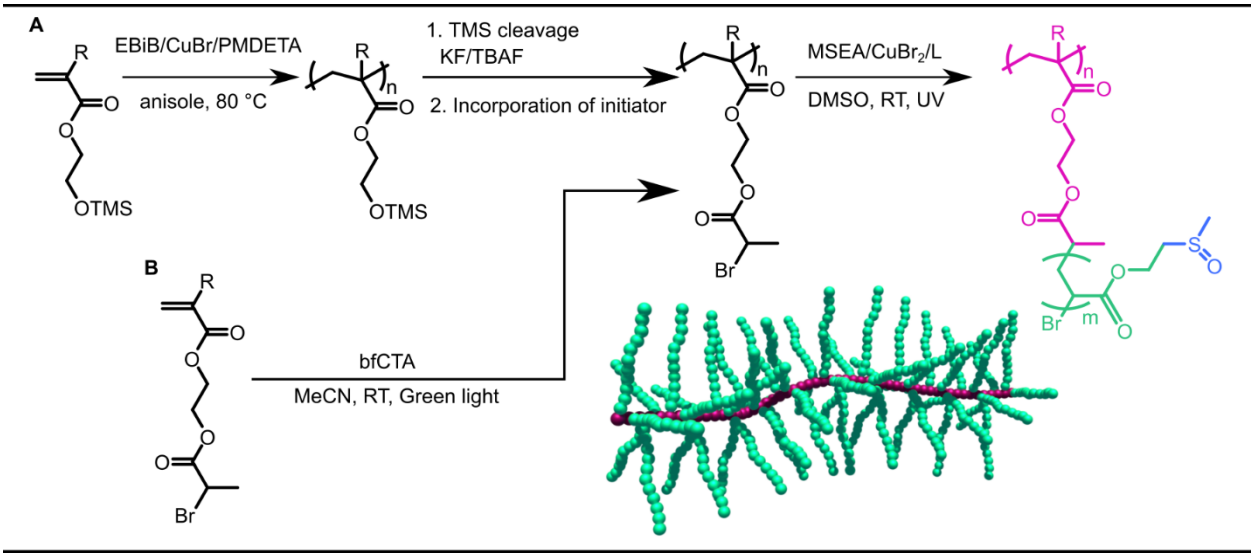

Figure 3.1. Synthesis of PMSEA MBs by (A) photoATRP from PBiBEM backbone prepared by ATRP and (B) PBiBEM backbone prepared by photoiniferter RAFT.

3.2 Materials and Methods

3.2.1 Materials

2-(Methylthio)ethanol (≥99%) was purchased from Alfa Aesar. Hydrogen peroxide solution (30%) was purchased from Fisher Scientific. Acrylic acid (≥99%), *N*-(3-(dimethylamino)propyl)-*N*′-ethylcarbodiimide hydrochloride (EDC, ≥99%), *N,N*-dimethylaminopyridine (DMAP, ≥99%), and copper bromide (≥99.99%) were purchased from Sigma-Aldrich. Acrylic acid was distilled under vacuum before use. Tris(2-dimethylaminoethyl)amine (Me_6TREN, 99%) was purchased from Alfa Aesar and used as received unless otherwise stated. Tris(2-pyridylmethyl)amine (TPMA), tris([(4-methoxy-2,5-dimethyl)-2-pyridyl]methyl)amine (TPMA*[3]), and 2-(methylsulfinyl)ethyl acrylate (MSEA) were synthesized according to previous procedures.[96] A bifunctional CTA, ethane-1,2-diyl bis(4-cyano-4-(((dodecylthio)carbonothioyl)thio)pentanoate) (bfCTA), was synthesized according to a previously reported procedure.[80] 2-(Trimethylsilyloxy)ethyl methacrylate (HEMA-

TMS, Aldrich, 96%), *n*-butyl methacrylate (BMA, Aldrich, >99%), and methyl methacrylate (MMA, Aldrich, >99%) were passed through a column filled with basic alumina prior to use to remove any polymerization inhibitor. 2-Hydroxyethyl methacrylate (HEMA, Aldrich, 98%) was purified using the following procedure: First, 2-hydroxyethyl acrylate (HEA) was dissolved in water to form a 33% solution. Then, the solution was washed five times with hexanes. Next, sodium chloride was added to the solution until the formation of a separate layer was observed. The top layer was separated and dried over $MgSO_4$ to obtain pure HEA. All solvents and other chemicals were of reagent quality and were used as received unless special treatments discussed below were applied.

3.2.2 Bottlebrush Polymer Synthesis

Synthesis of BiBEM

BiBEM was synthesized using the following procedure (**Scheme 3.*1***). HEMA (64 mL) was dissolved in dichloromethane (DCM) (1400 mL) and dried over $MgSO_4$. The salts were separated via filtration through a filter paper, and the solution was added directly to a 2 L three-neck round-bottom flask (RBF). Pyridine (47 mL) was added to the RBF. The flask was sealed with two septa and an addition funnel. Nitrogen was bubbled through the solution for 1 h. The flask was lowered into an ice bath before BiBBr (69 mL) was added to the addition funnel and was added dropwise to the solution overnight. The nitrogen pressure was positive for the duration of the experiment. Most pyridine salts were removed by filtration through filter paper. The crude reaction solution was poured into a 5 L beaker. The mixture was purified by trituration (stirring at 1400 rpm for 10 min in each round) against 2 L solutions of 0.05 M HCl, then 3× saturated sodium bicarbonate, and then 4× deionized water. The aqueous layer was decanted from the solution after each round.

The solution was dried over $MgSO_4$ and passed through a basic alumina plug before solvent evaporation on the rotary evaporator. Air was blown over the monomer overnight to remove trace DCM. The concentrated product was passed through a plug of silica before characterization. The monomer was stored inside of a freezer at −20 °C. The yield was 92 g (63%). The purity of the monomer was confirmed by ^1H NMR and GC-MS (99.2% purity by abundance).

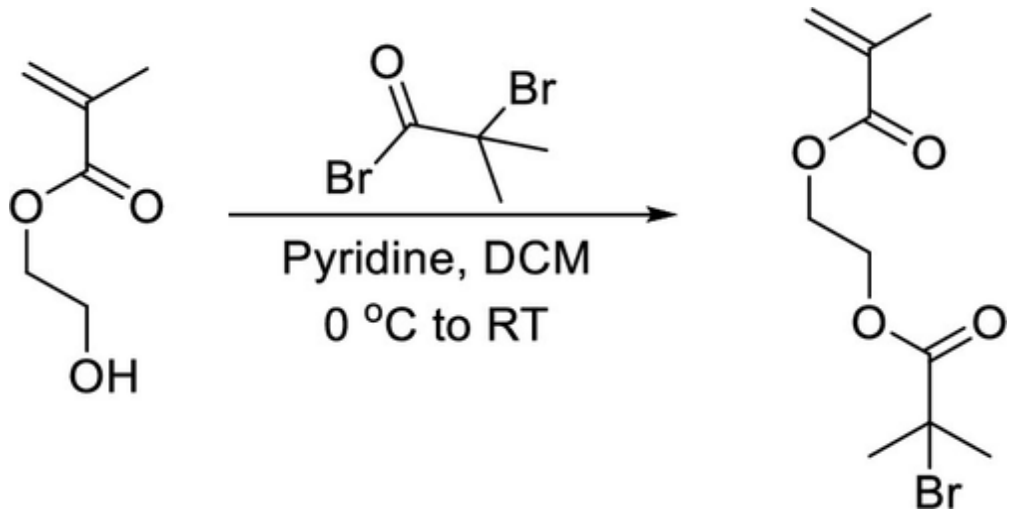

Scheme 3.1 Synthesis of BiBEM

Step 1: Synthesis of backbone for MBs by PhotoATRP

Synthesis of Poly(HEMA-TMS-co-PMMA) for MBs with 50% and 30% grafting densities

In a typical procedure, a dry 25 mL Schlenk flask was charged with ethyl α-bromoisobutyrate (EBiB, 6 mg, 0.031 mmol), $Cu^{II}Cl_2$ (6 mg, 0.006 mmol), TPMA (10 mg, 0.012 mmol), HEMA-TMS (5.0 g, 5.4 mL, 25 mmol), MMA (2 g, 2.2 mL, 20 mmol), and dimethylformamide (DMF) (1 mL). The solution was degassed by three freeze–pump–thaw cycles. The flask was sealed, evacuated, and backfilled with nitrogen five times and then placed under UV light. The reaction was stopped when the monomer conversion reached 48.9%. The monomer consumption was

calculated by the integration of MMA and HEMA-TMS vinyl groups signal (CHH═C–CH_3, 6.11 or 5.56 ppm) against the internal standard (anisole, *o*,*p*-Ar-H, 6.91 ppm). The A block was purified by three precipitations from hexane and then dried under vacuum for 16 h at room temperature.

Synthesis of Poly(HEMA-TMS) for MBs with 100% grafting densities

In a typical procedure, a dry 25 mL Schlenk flask was charged with ethyl α-bromoisobutyrate (EBiB, 12 mg, 0.062 mmol), $Cu^{II}Cl_2$ (1.22 mg, 0.012 mmol), TPMA (10 mg, 0.025 mmol), HEMA-TMS (5.0 g, 5.4 mL, 25 mmol), and DMF (1 mL). The solution was degassed by three freeze–pump–thaw cycles. The flask was sealed, evacuated, and backfilled with nitrogen five times and then placed under UV light. The reaction was stopped when the monomer conversion reached 27.8%. The monomer consumption was calculated by the integration of MMA and HEMA-TMS vinyl groups signal (CHH═C–CH_3, 6.11 or 5.56 ppm) against the internal standard (anisole, *o*,*p*-Ar-H, 6.91 ppm). Poly(HEMA-TMS) was purified by three precipitations from hexane and dried under vacuum for 16 h at room temperature.

Step 2: Synthesis of backbone for MBs by RAFT

Synthesis of Poly(BiBEM-co-MMA) for MBs with 50% and 30% grafting densities

The polymer from step 1a (2 g, containing 10 mmol of HEMA-TMS units), potassium fluoride (0.689 g, 12 mmol), and 2,6-di-*tert*-butylphenol (204 mg, 1 mmol) were placed in a 50 mL round-bottom flask. The flask was sealed and flushed with nitrogen, and dry tetrahydrofuran (THF) (30 mL) was added. The mixture was cooled in an ice bath to 0 °C, tetrabutylammonium fluoride solution in THF (1 M, 0.105 mL, 0.04 mmol) was injected to the flask, and this was followed by the dropwise addition of 2-bromoisobutyryl bromide (1.47 mL, 12.0 mmol) to form the macroinitiator. After the addition the reaction mixture was allowed to reach room temperature, and

stirring was continued for 24 h. The solids were filtered off, and the solution was precipitated into methanol/water (70:30, v/v %). The precipitated macroinitiator was redissolved in chloroform and passed through a short column filled with basic alumina. The filtrate was reprecipitated three times from chloroform into hexanes and dried under vacuum overnight at room temperature.

Synthesis of Poly(BiBEM-co-BMA) for MBs with 50% and 30% grafting densities

BiBEM (1.8 mL, 8.4 mmol), bifunctional CTA, ethane-1,2-diyl bis(4- 123 cyano-4-(((dodecylthio)carbonothioyl)thio)pentanoate) (bfCTA) (0.31 mL of a 0.226 g/mL stock solution in DMF, 84 μmol), BMA (2.68 mL, 16.8 mmol), MeCN (4.5 mL), and a magnetic stir bar were added to a 25 mL Schlenk flask. The flask was wrapped with aluminum foil and sealed with a glass stopper. It was sparged with nitrogen for 30 min. The first aliquot was removed for ^{1}H NMR analysis after degassing the syringe headspace. The reaction was lowered into the photoreactor and was started by turning on the green light. Aliquots were taken to determine the monomer conversion by ^{1}H NMR using the $-CH_2-$ methylene protons for the monomer and polymer within a range of 3.8–4.6 ppm at the internal standard. The conversion of BiBEM and BMA were tracked by their respective vinyl protons. BiBEM conversion was taken as the disappearance of vinyl peak A (6.14 ppm, singlet), and BMA conversion was taken as the disappearance of vinyl peak C (6.09 ppm, singlet). The number-average molecular weight ($M_{n,GPC}$) and dispersity ($Đ$) of each kinetic point were determined by THF GPC relative to linear PMMA standards. BiBEM reached 96% conversion, and BMA reached 98% conversion. GPC analysis of the crude backbone gave $M_{n,GPC}$ = 36 350 and $Đ$ = 1.32. The polymer macroinitiator was purified by precipitation into hexane once before it was dialyzed against acetone. The polymer was isolated as a film under vacuum. The final composition was confirmed by ^{1}H NMR.

Synthesis of polyBiBEM for MBs with 100% grafting densities

The polymer from step 1b (0.84 g, containing 4.15 mmol of HEMA-TMS units), potassium fluoride (0.289 g, 4.98 mmol), and 2,6-di-*tert*-butylphenol (86 mg, 0.690 mmol) were placed in a 50 mL round-bottom flask. The flask was sealed and flushed with nitrogen, and dry THF (30 mL) was added. The mixture was cooled in an ice bath to 0 °C, tetrabutylammonium fluoride solution in THF (1 M, 0.042 mL, 0.04 mmol) was injected to the flask, and this was followed by the dropwise addition of 2-bromoisobutyryl bromide (0.616 mL, 5.0 mmol) to form the macroinitiator. After the addition the reaction mixture was allowed to reach room temperature, and stirring was continued for 24 h. The solids were filtered off, and the solution was precipitated into methanol/water (70:30, v/v %). The precipitated macroinitiator was redissolved in chloroform and passed through a short column filled with basic alumina. The filtrate was reprecipitated three times from chloroform into hexanes and dried under vacuum overnight at room temperature.

Step 3: Synthesis of PMSEA Bottlebrush by Grafting-from via PhotoATRP in DMSO

In a typical procedure, a dry 5 mL Schlenk flask was charged with macroinitiator (from step 1 or 2) (4.3 mg, 0.04 μmol of PBiBEM), MSEA (500 mg, 3.1 mmol), TPMA (0.8 mg, 0.003 mmol), $Cu^{II}Br_2$ (as a stock solution, 0.1 mg, 0.0005 mmol), DMF (0.3 mL), and dimethylsulfoxide DMSO (2.0 mL). The solution was degassed by three freeze–pump–thaw cycles. The flask was sealed, evacuated, and backfilled with nitrogen five times and then placed under UV light. The first kinetic aliquot was taken using an air-free syringe after starting the reaction upon exposure to UV light. After various reaction times, kinetic samples were taken and quenched by exposure to air. The bottlebrush polymer was purified by dialysis against MeOH for 48 h using tubes with a pore size molar mass cutoff of 10 000 kDa.

Step 4: Synthesis of PMSEA Bottlebrush by Grafting-from via PhotoATRP in Acetonitrile

In a typical procedure, a dry 5 mL Schlenk flask was charged with macroinitiator (from step 2) (9.0 mg, 0.05 μmol of 2b), MSEA (500 mg, 3.1 mmol), TPMA[*3] (0.4 mg, 0.001 mmol), $Cu^{II}Br_2$ (as a stock solution, 0.2 mg, 0.002 mmol), DMF (0.3 mL), and acetonitrile (2.0 mL). The solution was degassed by three freeze–pump–thaw cycles. The flask was sealed, evacuated, and backfilled with nitrogen five times and then placed under UV light. The first kinetic aliquot was taken using an air-free syringe after starting the reaction upon exposure to UV light. After various reaction times, kinetic samples were taken and quenched by exposure to air. The bottlebrush polymer was purified by dialysis against MeOH for 48 h using tubes with a pore size molar mass cutoff of 10 000 kDa.

3.2.3 Equipment and Analysis

Proton nuclear magnetic resonance (^{1}H NMR) spectroscopy was performed using a Bruker 300 MHz spectrometer. In all cases deuterated chloroform ($CDCl_3$) was used as a solvent, except for the bottlebrush polymer, which was analyzed using deuterated DMSO (DMSO-d_6). ^{1}H chemical shifts are reported in parts per million (ppm) downfield from tetramethylsilane (TMS). Apparent molecular weights and molecular weight distribution measurements of polymers except for the bottlebrush polymer were measured by size exclusion chromatography (SEC) using Polymer Standards Services (PSS) columns (guard, 10^5, 10^3, and 500 Å), with THF or DMF as the eluent at 35 °C at a constant flow rate of 1.00 mL/min, and a differential refractive index (RI) detector (Waters). The apparent number-average molecular weights (M_n) and molecular weight distributions (M_w/M_n) were determined with a calibration based on linear poly(methyl methacrylate) (PMMA) standards and toluene as an internal standard.

3.2.4 Cell Cytotoxicity Experiments

Polymer Stock Solution and Dilution Preparation

Each MB polymer (250 μL) in methanol stocked at −80 °C (concentrations: 2–4 mg/mL) were sterile-transferred to autoclaved Eppendorf tubes. After drying, polymers 1 and 2 were resuspended in 250 μL of sterile DPBS, and polymers 3 and 4 were resuspended in 500 μL of sterile DPBS to a final concentration of 10 mg/mL. A serial dilution in sterile DPBS was performed to obtain solutions with final concentrations at 1000, 100, 10, 1, and 0.1 μg/mL (tests with HeLa, MCF-7, and U87 cells); 1000, 500, 100, 10, and 1 μg/mL (tests with Hep G2 and THP-1 cells).

Cell Culture

Dulbecco's modified Eagle's medium (DMEM), RPMI 1640 medium, fetal bovine serum (FBS), penicillin–streptomycin 100× solution, and Dulbecco's phosphate-buffered saline (DPBS) were provided by Wisent, Inc. (Saint-Bruno, QC, Canada). The MTS assay kit was from Abcam, Inc. (Toronto, ON, Canada). HeLa (human cervical cancer cells), U87 (human primary glioblastoma cell line), MCF7 cells (human breast cancer cell line), and Hep G2 (human hepatocyte cell line) were used for cytotoxicity evaluation and cultured in DMEM supplemented with 10% FBS and 1% streptomycin/penicillin. THP-1 (human monocyte cell line) was also used for cytotoxicity assays and cultured in RPMI 1640 medium, supplemented with 10% FBS, 1% streptomycin/penicillin, and 2-mercaptoethanol to a final concentration of 0.05 mM. The cells were maintained in T-75 flasks at 37 °C and 5% CO_2. After trypsinization, the cells were counted and resuspended in complete medium. Seeding density in 96-well plates was determined for each cell line to optimize the assays─HeLa, MCF-7, and Hep G2: 10×10^3 cells per well; U87: 5×10^3 cells per well; and THP-1: 15×10^3 cells per well.

Cells were incubated for 24 h to allow attachment or/and growth. Following attachment, the medium was changed and 10 μL of MB polymer dilution was added (n = 5/concentration), except for THP-1 (nonadherent cell line), for which the medium was not changed. One positive (treatment with DPBS alone) and negative (no cells) control were included in each plate (n = 5). Cells were incubated for 24 h in a cell culture incubator at 37 °C and 5% CO_2.

MTS Cell Proliferation Assay

Cell proliferation after polymer exposure was measured using the MTS Cell Proliferation Colorimetric assay kit (Abcam, Inc., product no. ab197010), used as recommended by the manufacturer. The absorbance was measured at 470 nm using a Tecan Spark microplate reader (Tecan, Austria). The absorbance was proportional to cell proliferation, and the results were expressed as the average percentage of cell proliferation ± SD.

3.2.5 Surface Forces Experiments

The surface forces apparatus 2000 (SFA 2000, SurForce, LLC, U.S.A.) was used to measure the interaction forces and the distance between two opposing and atomically flat mica surfaces covered with MB polymer. The distance between the surfaces was assessed using the fringes of equal chromatic order (FECO) via multiple beam interferometry (MBI).[99] Displacement of the surfaces was controlled by a coarse differential micrometer manipulated by hand and by a micromotor for the fine (subnanometer) displacement.[100]

Surface Preparation

Back-silvered mica surfaces were prepared by cutting freshly cleaved mica sheets with a thickness of 1–3 μm using a hot platinum wire and then coating one face with silver by physical vapor

deposition (Covap, Angstrom Engineering, Canada). Two back-silvered mica pieces having the same thickness were glued (silver side down) on cylindrical glass discs with a curvature of 2 cm. The glass discs carrying the mica sheets were mounted in a cross-cylindrical geometry in the chamber of an SFA and brought into contact in dry air to set the reference contact point. FECO were generated by multiple reflection of a white light beam between the two back-silvered mica sheets and were recorded using a spectrometer and a charge-coupled device (CCD) camera (Andor Technology, U.S.A.). After this calibration, the bottlebrush polymer solution was inserted in between the mica surfaces at a concentration of 100 $\mu g/mL^{-1}$ and left to adsorb for 45 min. Water was also added at the bottom of the SFA chamber to saturate the chamber and limit the evaporation of the liquid between mica surfaces.

Friction Force Measurements

For the assessment of friction force, each MB polymer was tested in at least 3 independent experiments at 2 different contacts in each experiment to ensure reproducibility. The friction force was measured at different normal loads ranging from 0.1 to 5 mN. Back and forth shear cycles were applied when the surfaces were in close contact. For each experiment, 4–10 shearing cycles were applied at each increasing load to ensure that the lubrication properties of the MB layer were stable. The surfaces were sheared past each other using a piezoelectric bimorph designed with a flexure point in the middle, which caused the surfaces to displace linearly as the voltage was applied. The bimorph drove the lower surface in a back-and-forth motion using a triangular wave function with a typical frequency of 50 mHz and an amplitude of 5 V (equivalent to 3 $\mu m/s^{-1}$) controlled by a function generator (Agilent 33250A, Agilent Technologies, Inc., U.S.A.). During sliding, the friction transmitted to the upper surface was measured by two vertical double-

cantilever springs equipped with four semiconductor strain gauges attached symmetrically to oppositely bending arms of the springs, thus forming the four arms of a Wheatstone bridge strain gauge system.[100] When a lateral force was applied to the upper surface, the strain gauges were used to measure the deflection with a signal conditioning amplifier (Vishay Measurements, 2310B), which outputs the signal to a computer data-acquisition system.

3.3 Results

3.3.1 Synthesis of PMSEA MBs

Grafting-from ATRP of MSEA from a poly(2-bromoisobutyryloxyethyl methacrylate) (PBiBEM) polymer with a degree of polymerization (DP) equal to 372 was used to find the optimal catalyst system. The efficiencies of ATRP catalysts with three different ligands─TPMA, TPMA^{*3}, and Me_6Tren─were compared. The reactions were stopped upon observing a significant increase in solution viscosity, at ~40% monomer conversion for all samples. Initially, experiments with 2-fold excess of ligand to $CuBr_2$ were performed. The catalyst with TPMA as a ligand required the longest time to reach a significant monomer conversion, 2 h (see **Figure S3.1**) for ~25% monomer conversion.. Polymerization was significantly faster with both TPMA^{*3} and Me_6Tren. Well-defined MBs with low dispersity were obtained for all three systems. No significant differences in dispersity or molecular weight of final brushes were observed despite different reaction times (**Table S3.1**).

Next, a series of experiments were performed using a 6-fold excess of ligand to $CuBr_2$. The reaction with Me_6Tren was significantly faster than those with TPMA or TPMA^{*3}. A clear trend

was observed with TPMA*[3] being slower than Me_6Tren and unmodified TPMA being the slowest (**Figure 3.2**).

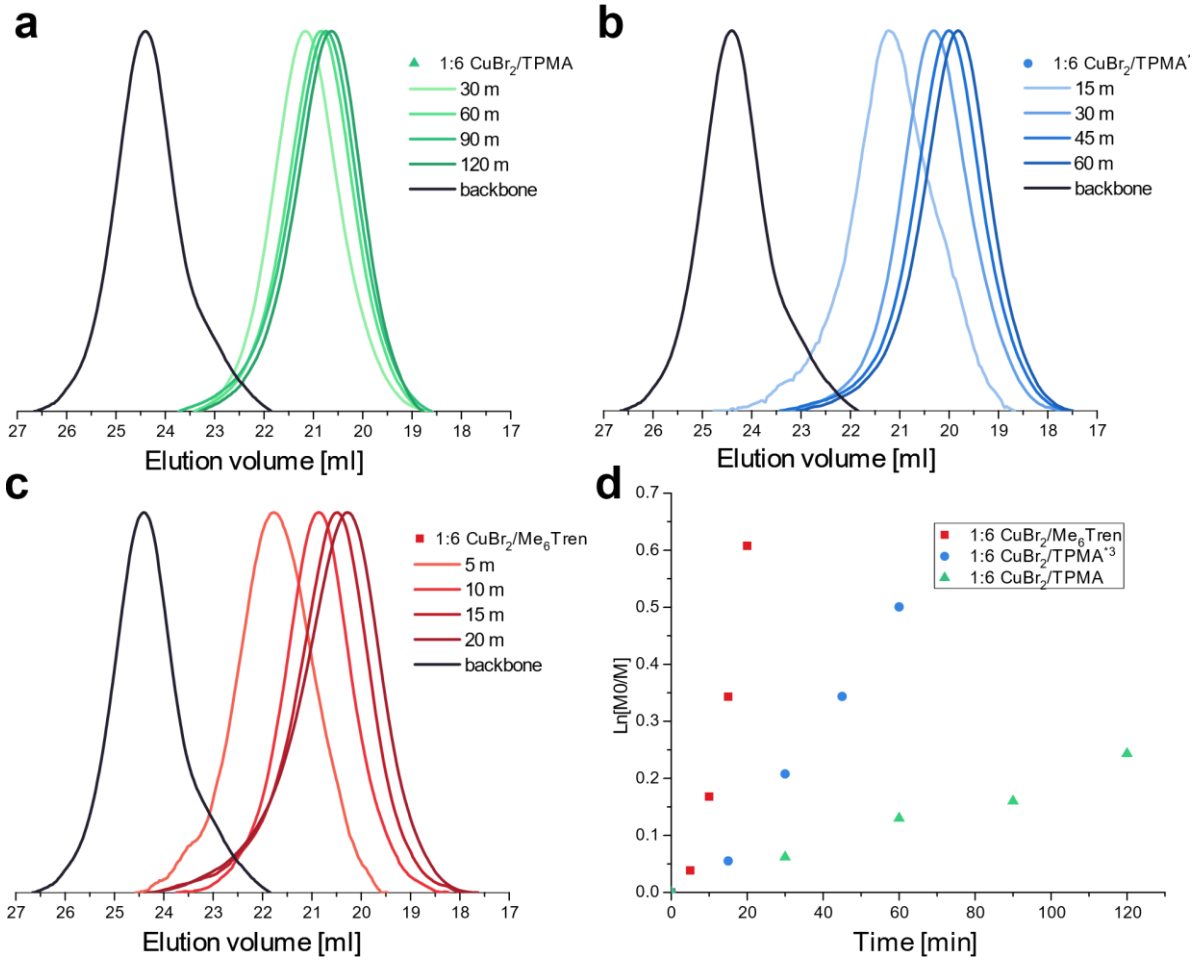

Figure 3.2. GPC traces of elution during the synthesis of P(BiBEM-*g*-PMSEA) with (a) 1:6 ratio of $CuBr_2$/TPMA, (b) 1:2 ratio of $CuBr_2$/TPMA*[3], and (c) 1:2 ratio $CuBr_2$/Me_6Tren. (d) Pseudo-first-order kinetic plots for the polymerization of poly(n-butyl acrylate) (PBA) molecular bottlebrushes. Irradiation by 360 nm at 4.9 mW/cm^2 at room temperature 25 °C, 75 vol % DMSO, 5% DMF. [MSEA]/[EBiB]/[CuBr2]/[L] = 200:1:0.03:0.18, x = 0.03.

In ATRP, an increase of polymerization rate with increasing excess of ligand to Cu is typically observed because the ligand acts as an electron donor helping the reduction of the Cu(II)

deactivator to the Cu(I) activator complex.[101, 102] The polymerization process was accelerated by an excess of Me6Tren, which contains four tertiary alkyl amine groups that act as more efficient electron donors than aromatic pyridines.

Then, a series of PMSEA MBs with different grafting densities and backbone lengths was synthesized. First, a series of backbones was prepared, with predetermined densities of ATRP initiation sites of approximately 30%, 50%, and 100%. Backbones with different densities of initiation sites were prepared by adjusting the content of MMA or BMA. A backbone with 100% grafting density was prepared by homopolymerization of HEMA-TMS. Backbones with a lower density of initiators were prepared by copolymerization of HEMA-TMS with MMA or BMA by photoATRP or BiBEM with MMA or BMA by RAFT, resulting in polymers where ~30% or ~50% of the repeat units contain the ATRP initiator functionality. Side chains were synthesized using grafting-from ATRP of MSEA. TPMA*[3] was used as the ligand to provide a short reaction time and greater control over the final side chain DP. **Table 3.1** contains detailed information about the structures of the prepared samples (GPC traces are provided in **Figure S3.3-S3.6**, and ^{1}H NMR spectra of samples MB1 and MB3 are provided as examples in **Figure S3.7 and S3.8**).

Table 3.1. Summary of Characterized PMSEA-MB Samples (See Figure S2 for Schematic of the Structures)

Entry	Backbone DP	Grafting density	Side chain DP	$M_{n,th} \times 10^{-3}$	Đ
MB1	221	~50%	55	940	1.29
MB2	487	~50%	54	2290	1.19
MB3	292	~30%	64	1040	1.25
MB4	372	~100%	55	3907	1.20

3.3.2 Cellular Toxicities of the Different PMSEA MBs

To evaluate the toxicities of the PMSEA MBs, we chose three epithelial cell lines coming from different organs─cervix, brain, and breast epithelium─and in addition two more cell lines, one from the liver (hepatocytes) and another one from the mononuclear phagocyte system (macrophages). These cell lines are representative of tissues most likely exposed to nanomaterials entering the bloodstream. The polymers dissolved in DPBS did not significantly affect the proliferation of immortalized cancer cells, as shown in **Figure 3.3**. From the proliferation assay, no lethal concentration (LC50) could be extracted in the range of polymer concentration tested; therefore, PMSEA MBs appeared to be well-tolerated even at the maximum concentration tested (1 mg/mL). More variability was observed with the MCF7 cell line, but no trend or explanation could be identified. No changes of cell morphology upon MB polymer exposure were detected, suggesting that the MB surface groups did not affect the cell membrane integrity (see **Figure S3.9**). These results suggest the suitability of PMSEA MBs for therapeutic intervention such as drug delivery, imaging, and lubrication, among others.

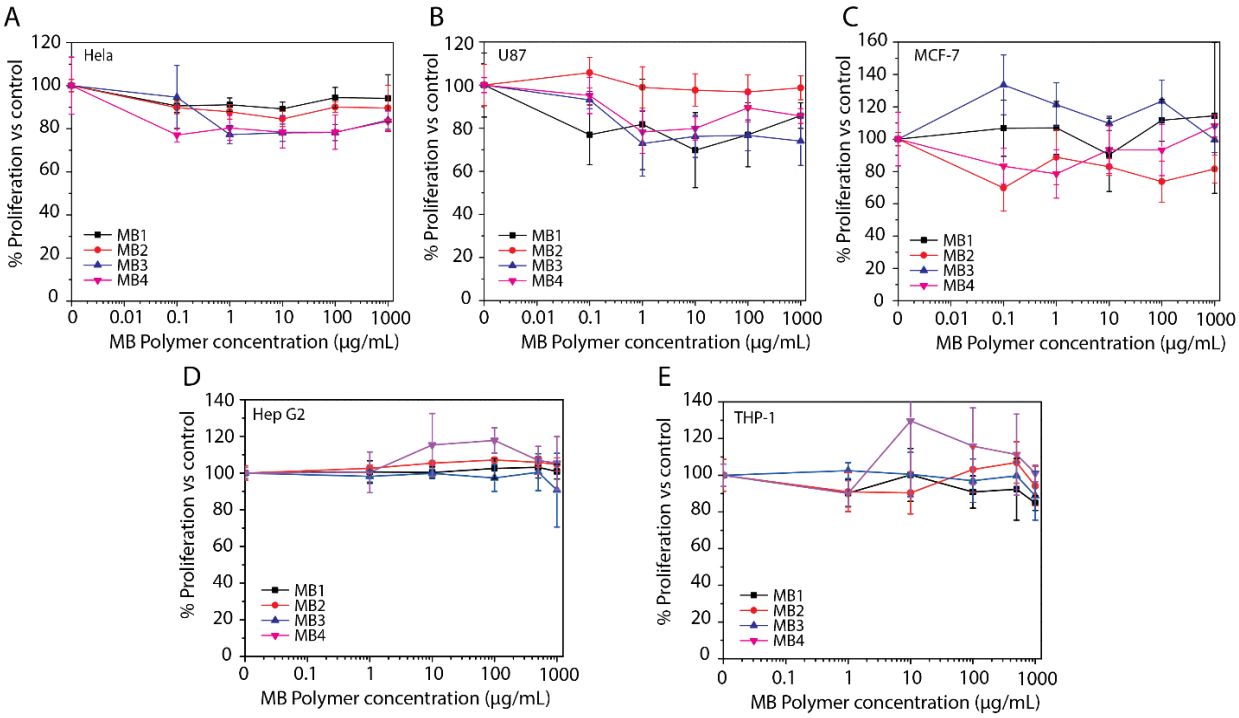

Figure 3.3. PMSEA MBs do not impact cell proliferation in several cell lines. (A) HeLa, human cervical cancer cell line; (B) U87, human primary glioblastoma cell line; (C) MCF-7, human breast cancer cell line; (D) Hep G2, hepatocyte cell line; (E) THP-1 human monocyte cell line. Cells were exposed for 24 h to different concentrations of PMSEA MBs (n = 5) prior to cell-proliferation assays. Results are expressed as a percentage of proliferation relative to DPBS-treated cells (control).

3.3.3 Lubrication Properties of the Bottlebrush Polymers

In a first series of tests, the different PMSEA MBs were independently evaluated for their tribological properties against mica surfaces. Mica was chosen as a substrate because it is the most reliable material for surface forces measurements using the SFA. As shown in **Figure 3.4A**, the tested polymers exhibited different tribological behaviors depending on their architecture. The measured friction force showed a nonlinear dependence with the applied normal load for all the

polymers, a behavior that will be explained in detail later. An effective friction coefficient, μ_{eff}, was estimated using the relationship $\mu_{eff} = dF_s/dF_n$.

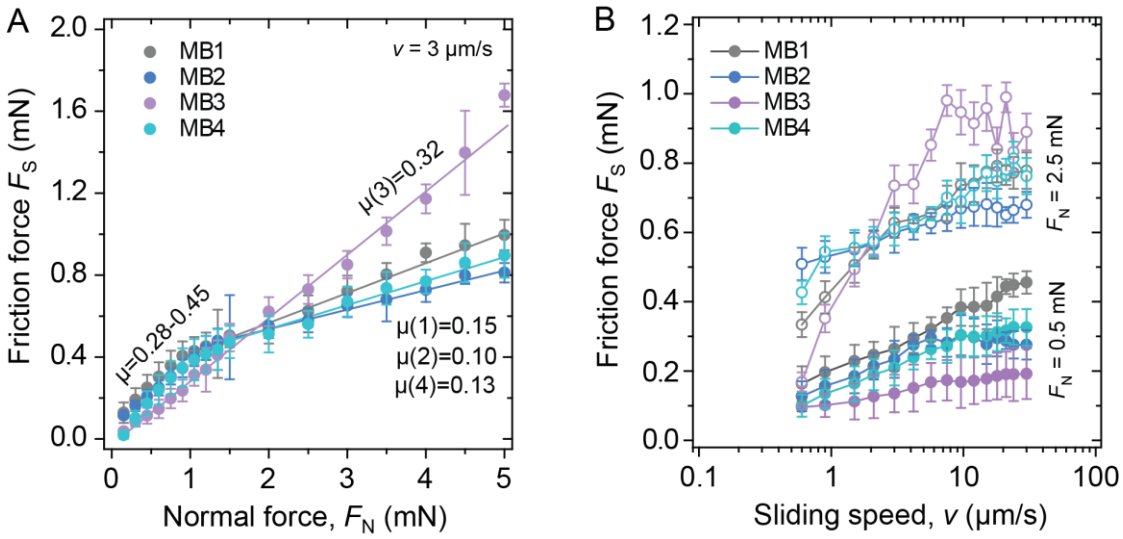

Figure 3.4. (A) Tribological testing of the 4 different PMSEA MBs in water at 100 μg/mL. Evolution of the friction force with the normal force applied at a constant sliding speed of 3 $\mu m/s^{-1}$. (B) Friction force vs sliding speed at normal loads of 0.5 mN (filled symbols) and 2.5 mN (open symbols).

As can be seen in **Figure 3.4A**, at a normal force $F_N < 1$ mN, a high friction coefficient was measured with μ_{eff} varying between 0.28 and 0.45 depending on the polymer, and for $F_N > 1$ mN, μ_{eff} was found to vary between 0.104 and 0.154. The coefficient of friction, μ_{eff}, of this load regime was reduced by ~55–70% compared to the low F_N regime. The nonlinear relationship between F_S and F_N was not clearly observed for MB3; therefore, its coefficient of friction remained constant in the whole range of normal force tested but still similar to the values obtained for the other polymers in the low-load regime (μ_{eff} = 0.32). The nonlinearity between F_S and F_N observed for MBs 1, 2, and 4 can be explained by assuming that the shear stress

is independent of the load and that there is a Hertzian contact between the two surfaces. In that approximation, F_S and F_N are proportional as $F_S \propto F_N^{2/3}$ (**Equation 3.1**) and the friction coefficient *m* defined as $\mu = F_s / F_N$ varies as $\mu \propto F_N^{-1/3}$.[103]

As can be seen in **Figure 3.5A**, fitting the experimental result with **eq 3.1** was not possible for MB3 but was possible for the other polymers (only the fitting for MB4 is shown for clarity). When monitoring the film thickness during sliding at constant speed, $v = 3$ μm/s, it appears that the MB3 lubricating film reaches values close to 2 nm at the highest applied load ($F_N = 5$ mN), which corresponds to the thickness of a monolayer of MB polymer (**Figure 3.5B**). The lubricating film at such a high load was the thinnest for MB3 and increased in the order MB3 > MB1 > MB4 > MB2. The increase of the film thickness from MB3 to MB1 and to MB4 is correlated to the increase of the side chain grafting density from 30% to 100% in these polymers. The film thickness of MB2, which has a chain grafting density of 50%, identical to that for MB1, was the largest, probably due to the fact that the backbone length of this polymer was the longest of the series of PMSEA MBs. The values of the hard wall thickness (measured at the highest compression) provide some indications of the conformation of the polymers under confinement. The increase of the hard wall thickness with the length of the backbone of the polymer suggests that its conformation is not flat on the surface, even under high compression, but rather coiled or possibly entangled with other chains.

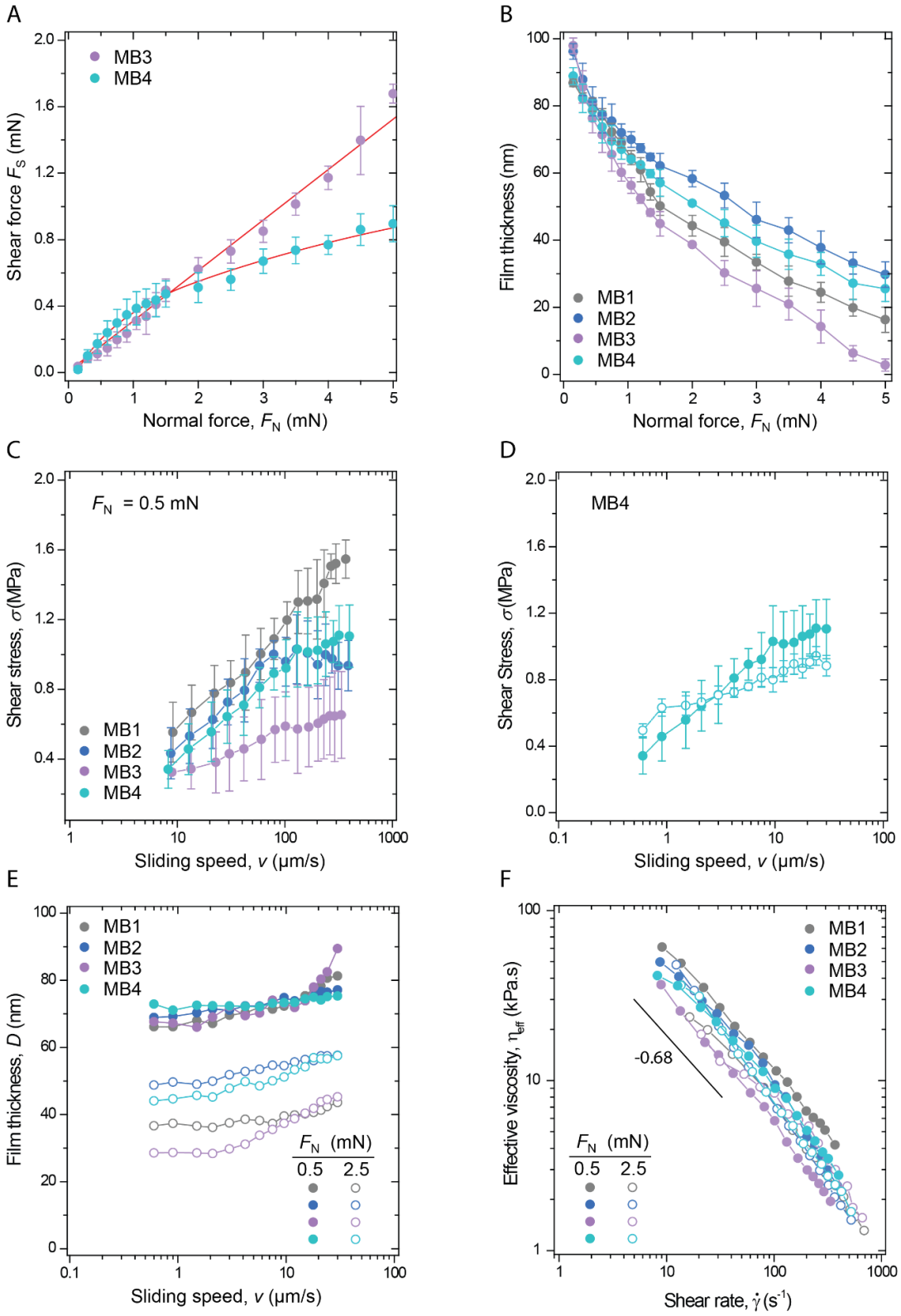
A
Shear force F_S (mN)
Normal force, F_N (mN)
MB3
MB4
B
Film thickness (nm)
Normal force, F_N (mN)
MB1
MB2
MB3
MB4
C
Shear stress, σ(MPa)
F_N = 0.5 mN
Sliding speed, v (μm/s)
MB1
MB2
MB3
MB4
D
Shear Stress, σ(MPa)
MB4
Sliding speed, v (μm/s)
E
Film thickness, D (nm)
Sliding speed, v (μm/s)
MB1
MB2
MB3
MB4
F_N (mN)
0.5 2.5
F
Effective viscosity, η_{eff} (kPa.s)
Shear rate, $\dot{\gamma}$ (s^{-1})
-0.68
MB1
MB2
MB3
MB4
F_N (mN)
0.5 2.5

Figure 3.5. (A) Representative evolution of the shear force as a function of the applied normal force for two bottlebrush polymers behaving significantly differently. (B) Thinning of the polymer film during the shear test. (C) Evolution of the shear stress with the sliding speed for all 4 polymers at low applied normal force and (D) comparison of the shear stress at two different loads. (E) Increase of the lubricating film thickness with the sliding speed at two different applied normal forces and (F) evolution of the effective viscosity with the shear rate at the same two applied normal forces.

The large values of the lubricating film thickness at $F_N < 0.5$ mN for all of the polymers also suggest that the lubrication mechanism should be dominated by hydrodynamic lubrication. This could be corroborated by three independent observations. First, in **Figure 3.4B** and **3.5C**, the dependence of F_S or the shear stress σ with the sliding speed shows a logarithmic increase, which has been reported for several polymeric lubricating materials exhibiting complex rheological behavior.[104, 105] Second, for all four PMSEA MBs, the shear stress extrapolates to zero at zero speed, as shown in **Figure 3.5C**, and the shear stress was weakly dependent on the normal force F_N (**Figure 3.5D**). Third, we observed a slight increase of the film thickness with the sliding speed at high and low applied loads (thin and thick lubricating films, **Figure 3.5E**), which is also a strong indicator of hydrodynamic lubrication. These observations point to a hydrodynamic dissipation mechanism of the friction force, as already reported for polymeric melts.[106]

For a confined fluid, where hydrodynamic dissipation is expected to dominate, an effective thin film viscosity, η_{eff}, can be defined as $\eta_{eff} = F_S D/Av$, where A is the contact area and D is the film thickness. For separation distances that are several times larger than the characteristic size of the molecules constituting the lubricating film, η_{eff} is expected to equal the bulk viscosity. In the present case, this situation is expected to happen when D is superior to a few hundred nanometers

based on the size of the backbone of the polymers, which is larger than the separation distance measured during the tribological tests. In **Figure 3.5F** is shown the dependence of η_{eff} with the shear rate, $\dot{\gamma}$, for the four different polymers. The effective viscosity is clearly decreasing as $\dot{\gamma}$ increases and follows a power law $\eta_{eff} \propto \dot{\gamma}^n$, with n having the experimental value of $n = -0.68 \pm 0.05$ for all of the polymers. This experimental value is close to the theoretical value of $-2/3$ expected for nonentangled polymer melts[107] and is significantly lower than the value of $n = 1$ reported for polybutadiene melts with molecular weights higher than the molecular entanglement weight, M_e.[108] A similar value for n was obtained for physisorbed polyethylene glycol brushes on mica surfaces in water.[109] Compared to linear polymers, bottlebrush polymers have the singular property to exhibit low entanglement density or high M_e. The scaling of M_e with the molecular diameter of the bottlebrush chain, Δ, is found to scale as $M_e \approx \Delta^3$.[110] Therefore, it is not surprising that the rheological behavior of the MB polymers is close to what is expected for nonentangled polymer melts even when the film thickness D is far larger than Δ. Experimental data show that there are no significant differences in thin film viscosity, η_{eff}, among the 4 polymers, which is likely due to the fact that all of their side chains have the same DP_n and, therefore, the same value of Δ. Data in **Figure 3.5F** also show that differences in η_{eff} values between the different polymers are more pronounced at low applied load (large separation distances) than at high applied load (small separation distances). Because the 4 polymers have a backbone DP_n ranging from 219 up to 497, this observation suggests that the thin film viscosity of bottlebrush polymers under high confinement does not depend on the polymer backbone length.

3.4 Conclusion

In this study, a series of molecular bottlebrushes with sulfoxide-containing side chains was synthesized. Kinetic experiments on photoATRP of MSEA from polyacrylate backbones showed significantly faster polymerization with Me_6Tren compared to TPMA or TPMA*[3] when a high excess of ligand was used. PMSEA MBs with theoretical grafting densities of 30%, 50%, and 100% exhibited excellent toxicity profiles in vitro. SFA tests were performed to analyze the lubricative properties of PMSEA MBs. Lubrication performance depends strongly on the grafting density of pendant chains and is tunable. Compared to other polyelectrolyte and zwitterionic hydrophilic MBs, PMSEA MBs exhibited a relatively high coefficient of friction. However, no signs of wear were observed with increasing applied loads, evidencing promising protective properties of PMSEA MBs. Different tribological behaviors were shown for PMSEA MBs with different grafting densities. PMSEA MBs with a grafting density of ≥50% exhibited a nonlinear relationship between the coefficient of friction and the applied force. Additionally, highly confined PMSEA MBs exhibited a rheological behavior characteristic for nonentangled polymer melts. Given the straightforward synthesis, excellent toxicity profile, and unique lubricating properties with improved wear protection, we believe that PMSEA MBs are promising candidates for biomedical applications such as biolubricants for medical devices such as contact lenses or for topical applications.

3.5 Supporting information

Experimental Details

PMSEA grafting-from optimization

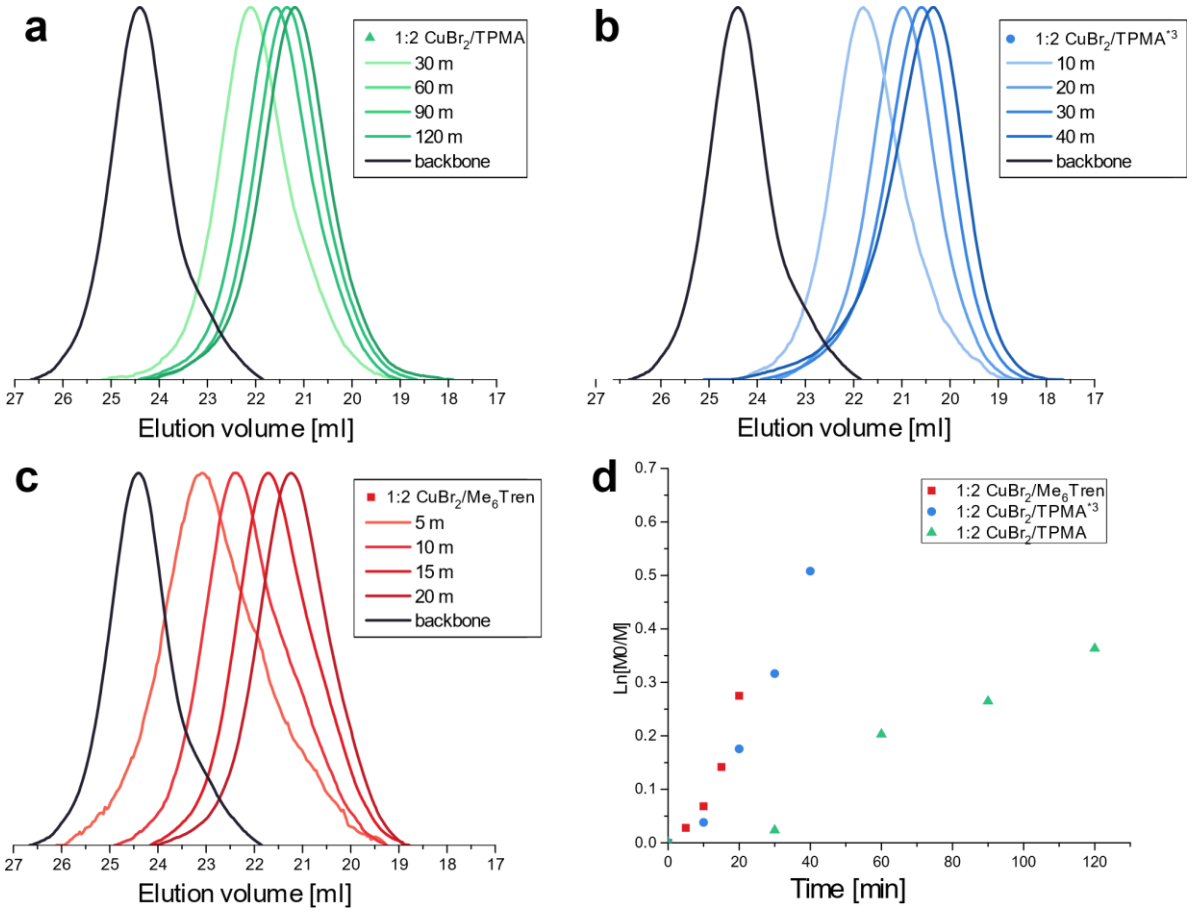

Figure S3.1. Gel permeation chromatography (GPC) traces evolution during the synthesis of P(BiBEM-g-PMSEA) with (a) 1:2 ratio $CuBr_2$/TPMA,(b) 1:2 ratio Cu/TPMA^{*3}, (c) 1:2 ratio $CuBr_2$/Me_6Tren, (d) Pseudo-first order kinetic plots for the polymerization of PBA molecular bottlebrushes. Irradiation by 360 nm at 4.9 mW/cm2 at room temperature 25 ºC, 75 vol.% DMSO, 5% DMF. [MSEA]:[EBiB]: [CuBr2]: [L]= 200:1:0.03:0.06, x = 0.03.

Table S3.1. PhotoATRP grafting-from of MSEA with different ligands and different $[L]_0/[CuBr_2]_0$ ratios.

Entry	Ligand	$[L]_0/[CuBr_2]_0$	Time (min)	Conv.[b] (%)	$M_{n,th} \times 10^{-3}$	$M_{n,GPC} \times 10^{-3}$	Đ
1	TPMA	2	120	39	4700	492	1.41
2	TPMA^{*3}	2	40	30	3620	450	1.39
3	Me_6Tren	2	20	24	2890	333	1.26
4	TPMA	6	120	22	2650	444	1.22
5	TPMA^{*3}	6	60	40	4820	580	1.18

6	Me_6Tren	6	20	46	5540	491	1.38

PMSEA MB samples for characterization

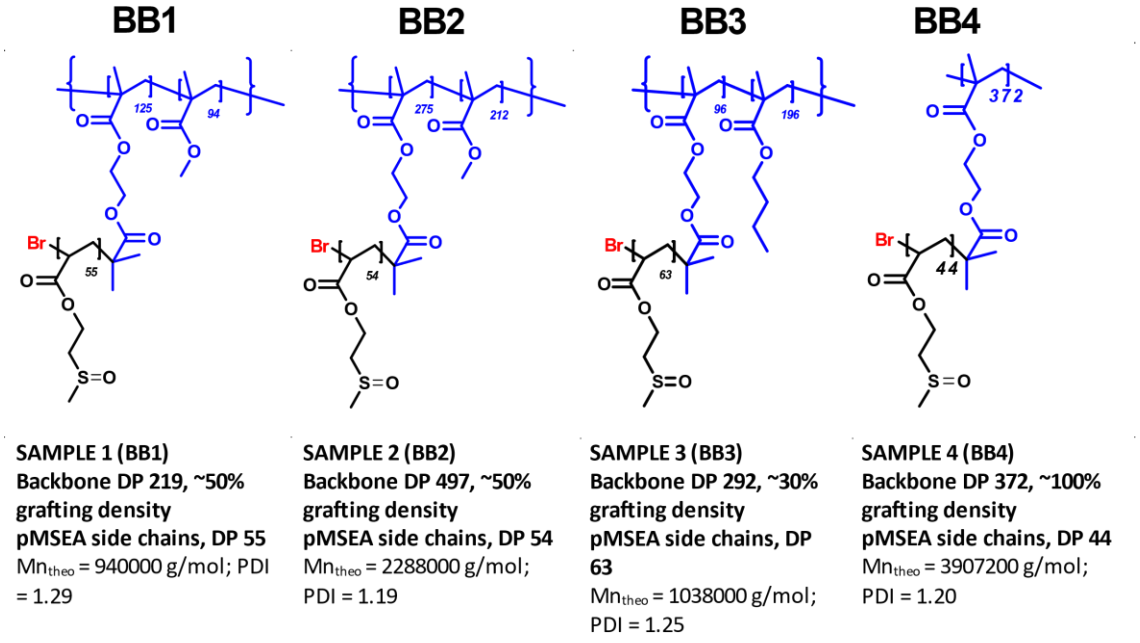

Figure S3.2. Schematic representation of synthesized PMSEA-MBs with different compositions.

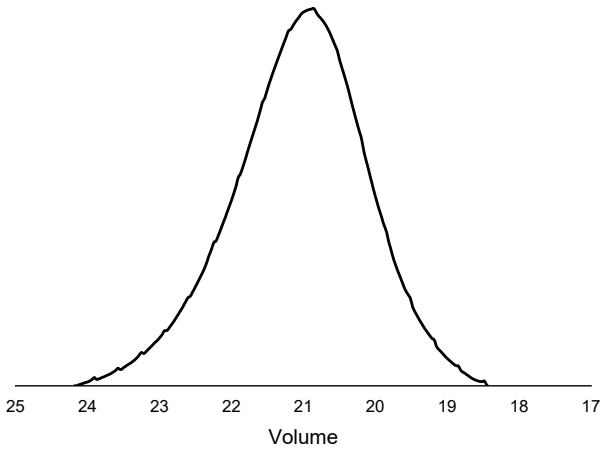

Figure S3.3. GPC trace of sample. BB1

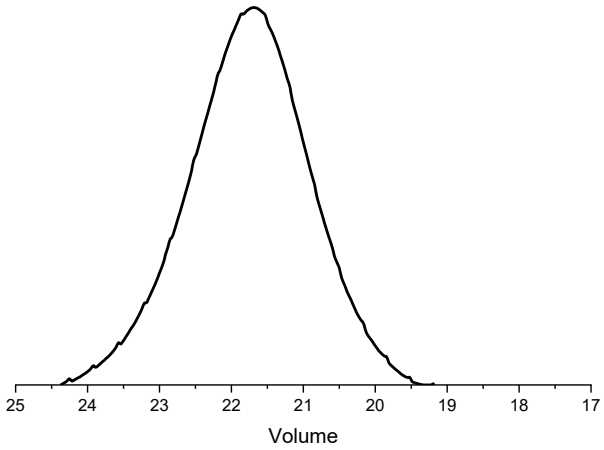

Figure S3.4. GPC trace of sample. BB2

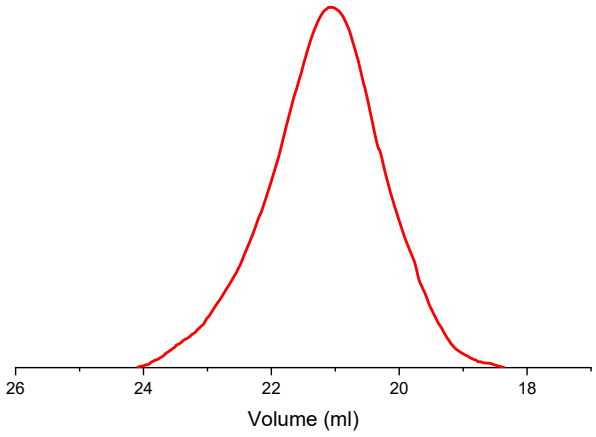

Figure S3.5. GPC trace of sample BB3

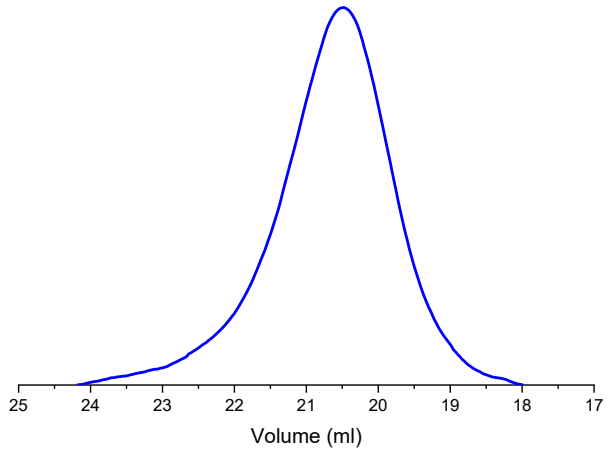

Figure S3.6. GPC trace of sample BB4

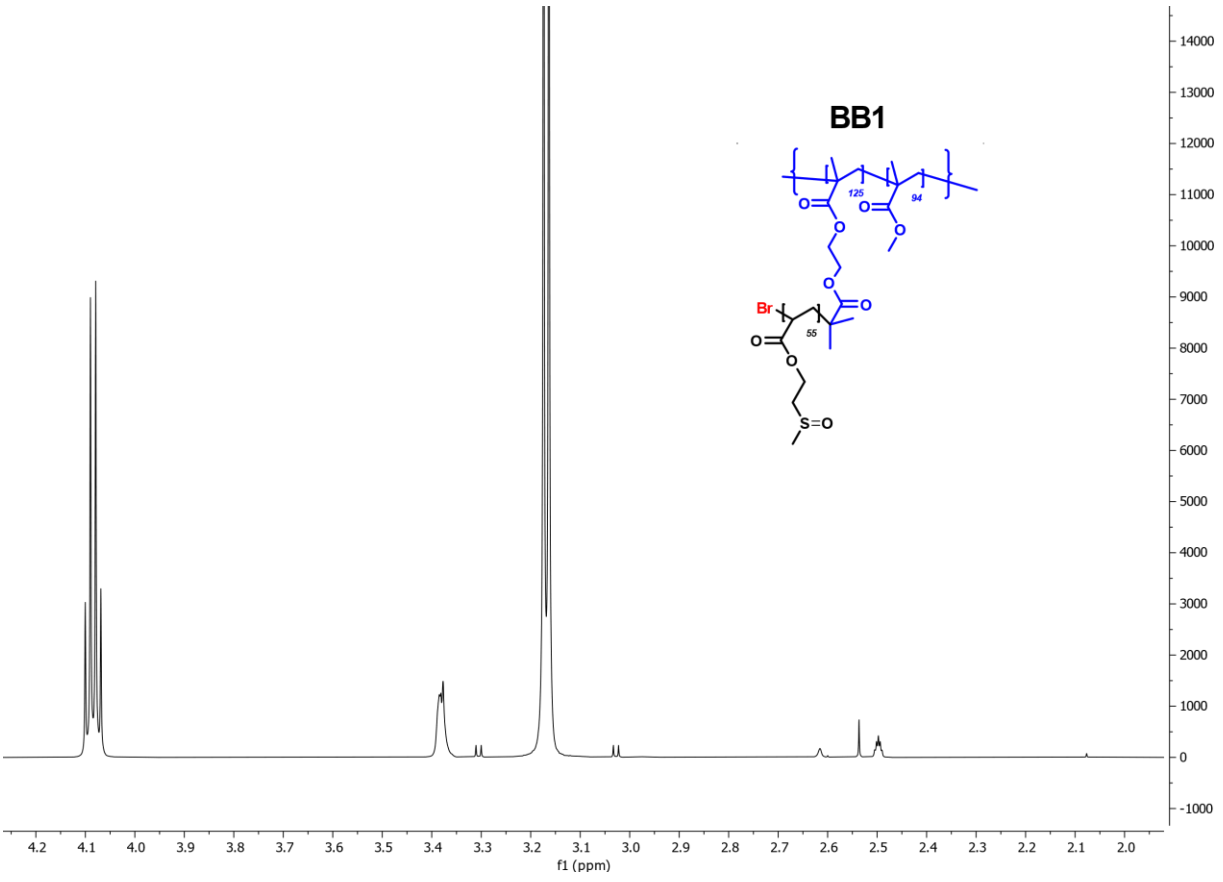

Figure S3.7. ^{1}H NMR spectrum of Sample BB1

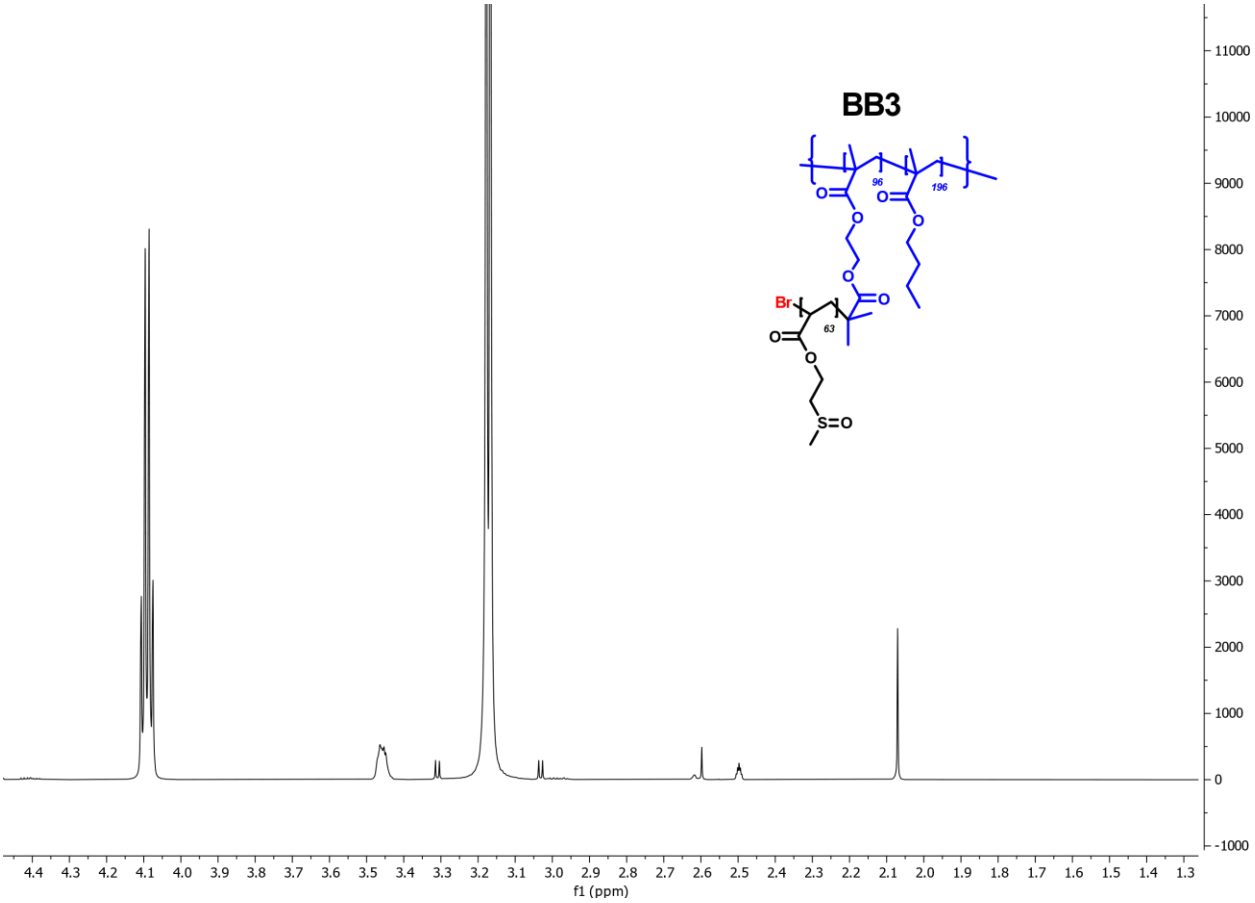

Figure S3. 8. ^{1}H NMR spectrum of Sample BB3

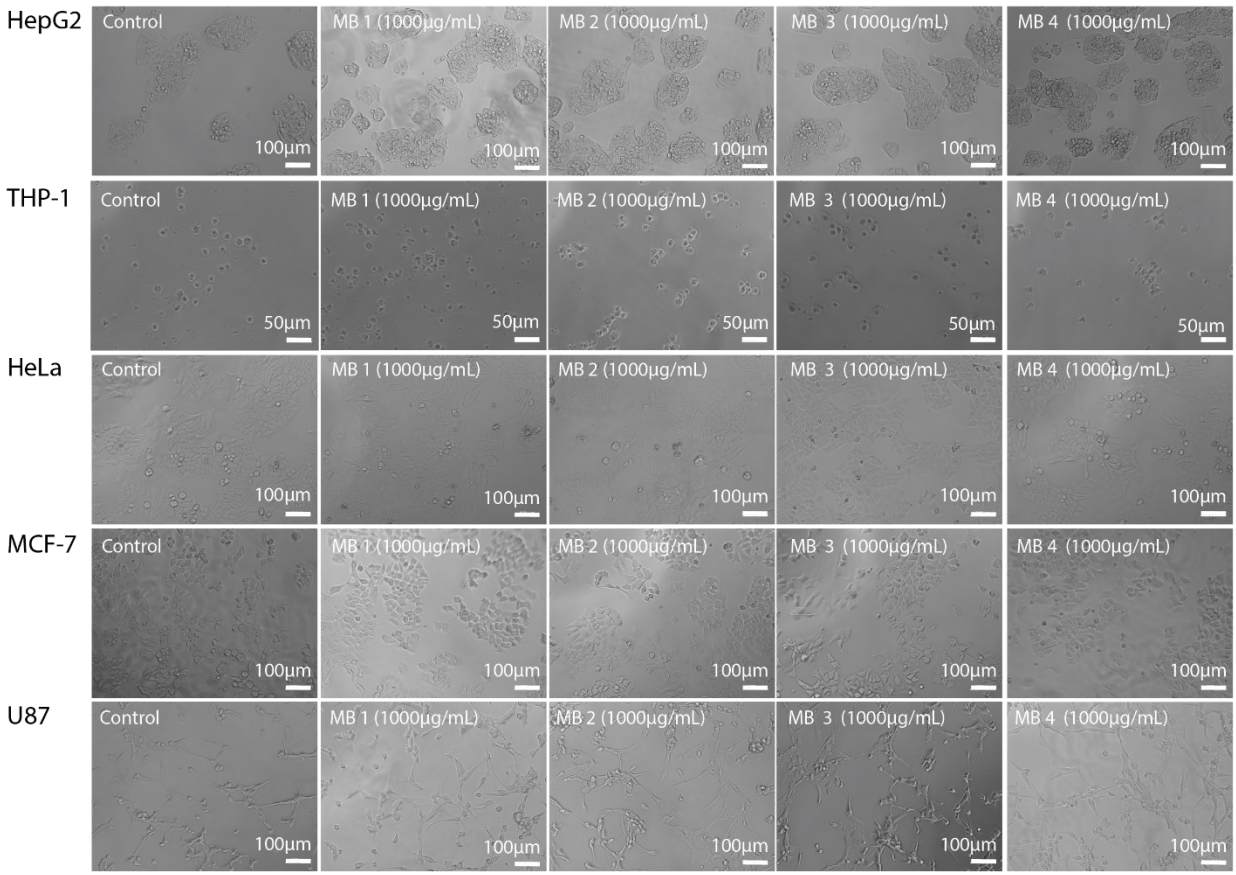

Figure S3.9. Evolution of cell morphology upon exposure to the different MB polymers. Dose concentration is indicated on each photo. Note: THP-1 are non-adherent cells, therefore they appear as much smaller than the other cell lines. Cells were imaged on an AxioObserver microscope (Zeiss) equipped with an AxioCam MRm camera (Zeiss) in Phase contrast mode using 5X, 10X and 20X objectives. Images were acquired and processed with Zen 2.3 (Bleu edition) (Carl Zeiss Microscopy, GmbH, 2011).

Author Information

Corresponding Authors

Krzysztof Matyjaszewski - *Department of Chemistry, Carnegie Mellon University, Pittsburgh, Pennsylvania15213, United States*; Email: km3b@andrew.cmu.edu

Xavier Banquy - *Faculty of Pharmacy, Université de Montréal, Montréal, QuébecH3C 3J7, Canada*; *Department of Chemistry, Faculty of Art and Science, Université de Montréal, Montréal, QuébecH3C 3J7, Canada*; *Institute of Biomedical Engineering, Faculty of Medicine, Université de Montréal, Montréal, QuébecH3C 3J7, Canada*; Email: xavier.banquy@umontreal.ca

Authors

Mateusz Olszewski - *Department of Chemistry, Carnegie Mellon University, Pittsburgh, Pennsylvania15213, United States*

Duy Anh Pham - *Faculty of Pharmacy, Université de Montréal, Montréal, QuébecH3C 3J7, Canada*

Sara González Bolívar - *Faculty of Pharmacy, Université de Montréal, Montréal, QuébecH3C 3J7, Canada*

Jean-Michel Rabanel - *Faculty of Pharmacy, Université de Montréal, Montréal, QuébecH3C 3J7, Canada*

Michael Martinez - *Department of Chemistry, Carnegie Mellon University, Pittsburgh, Pennsylvania15213, United States*

Author Contributions

M.O. and **D.A.P**. contributed equally to this work.

Notes

The authors declare no competing financial interest.

Acknowledgments

Financial support from NSF (DMR 2002747) is acknowledged. X.B. is grateful for the financial support of NSERC (Discovery grant) and the Canada Research Chair program (CRC Tier 2). D.A.P. acknowledges the financial support of the Faculty of Pharmacy at Université de Montréal.

CHAPITRE 4 : DEUXIEME ARTICLE

A triblock bottlebrush polymer mitigates frictional wear of biological and medical surfaces.

Duy Anh Pham [a], Chang-Sheng Wang [a], Hu Zhang [a], Jean-Michel Rabanel [a], Line Séguy [a], Xavier Banquy [ab*]

a: Faculty of Pharmacy, Université de Montréal, Montréal, Québec H3T 1J4, Canada

b: Department of Chemistry, Faculty of Art and Science, Université de Montréal, Montréal, QC, H3C 3J7, Canada

* Corresponding author: xavier.banquy@umontreal.ca

Abstract

In the past decade, polymers with bottlebrush structure (BB) hold promise for moderating friction and wear problems in biomedical field. In this work, we report the tribological properties of a synthesized triblock polymer with the central block having a bottlebrush structure and two grafted lateral parts providing strong adhesion to the surfaces. Contact lens, rat cartilage and rabbit eye have been selected as the model surfaces to investigate the adsorption/desorption, lubrication, and wear resistance of the synthesized polymer. The affinity kinetics of polymer on each surface was monitored using the fluorescent microscopy or a LigandTracer instrument depending on the surface morphology, and it shows that the polymer can adsorb on all substrates in a short time. Surface Force Apparatus (SFA) reveals that the adsorbed polymer layer possesses high performance of lubrication and stays ultra-stable under multiple shear cycles and high compression. Due to the entanglement of BB polymer, tribological properties and biocompatibility

of the synergy between BB and hyaluronic acid (HA) were also evaluated in the cartilage and the ocular surface section.

Keywords: Bottlebrush, bio-lubrication, bio-affinity, bio-interface, osteoarthritis, dry eye, contact lens.

4.1 Introduction

Friction exists in any motion in the universe where an object slides along a surface. It creates a force in the opposite direction of the motion and can damage the interface of the surface in some cases.[111] The friction inside the human body is not an exception, it is created in bone joints like elbow, knee, ankle, shoulder during motion or in the ocular surface where the eye slides along the eyelid during blinking.[2] In the healthy state, the body uses various methods to decrease friction by complex bio-lubrication systems. For example, the synovial fluid between the joints decreases friction and prevents wear of the cartilage.[3] Another example comes from the ocular surface where the lacrimal film plays a critical role in the health of the eyes by its hydration, lubrication and prevention of foreign particles.[112] Malfunction of these bio-lubrication systems cause frictional diseases like osteoarthritis or dry eye. Based on the statistical study, the prevalence of osteoarthritis rose from 247.51 million in 1990 to 527.81 million in 2019,[113] while dry eye in the population varies from 5% to 34% depending on the country and increases linearly with age.[18] One key rule is to find a cure the friction-related disease at an early stage.

Bottlebrush (BB) polymers, inspired by lubricin which is one key component in the synovial fluid, were synthesized and found to have excellent lubricant properties and capacity of protecting different kinds of surface over a long period of time.[65, 72] Generally, BB is composed of a backbone

with covalently attached pendent side chains. BB is characterized by three unique features: a) a large amount of side chains; b) an extended backbone due to steric repulsion (or electrostatic repulsion if any) between the side chains; and c) uniform spatial occupancy due to chain entanglement and the flexible conformation of each molecule.[114] Over the past 10 years, the development of advanced synthetic techniques has enabled increasingly precise control of their various architectural parameters such as the orientation of their backbone and side chains as well as their grafting densities.[60, 114, 115] The versatility in architectural designs provides great flexibility to tune the rheological properties and the lubricant properties, which are promising for coating applications.[59, 62]

In this work, we report the remarkable ability in protecting the tissue interfaces against frictional threats of a triblock BB polymer, which is composed of a flexible MMA backbone decorated with polyzwitterionic branches of poly(2-methacryloyloxyethyl phos-phorylcholine) (pMPC), and 2 adhesive blocks (A) containing a positively charged amine monomer (quaternized2-(dimethylaminoethyl) methacrylate, qDMAEMA) and a hydrophobic (methyl methacrylate, MMA) monomer (i.e. ABA polymeric structure) and its mixture with hyaluronic acid (HA). Rat cartilage, rabbit eyes and contact lenses were used as model surfaces. The intensity and the affinity of adsorption and desorption of ABA molecules onto the surfaces were measured by using a fluorescent microscopy and a LigandTracer, while the friction test was performed using a surface force apparatus (SFA 2000).

4.2 Materials and methods

4.2.1 Materials

Hyaluronic acid (sodium salt) (M_n = 500 kDa) was purchased from Lifecore Biomedical, Inc.. B and ABA polymer were synthesized using atom transfer radical polymerization (ATRP) polymerization method (Scheme SI). All other reagents were purchased from Sigma-Aldrich. PBS was prepared via the procedure of Sigma.[116] Artificial tear fluid (PH 7.4) was formulated according to Geigy formula.[117]

Concerning the surfaces tested, contact lens were purchased from ACUVUE OASYS. Ruby muscovite mica, grade 1, was purchased by S & J Trading Inc. PDMS membranes were prepared by mixing the elastomer with the curing agent with the ratio 10:1 via the PDMS protocol.[118] Rabbits raised without fertility and growth hormones were purchased from a local butcher Fernando (Montreal, Quebec). Eight-week-old male Lewis rats were purchased from Charles River Canada (Saint-Constant, Quebec) and housed under standard conditions. All procedures were conformed to the Canadian Council on Animal Care guidelines.[119]

Osteoarthritis was surgically induced in male rats by transection of the right anterior cruciate ligament. Rabbit eyes were collected from the rabbits raised without fertility and growth hormones which were purchased from a local butchery. Dry condition was induced in rabbit eyes by exposing them under the hood in 1h after gluing them into the support.

4.2.2 Polymer solution preparation

B, ABA and HA solutions were prepared by dissolving them into Milli-Q water at a stirring speed of ~300 rpm using a magnetic bar for at least 12 h at room temperature (**Figure S4.1**). During

stirring, the glass container was sealed with an air-tight film to minimize water evaporation. The mixed solutions were prepared by mixing the desired solutions at a volume ratio of 1 to 1 and then stirred for 1 h.

4.2.3 Surface force apparatus

The friction force, *F*, was measured using Surface Force Apparatus (SFA 2000, SurForce LLC, United States) equipped with a bimorph slider. At the same time, the normal force, *L*, was monitored via a high-resolution sensor and controlled using the motor of SFA, as shown in **Scheme 4.1**.

For tribological measurements of mica surfaces, the freshly cleaved back-silvered mica surfaces were glued (epoxy glue Epon 1004F) on glass cylindrical disks with a curvature, *R*, of 2 cm under a laminar flow hood. The disks were then mounted in the SFA chamber in a cross cylindrical configuration. 100 μL/mL of polymer solution was injected between the surfaces and left for adsorption for 1 h before frictional experimentation.

For tribological measurements of contact lens and corneas, supports having a similar curvature of the lens and eyes were designated using the software Autodesk Inventor Professional and printed by a 3D printer (Formlabs Form 3+). Prior to each experiment, contact lens or cornea was glued to its support and then immersed in the polymer solution at a concentration of 100 μg/ml. After coated with the polymers, the surfaces were mounted in SFA where they are sheared against the flat glass disc (in the case of the lens) or a PDMS membrane mimicking the eyelids (in the case of the eye) under different loads, *L* (**Scheme 4.1**).

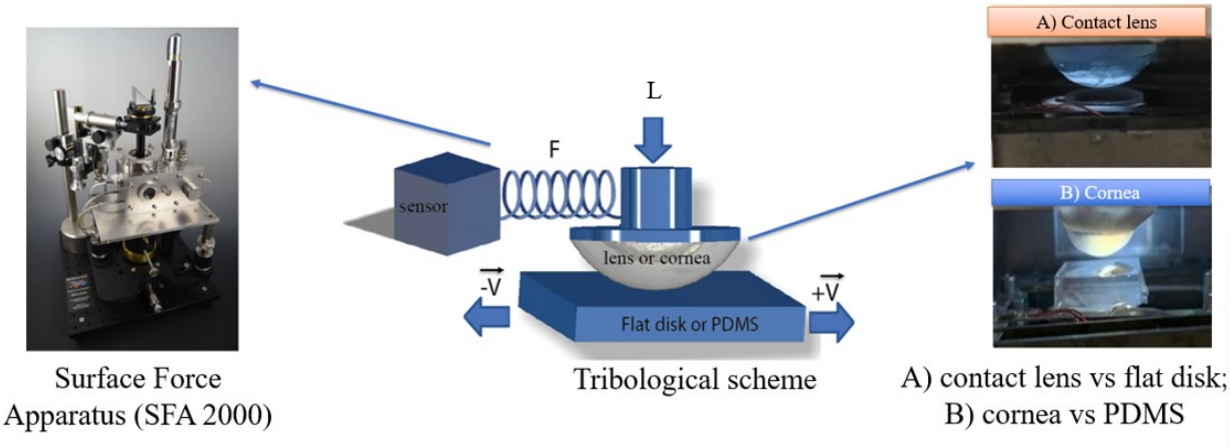

Scheme 4.1. Scheme of surface configuration in SFA A) contact lens and clean flat glass disc; B) cornea and PDMS membrane mimicking the eyelid. *SFA 2000 image was obtained via https://surforcellc.com/surface-forces-apparatus-techniques-measuring-surface-forces/.*

4.2.4 Atomic force microscopy

AFM imaging was performed on a Nanoscope V Dimension Icon/Fastscan AFM (Bruker, USA) in PeakForce Tapping mode in air. Scanasyst-air silicon tips (on nitride cantilever) with a resonance frequency of 50-90 kHz and a spring constant of ~0.4 N/m were used. Aliquots of BB polymer solutions were diluted with pure water at a concentration of 25 µg/mL and deposited on freshly cleaved mica. After one hour of adsorption, the remnant polymer solution was gently removed, and the surface was carefully rinsed with MiliQ water. The contour length of the BB polymer was obtained by analyzing AFM images using the Nanoscope analysis program.

4.2.5 LigandTracer

The real-time affinity of polymer on the cornea and the antifouling properties of polymer layer on the contact lens were measured with LigandTracer Green (Ridgeview Instruments AB). In brief, a

petri-dish with a local area glued with cornea or contact lens and a reference area is placed on an inclined and rotating support. 3 mL PBS solution was added to the petri dish and a Red-NIR detector (excitation/emission: 632-671 nm) is mounted above the upper part of the dish to monitor the change in the fluorescent intensity on the target surfaces. A baseline was recorded by collecting the signals from target surfaces and reference area every 30s during each rotation. Then, Cy5-labelled polymer solution was added to obtain the adsorption curve. Finally, the incubation solution was replaced by PBS to record the dissociation of the polymer. The data was analyzed, and the affinity constants were deducted from a corresponding model in TraceDrawer 1.9.2 (Ridgeview Instruments).

4.2.6 Fluorescent microscopy

A ZIESS ApoTome.2 fluorescence microscope was used to measure the intensity of polymer adsorbing to the contact lens. This involved monitoring the fluorescence evolution of the concentration of the Cy5-polymer on the lens surface for adsorption-desorption kinetics studies. Results are analyzed with Ziess ZEN software and processed with ImageJ. The laser excitation wavelength was 651nm. Different than LigandTracer procedure, the lens didn't need to be glued to a surface, so its shape can be kept unchanged during the experiment. The protocol and the equations used to convert the fluorescent intensity to the quantity of polymers adsorbed onto the lens surface are presented in **SI** accompanied by 2 image examples in **Figure S4.3**.

4.2.7 Cell viability (synoviocytes, chondrocytes, osteoblasts)

Synoviocytes, chondrocytes and osteoblasts viability were evaluated by 3-(4,5-dimethyl-thiazoyl)-2,5-diphenyl-SH-tetrazolium bromide (MTT) assay in 96-well plates (Fisher Scientific Company).

After being pre-treated with BB solution for 24 hours, the cells were incubated in the solution containing 0.5 mg/ml MTT reagent (Sigma-Aldrich) for 15 min at 378C. Then, 100 ml of solubilization solution (0.04 M HCl–isopropanol) was added, and the absorbance was read at 570 nm with the micro-ELISA Vmax photometer (Bio-Tek Instruments).

2.8 Matrix metalloproteinases (MMP3 and MMP13) progression

MMP-3 and MMP-13 levels of chondrocytes pre-treated with BB solution were assessed by using enzyme immunoassay (Cayman Chemical) and enzyme-linked immunosorbent assay (ELISA) kits (R&D Systems, Minneapolis), respectively. All assays were performed in duplicate, and the absorbance was measured with a micro-ELISA Vmax photometer (Bio-Tek Instruments).

4.2.8 Compressive modulus study

An automated 3-dimensional mapping mechanical tester (March-1 v500css, Biomomentum) was used to study the compressive modulus of arthritis cartilages treated by PBS, HA and ABA-HA, and healthy cartilages were used as control surfaces. When moving to a predefined coordination on the cartilage interface, the tester detected the height and orientation of the surface and simultaneously recorded the normal force loading to the indenter. The instantaneous modulus at each position in cartilage region was then obtained by fitting the load-displacement curve (with corresponding thickness) to an elastic model in indentation.[120]

4.2.9 Rheological study

Rheological measurements of BB solutions were realized by using TA Instruments AR2000 stress-controlled rheometer (USA). A cone plate (d = 40 mm, angle = 2°) was used for all experiments.

During the experiment, strain sweep measurements were conducted at a constant frequency (f = 1 Hz) at 37 °C. Mineral oil was used to prevent the dehydration of the solution. Each test was replicated three times.

4.3 Results and discussions

4.3.1 Morphology study

Figure 4.1 shows the chemical structures (left) and the morphology (right) of B and ABA. Both polymers clearly exhibit the characteristic of brush structure where the side chains cover all the backbone of each molecule. Image analysis reveals that B has a contour length of 121.6 ± 9.6 nm and ABA is 126.5 ± 8.8 nm, whereas the average width of 'B' is 74.7 ± 5.8 nm and for the triblock polymer 'ABA' is 85.1 ± 6.4 nm. This is as expected because the only difference between the two polymers lies in the small terminal blocks.

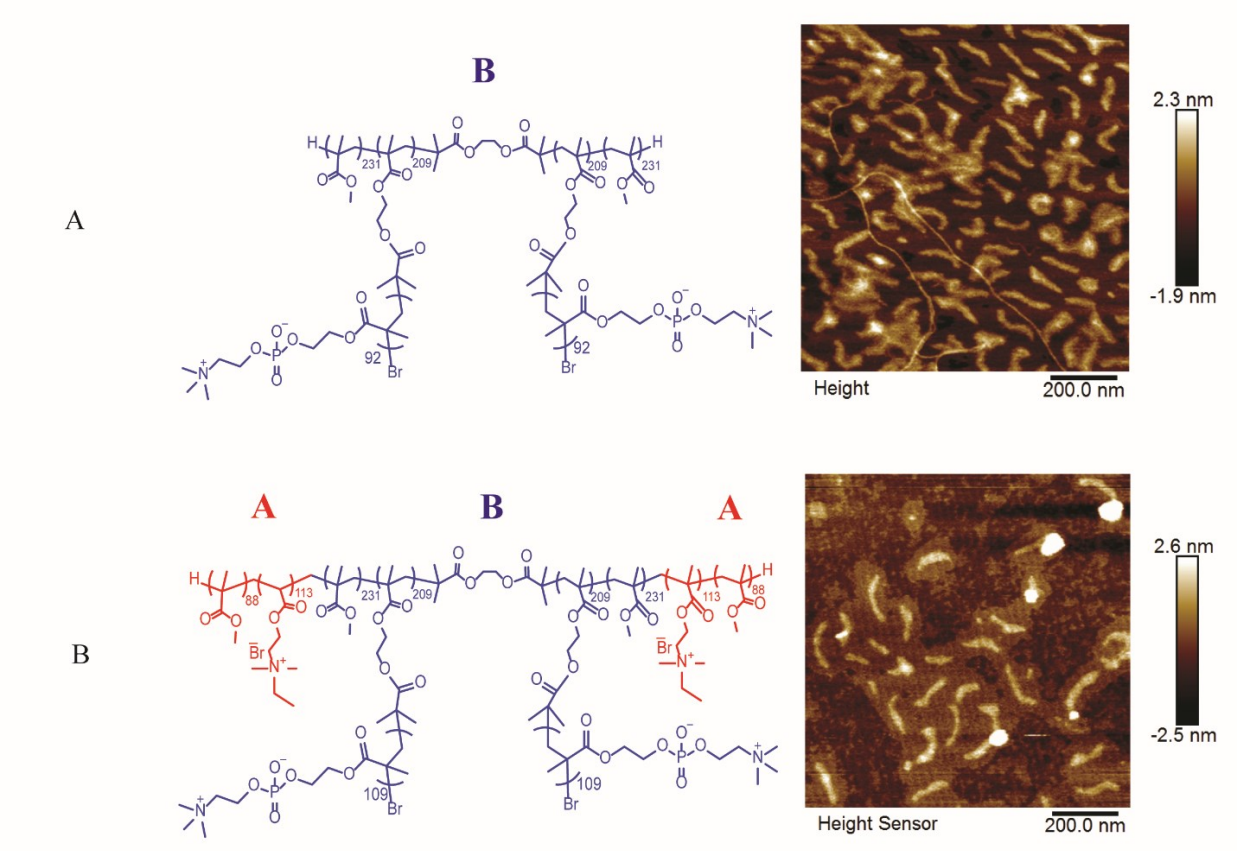

Figure 4.1. Chemical structure and morphology characterized by AFM (for a 1 μm square grid) of: A) monoblock bottlebrush 'B'; B) triblock bottlebrush 'ABA'.

4.3.2 Lubrication capacity on cartilage surfaces

The viscoelastic behaviors of the solutions containing HA and ABA at the concentration of 1.5 mg/mL are shown in **Figure 4.2A**. ABA has slightly wider viscoelastic regimes compared to HA, and G' is above G" for all the sample solutions, exhibiting solid-like behavior. At strain values beyond the linear viscoelastic regime, both G' and G" decrease due to the break of the transient network structure. At a critical strain value, G' becomes smaller than G", displaying a liquid-like behavior. The liquid-like behavior at large strains indicates that the BB polymers can be injected in-between the cartilages.

Injecting ABA into synovial fluid may lead to the complexation between ABA and HA via electrostatic attraction. Low cell toxicity is a precondition for in vivo applications. Therefore, we evaluated cell toxicity of HA, ABA and the mixture thereof (ABA-HA) using three cell lines that are related to cartilage lubrication [121, 122] and bone regeneration [123-125] including fibroblast-like synoviocytes , chondrocytes and osteoblasts. The results are shown in **Figure 4.2B-D**. As expected, HA does not show any cell toxicity and it even promotes the proliferation of synoviocytes cells. ABA exhibits slight toxicity against the synoviocytes cells (causes ~5% dead cells), but it promotes the reproduction of the other two cell lines slightly. The mixture combines all the advantages in one, that is to say, it decreases the cell toxicity of ABA against synoviocytes cells but keeps the friendliness to the other cells. Overall, ABA exhibits good biocompatibilities for all the three cell lines, and the biocompatibility can be enhanced in the presence of HA.

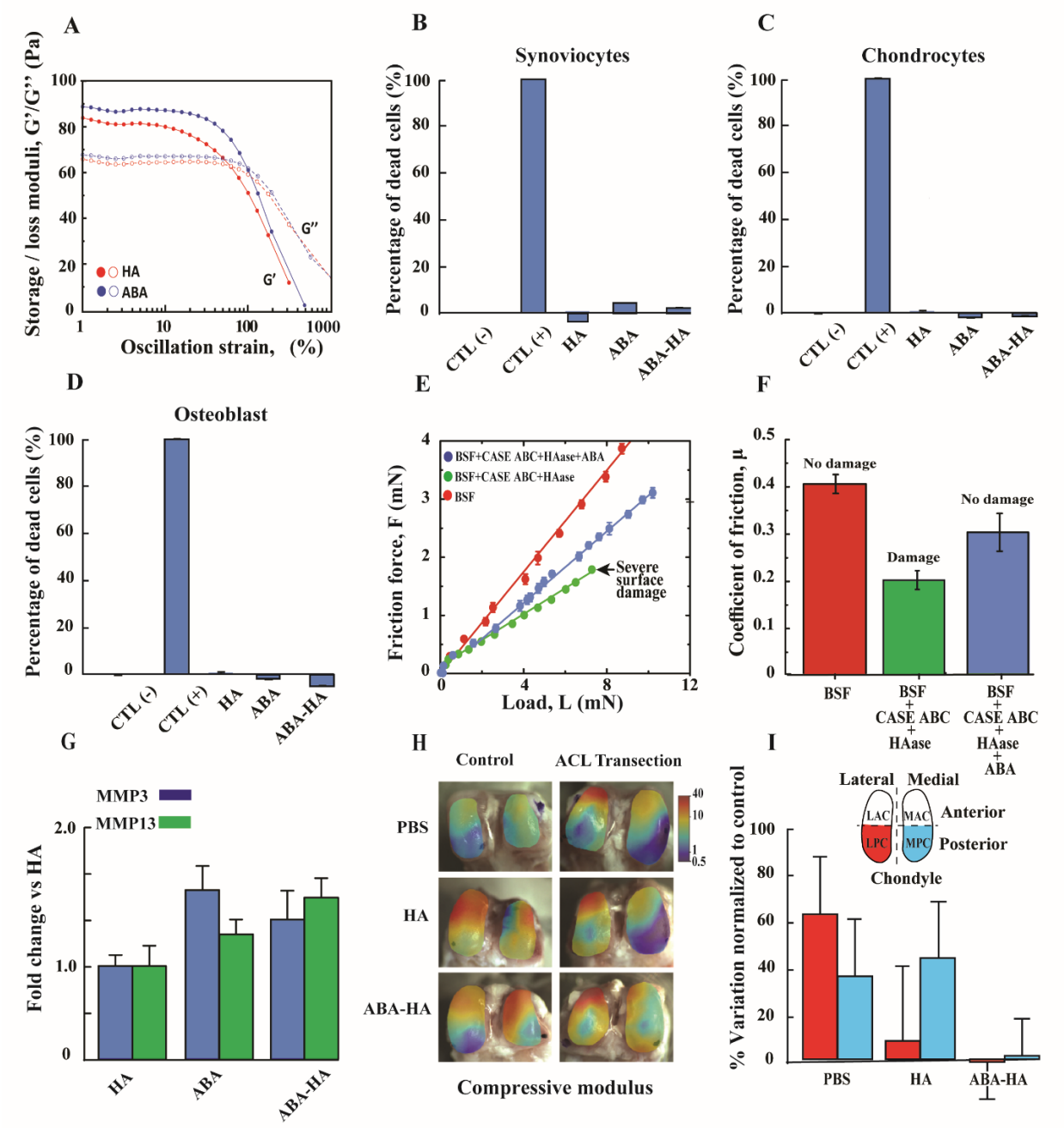

Figure 4.2. Impacts of BB (1.5%, w/v) and HA (1.5%, w/v) solutions on the cartilages: A) Rheology properties of the samples; Percentage of dead cells of : B) Synoviocytes; C) Chondrocytes; D) Osteoblast. ; E) Evolution of friction force with applied load on mica surfaces; F) Comparison of friction coefficient; G) Fold change of MMP3 and MMP13 on ABA and ABA-

HA vs HA; H) Instantaneous compression modulus profile on the cartilage between PBS, HA and ABA-HA; I) Proportion of compression modulus on the cartilages after ACL transection varied by PBS, HA and ABA-HA.

Chondroitinase ABC (case-ABC) is an enzyme used together with glucosamine to treat osteoarthritis (OA) in recent years. [126, 127] On mica surface, the enzyme can decrease the friction coefficient of BSF (bovine synovial fluid) by two-fold, as shown in **Figure 4.2E**. However, the surfaces are severely damaged at a load of 8 mN. Adding ABA to this treating formulation maintains the low friction coefficient and can well protect the surfaces from being damaged (**Figure 4.2E-F**).

In order to ensure the safety on the cartilage, it is also important to check the expression of matrix metalloproteinases (MMPs), which is closely related to the cell behaviors such as cell proliferation, migration, and differentiation, etc. [128] Overproduction of some MMPs can lead to the imbalance of cartilage matrix turnover, which then causes cartilage degradation [129-131]. For example, multiple studies revealed that MMP3 upregulates very early in degeneration process, [132] whereas MMP13 is one of the key factors in the pathology of OA due to its ability to cleave interstitial fibrillar collagens. [133] It was found that MMP3 expression was increased 1.5-fold in ABA and 1.3-fold in ABA-HA, while MMP-13 expression was increased 1.2-fold in ABA and 1.4-fold in ABA-HA (**Figure 4.2G**). The slight increase ensures the safe injection of ABA solution on the cartilages.

Anterior cruciate ligament (ACL) transection, a well-established surgical model of OA,[134, 135] was used here to evaluate the compressive modulus profiles to show the treatment effectiveness of ABA-HA (**Figure 4.2H**). For healthy cartilages, the results show that the presence of HA and ABA-HA leads to an overall increase in the compressive modulus compared to PBS. As for the ACL transection cartilages, a big blue region where the compressive modulus was decreased

heavily appeared in both cases of PBS and HA, it presents the risk of cartilage breaking under high load. In contrast, after being treated by ABA-HA, the arthritis cartilage has almost the same stiffness as the healthy cartilage. The stability of cartilages treated by ABA-HA is also demonstrated in **Figure 4.2G** where the variation in cartilage stiffness is shown from anterior to posterior region after ACL transection. In detail, in lateral compartment, the variation is about 62 % for PBS, 7 % for HA, and 2 % for ABA-HA treatment. In medial compartment, the variation is about 37 % for PBS, 42 % for HA, and 2 % for ABA-HA treatment.

In osteoarthritis, the deficiency of the lubrication capacity of the synovial fluid leads to degradation, degeneration, and finally destruction of the cartilages of the joints [5, 9]. Having a low toxicity on cartilage and synovial fluid, ABA-HA injection is promising in osteoarthritis treatment when providing lubrication and stiffness stability to the cartilage surface.

4.3.3 Lubrication capacity on the ocular surface (cornea)

The real time adsorption and desorption of B, ABA, B-HA and ABA-HA on the ocular surface (cornea) was shown in **Figure 4.3A**. The fluorescent intensity increases steeply in the first 30 min followed by a slower continuous process at each concentration. When replacing the polymer solution with PBS, a fast desorption was observed, with the fluorescent intensity decreasing ~40-50 % in the first 30 min. The adsorption-desorption curve was then fitted to 1:1 or 1:2 interaction model **(Figure S4.2)**. The strong deviation of 1:1 model from the experimental data indicates that the interaction was not adequately described by a 1:1 binding process. In comparison, the 1:2 interaction model can well describe the experimental data, which indicates that there are two interaction populations that differ in their binding stability, possibly related to hydrogen bonding and electrostatic forces. [136] The association rate constants K_a and dissociation rate constants K_d can

be obtained, and the results are displayed in **Figure 4.3B**. No significant difference is observed among difference samples.

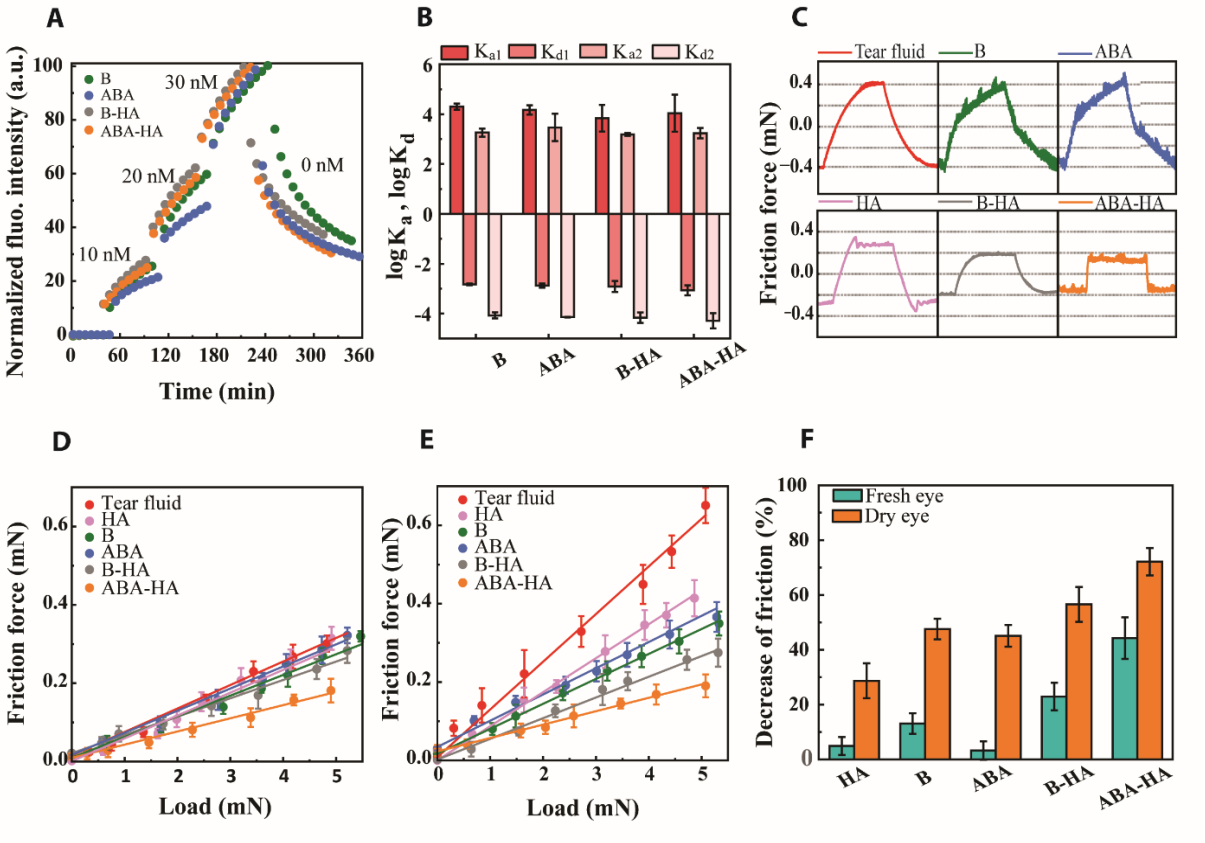

Figure 4.3. Impact of BB (0.1%, w,v) and HA (1%, w/v) solutions on the ocular surface (cornea) **:** A) Adsorption/ Desorption of the polymers on the cornea; B) Affinity kinetic of the polymers on the cornea; C) Friction signals of dry corneas coated with different polymers during tribological experiments; D) Evolution of friction force with applied load for the fresh cornea; E) Evolution of friction force with applied load for the dry cornea; Decrease of friction of the cornea coated by the polymers comparing to the neat cornea in tear fluid.

HA is known to play an important role in eye hydration and lubrication.[140, 141] Without HA (i.e. B and ABA), the friction trace of cornea exhibits a stick-slip pattern, where the kinetic one increases

as a function of time between the surface (**Figure 4.3C**). In fact, the shape of a friction curve is affected not only by the shear force but also by the adhesion and the deformation of the surface.[142] By comparison, a steady state can be reached for all the samples containing HA. It appears to indicate that HA allows the cornea to slide smoothly with a constant kinetic friction force after exceeding static friction. The steady state is reached almost immediately when reversing the siding direction using ABA-HA as a lubricant. The friction force increases linearly with the normal load for both fresh and dry eyes (**Figure 4.3D-E**). The friction curves pass through 0, an indication of the negligible contribution from adhesion.[143] For fresh eyes, all the formulations provide similar friction coefficient, except for ABA-HA, which shows slight better lubricant properties. In comparison, the friction coefficient of dry eyes is ~1.5 times higher than the fresh ones. The formulations reduce the friction more efficiently for the abnormal corneal surfaces, as indicated by **Figure 4.3F**. ABA-HA is the most promising formulation for treating friction-related eye diseases when providing the lowest coefficient of friction in both states of eye.

Dry eye is a condition in which the patient doesn't have enough quality tears to lubricate and protect the eye, leading to the irritation, the inflammation or the bacterial infection of the ocular surface.[13, 14] Adsorbing to the cornea via electrostatic and hydrogen bonding forces, ABA-HA formulation provides an insight into the dry eye treatment after demonstrating its ability to regenerate hydration and lubrication on the corneal surface.

4.3.4 Lubrication capacity on contact lens

Like the cornea study, we also checked the adsorption and desorption of polymer molecules on the contact lens, as shown in **Figure 4.4A**. Similar adsorption-desorption curve was observed for B and ABA. A plateau appears after an adsorption time of ~90 min, indicating that an equilibrium is reached between the adsorption and desorption processes. In the desorption phase, the fluorescent

intensity decreases by 60-70% and remains almost unchanged after 90 min. ABA has slightly higher adsorption rate and less tendency to detach from the surface compared to B, probably due to the terminal adhesive blocks.

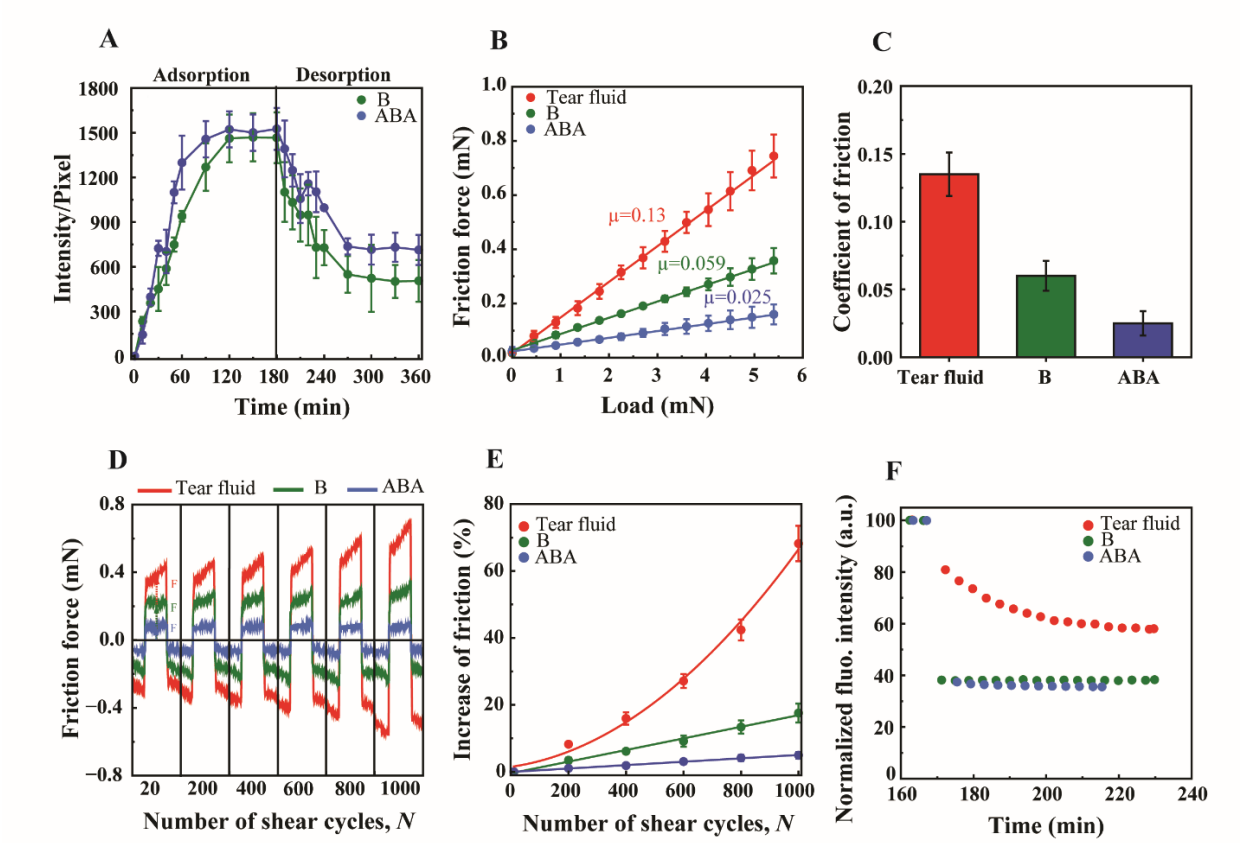

Figure 4.4. Impacts of BB solution (0.1%, w/v) on the contact lens **:** A) Adsorption/Desorption of the polymers on contact lens; B) Evolution of friction force with applied load for the contact lens with and without polymers; C) Comparison of friction coefficient of the contact lens; D) Friction force signals of the contact lens after N shear cycles; E) Evolution of friction force of the contact lens with the number of shear cycles N; F) Percentage of rhodamine quantity washed out from the contact lens over time.

The friction force also increases linearly with the applied load for all the tested samples, as shown in **Figure 4.4B**. The friction coefficient decreases upon adding the BB polymers to the artificial

tear solutions, with $\mu = 0.059$ for B and $\mu = 0.025$ for ABA. This different performance in lubricant properties is from the terminal groups, which are expected to induce different conformations on surface. Beside the lubrication, the stability of the polymeric layer under repeated shearing becomes important, as humans blink their eyes around 15,000 times a day.[144] Considering the limit of the equipment, we performed 1,000 shear cycles to check the evolution of the friction of contact lens in tear solutions with and without polymer under a load of 3 mN (**Figure 4.4D**). In general, the friction force increases with the number of shear cycles, and the increase is up to ~80 % after 1000 shear cycles in BB polymer free tear solutions (**Figure 4.4E**). In comparison, the increase becomes much less pronounced in the presence of BB polymers, with only ~10 % for B and ~5 % for ABA, highlighting the role of BB polymer in improving the lubricant properties. Besides, the time to reach a steady state is also greatly reduced in the presence of BB polymers.

Protein adsorption on the contact lens may lead to bacterial adhesion and then reduce the optical quality and oxygen permeability.[145, 146] It would be important to check the anti-fouling properties of BB polymer coated contact lens. The results show that the two BB polymer can reduce the protein adsorption (40% vs 60% in BB polymer free case), as shown in **Figure 4.4F**. This is probably because of the hydrated phosphorylcholine groups, which are known to have excellent anti-fouling properties.[147, 148]

Wearing contact lens for long period of time can cause dry eye, in severe conditions it can decrease the entire corneal thickness or increase the chance of bacterial infection.[16, 149] In this section, we demonstrated that immersing contact lens in BB solution can enhance its lubrication and prevent bacterial infection from the environment.

4.4 Conclusion

Affinity studies demonstrated that BB polymers can quickly adsorb on different bio-surfaces via hydrogen bonds and electrostatic interactions. When absorbing onto the surface, BB polymers form a protective layer that lubricate it and reduce the infection risks. In this paper, the triblock BB polymer ABA have proven its intense lubrication when applied in the cartilage, the eye, and the contact lens. In particular, the tribological properties and the biocompatibility of ABA can be enhanced in the presence of HA. Having high performance in lubrication and good interaction with HA, ABA polymer is promising to be used as a principal element for the new treatment relating to the deficiency of bio-lubricant system.

4.5 Supporting information

4.5.1. Materials for BB polymer synthesis

All compounds were bought from sigma-Aldrich unless otherwise stated. Methyl methacrylate (MMA), 2-(trimethylsilyloxy)ethyl methacrylate (HEMA-TMS) and 2-(dimethylamino)ethyl methacrylate (DMAEMA) were purified by passing through a short basic Al_2O_3 column. 2-Methacryloyloxyethyl phosphorylcholine (MPC) was recrystallized from acetonitrile and dried under vacuum.. Copper(I) bromide (CuIBr, 99.999%), copper(II) bromide (CuIIBr2, 99.999%), 4,4′Dinonyl-2,2′-dipyridyl (dNbpy, 97%), Tris(2-pyridylmethyl)amine (TPMA), tributyltin hydride (97%), potassium fluoride (KF, 99%), tetrabutylammonium fluoride (TBAF, 1M solution in THF), α-bromoisobutyryl bromide (98%), bromoethane (98%), copper(I) chloride (CuICl, ≥99.995% trace metals basis), copper(II) chloride (CuIICl2, ≥99.995% trace metals basis, anhydrous), 2,2′-bipyridyl (bpy, 99%), and were used without any additional purification.

Ethylene bis(2-bromoisobutyrate) (diBr) were synthesized according to previously published procedures.[150, 151]

4.5.2. BB polymer synthesis strategy

The Synthesis of ABA-bottle brush polymer was followed by references with some modifications.[62, 65, 70] The modified synthesis procedure was described.

a) Synthesis of poly[(HEMA-TMS)400-stat-PMMA400) (B block copolymer)

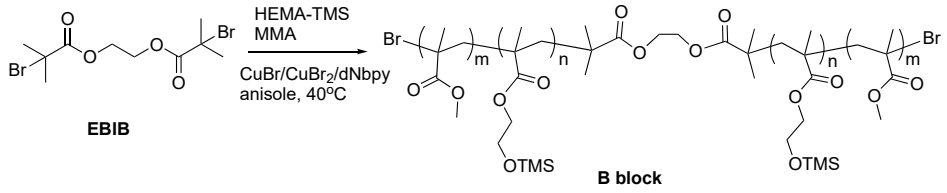

Scheme S4.1. Synthesis procedure of B block copolymer

A dry 25 mL Schlenk flask was charged with EBIB (8.2 mg), CuIIBr2 (6.1 mg), dNbpy (134 mg), HEMA-TMS (9.28g, 10 mL), MMA (4.59 g, 4.8 mL) and anisole (3.0 mL). The solution was degassed by three freeze-thaw cycles. During the final cycle, the flask was filled with nitrogen and CuBr (15.8 mg) was quickly added to the frozen reaction mixture. The flask was sealed, evacuated and backfilled with nitrogen five times, and then immersed in an oil bath at 40 °C. Reaction was stopped after 5h 30 min. via exposure to air. An aliquot was taken for recording the NMR. The monomers conversion ratio was calculated by the integration of MMA and HEMA-TMS vinyl groups signal (*CHH*=C-CH3, 6.11 ppm or 5.56 ppm) against the hydrogen of the backbone (-CH2-C(*CH3*)-, 0.75-1.0 ppm). The polymer was purified by precipitating the solution into cold methanol twice (cooled with dry ice and isopropanol). The

product was redissolved in $CHCl_3$ and passed through a short natural Al_2O_3 column. After evaporating most of the solvent, the concentrated polymer solution was precipitated into cold methanol again to get the final product. The conversion ratio was 21.5% calculated from the integral of NMR peaks meaning the m=231 and n=209.

b) Synthesis of poly[(DMAEMA-stat-MMA)-b-(HEMA-TMS-stat-MMA)-b- (DMAEMA-stat-MMA)] (ABA block copolymer first stage)

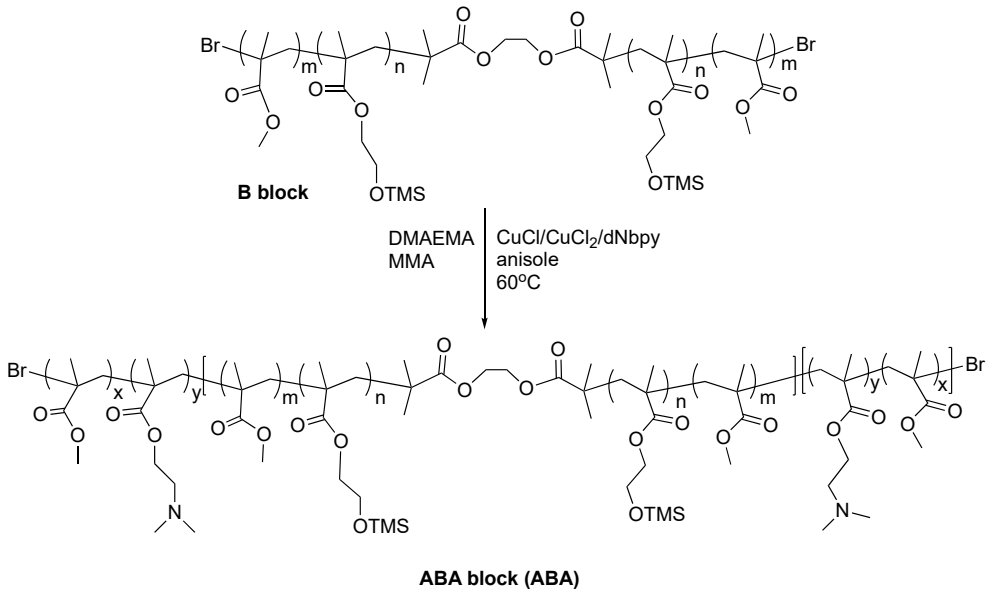

Scheme S4.2. Synthesis procedure of the first stage of ABA block copolymer

A dry 25 mL flask was charged with B block copolymer (1.1 g, 0.0084 mmol). 4.0 mL anisole was added into the flask and stirred overnight to make sure the B block was completely dissolved. CuCl2 (0.56 mg, 4.2 μmol), dNbpy (0.0343 g, 0.084 mmol), DMAEMA (2.10 g, 2.26 mL, 13.4 mmol), MMA (1.34 g, 1.42 mL, 13.4 mmol) were then added into the flask. The solution was degassed by three freeze-pump-thaw cycles. During the final cycle, the flask was filled with nitrogen and opened; CuCl (0.0033 g, 0.0336 mmol) was quickly added to the frozen reaction mixture. The flask was re-sealed, evacuated and back-filled with nitrogen three times,

and then immersed in an oil bath at 60 °C. Reaction was stopped after 28 h. via exposure to air. An aliquot was taken for NMR to check the conversion ratio before purifying the polymer. The product was precipitated from cold hexanes three times, re-dissolved in chloroform and passed through neutral alumina. The solvent was removed, and the purified product was dried overnight under vacuum at room temperature. The conversion ratio was 14.7 % calculated from the integral of NMR peaks, meaning x is 88 and y is 113.

c) Removal of the end bromide of ABA block copolymer (ABA-H).

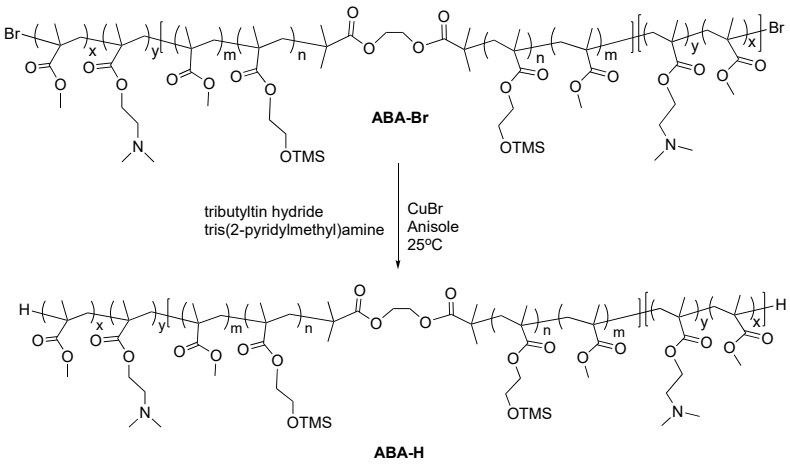

Scheme S4.3. Procedure of removal of the end bromide of ABA block copolymer, leads to ABA-H

The polymer ABA-Br (1.35 g, 0.0073 mmol), tributyltin hydride (0.043g, 0.146 mmol, 0.039 mL), tris(2-pyridylmethyl)amine (0.010 g, 0.0352 mmol), and anisole (8.0 mL) were placed in a 25 ml Schlenk flask. The reaction mixture was deoxygenated by two freeze–pump–thaw cycles. During the last cycle CuBr (0.0025 g, 0.0176mmol) was added to the frozen mixture. The flask was sealed, evacuated and back-filled with argon. The reaction mixture was thawed

and stirred at 25 ºC for 24 h. The polymer was purified by dialysis against THF:MeOH (2:1) then acetone for 48 h using tubes with a pore size molar mass cut off 50,000 kDa. The polymer is then dried under vacumn.

d) Quaternization of ABA-H copolymer (qABA)

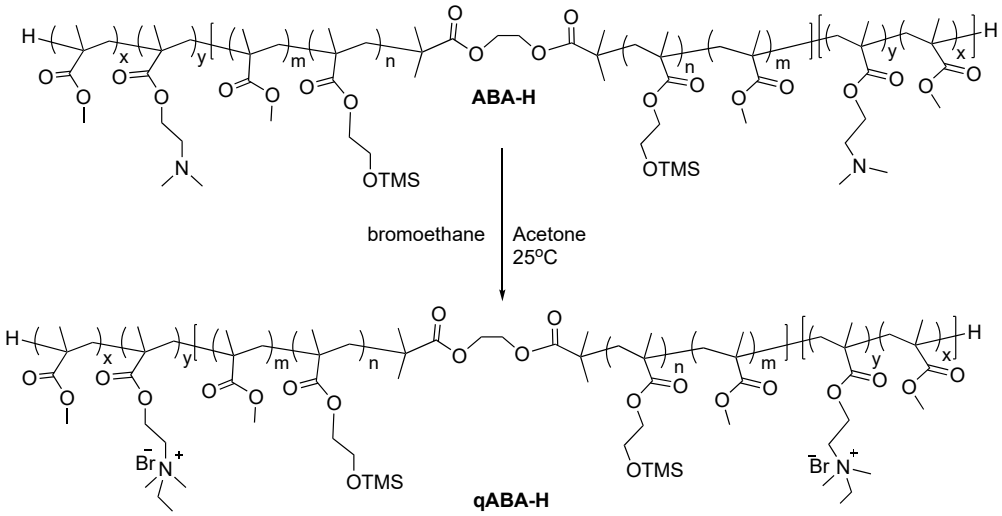

Scheme S4.4. Quaternization of ABA-H copolymer

0.19 g of ABA-H polymer was taken into a 25 mL bottom round flask. 9 mL acetone was added into this flask to dissolve the polymer. The solution was cooled in an ice bath to 0 °C. 0.17 mL bromoethane (0.254 g, 2.3 mmol) was firstly diluted in 1 mL acetone and then added slowly into the polymer solution. The reaction was stirred at 25ºC for the next 48 h. The solvent was removed, and the product was dried under vacuum at room temperature and directly used in the next step without further purification.

e) Deprotection of the TMS group and synthesis of the macro-initiator (qABA-Br)

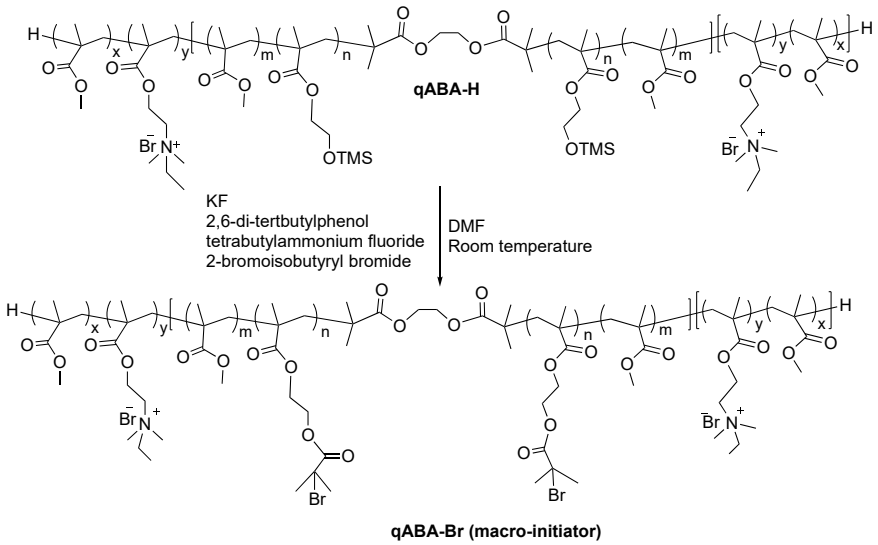

Scheme S4.5. Synthesis of the macro-initiator for ABA (qABA-Br)

The qABA-H polymer (0.25g)， potassium fluoride (0.087g) and 2,6-di-tertbutylphenol (0.025 g) were placed in a 25 mL round bottom flask. The flask was sealed, flushed with argon, and anhydrous DMF (8 mL) was added. The mixture was cooled in an ice bath to 0 oC, tetrabutylammonium fluoride solution in THF (1M, 1.2 mL,) was added to the flask, followed by the drop-wise addition of 2-bromoisobutyryl bromide (0.35 g, 0.19 mL,). After the addition, the reaction mixture was allowed to reach room temperature and stirring was continued for 24 h. The solids were filtered off, and the solution was dialyzed with methanol and acetone and dried under vacuum.

f) Synthesis of qABA-gMPC bottle brush polymer

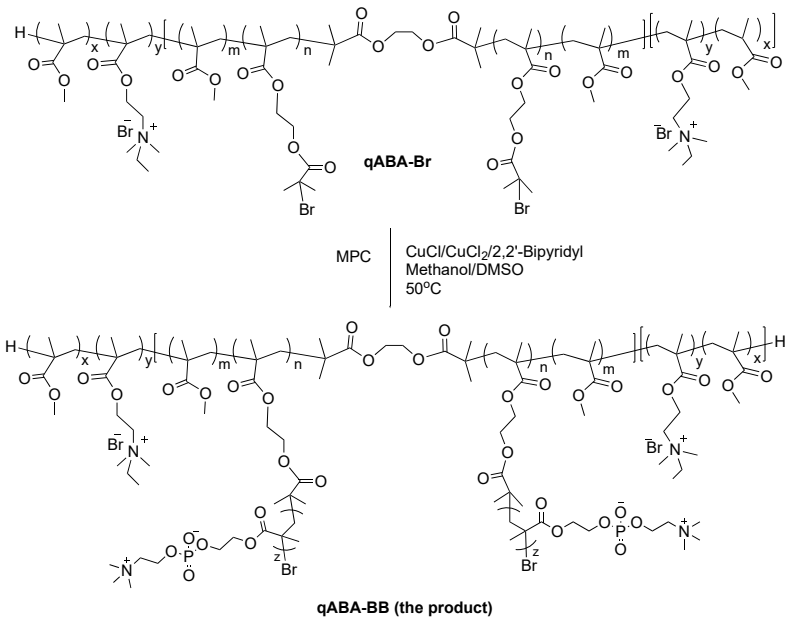

Scheme S4.6. Synthesis procedure of the final stage of ABA block copolymer

A dry 5 mL bottom round flask was charged with CuCl2 (0.12 mg), CuCl (0.64 mg) and 2,2′-Bipyridyl (2.54 mg). The flask was sealed with stopper and black tape. In the meantime, qABA-Br macroinititor (2.5 mg) was first dissolved in DMSO (0.5 mL) (non-anhydrous) under stirring for 30 min in a separated vial. Then, MPC (256 mg) and methanol (0.8 mL) was added into this vial. A stainless steel cannulas was used to connect the flask the vial. Then the solution (in the vial) was degassed by four freeze-pump-thaw cycles. During the final cycle, the flask was thaw to room temperature filled with nitrogen. The whole system was turned to vacuum for a few second then the cannula was inserted into the solution. The system was quickly switched to argon to push the solution from the vial to the flask. The flask was sealed tightly after removal of the cannula. The mixture was put in a pre-heated oil bath at 50°C. Reaction was stopped after 3h. via exposure to air. The polymer was purified by dialysis against methanol. After purification, the polymer was kept in methanol and stored in refrigerator. The monomers consumption calculated by NMR was 53%. Thus, the repeating unit of side chain (z), MPC, is

106.

4.5.3. Characterization of Bottlebrush Polymer

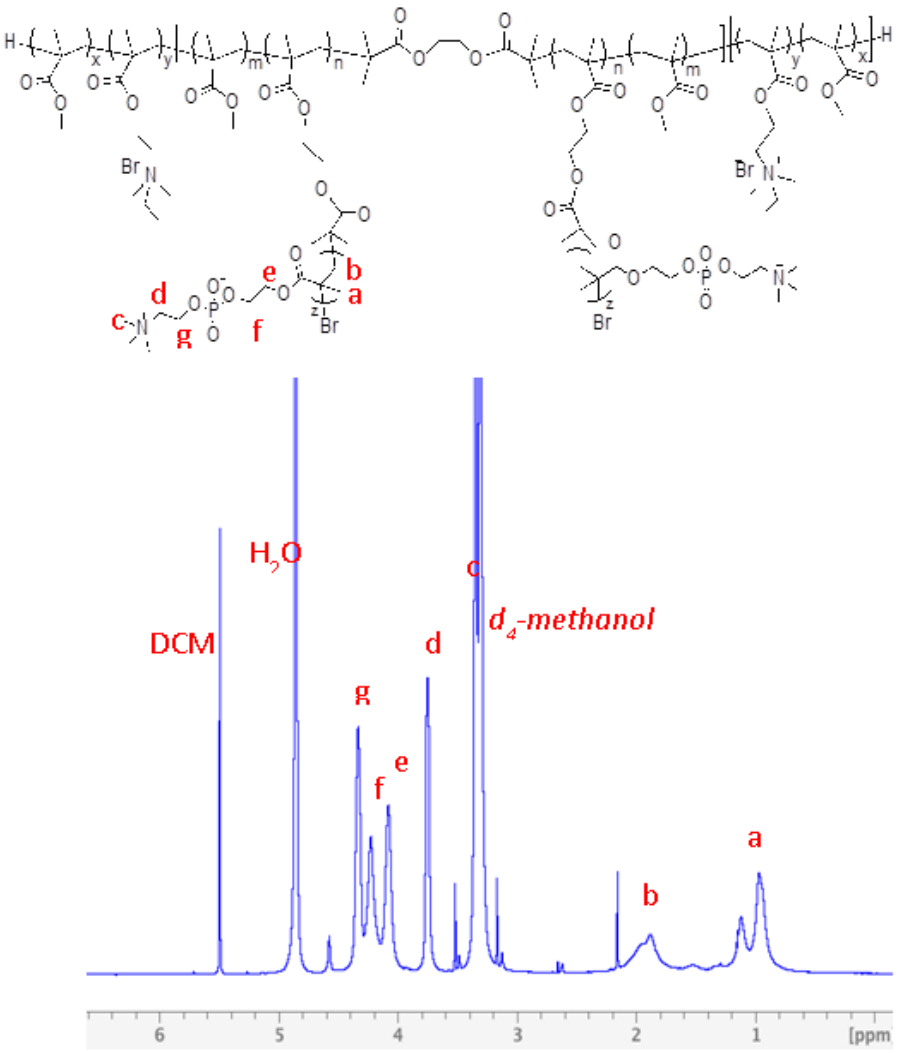

Scheme S4.7. Characterization of ABA

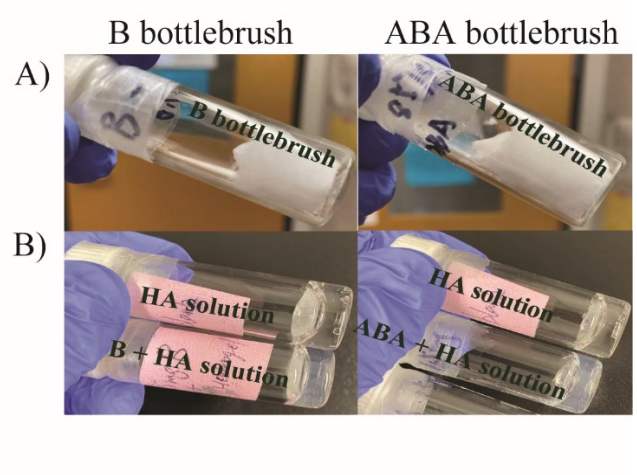

Figure S4.1. Images of: A) Bottlebrush B and ABA powder; B) Solution of HA, B-HA, and ABA-HA in miliQ water.

4.5.4. LigandTracer data fitting

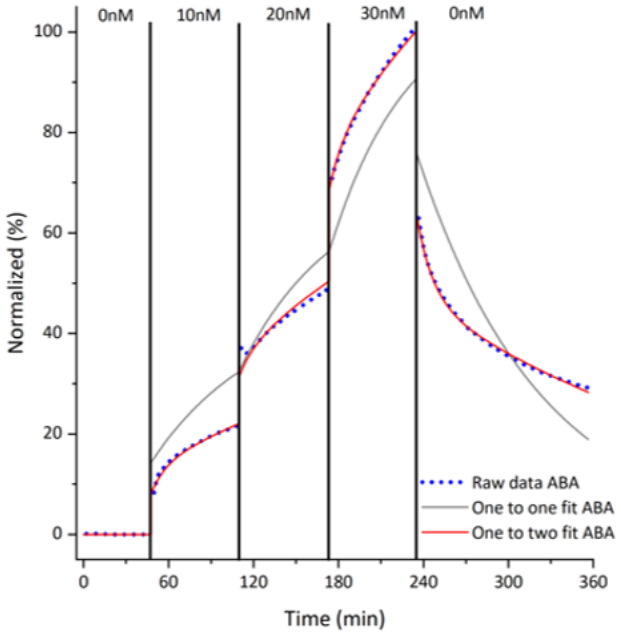

Figure S4.2. Typical example of kinetic affinity of ABA fitted by "one-to-one" and "one-to-two" models.

4.5.5. Fluorescent microscopy test

For each affinity test with the fluorescence microscopy, the contact lenses are immersed in a fluorescent polymer solution. After each defined interval of time t, the lenses are removed from the polymer solution, rinsed with distilled water and photographed. Measurements on the polymer-free contact lens *I(0)* were used as references. The fluorescent intensity *I(t)* is analyzed by ImageJ and the calculated surface area S is normalized by the pixel unit. Based on the grafting ratio between polymer/cy-5, we deduce the amount of polymer adsorbed to the surface *A(t)* as a function of time, which correlates with the growth in Cy5 intensity measured during the experiment (**Equation S4.1**).

$$A(t) \propto \frac{I(t)}{S(t)} - \frac{I(0)}{S(0)}$$

Equation S4.1

Desorption kinetics are studied using the same technique. The contact lenses are immersed in the prepared tear solution to quantify the amount of polymer desorbed from the surface. The amount of polymer desorbed from the surface as a function of time *D(t)* is linearly proportional to the decrease in Cy5 intensity measured during the experiment (**Equation S4.2**).

$$D(t) \propto \frac{I'(0)}{S'(0)} - \frac{I'(t)}{S'(t)}$$

Equation S4.2

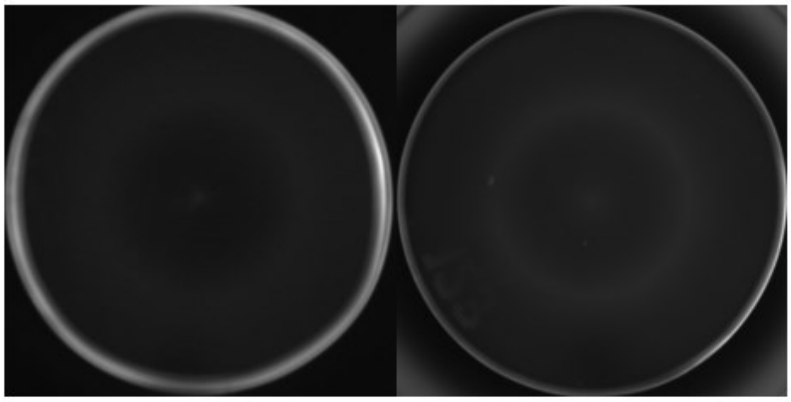

Figure S4.3. Photos of the lens without polymer (left) and the lens emerged in polymer solution for 1h (right).

Conflict of interest

The authors declare that they have no known competing financial interests or personal relationships that could have appeared to influence the work reported in this paper.

Acknowledgement

X.B. is grateful for the financial support of NSERC (Discovery grant) and the Canada Research Chair program (CRC Tier 2). D.A.P. acknowledges the financial support of the Faculty of Pharmacy at Université de Montréal.

CHAPITRE 5 : DISCUSSION GENERALE

L'objectif principal du projet, visant à mettre en corrélation la structure chimique du BB et sa capacité de protection sur les différents types de surface, a été atteint avec succès dans ce projet.

En répondant au premier objectif (défini dans la section **2.2**), le premier article de la thèse a déterminé l'impact de la densité de greffage (DF) et du squelette du polymère en brosse PMSEA sur ses propriétés tribologiques à la surface du mica.[72] Les résultats de SFA ont montré que le coefficient de frottement des BBs dépend linéairement et fortement de la densité de greffage quand leur densité reste en-dessous du niveau seuil (DF $\leq$ 50 %). Au-dessus du niveau seuil (DF $\geq$ 50 %), la modulation de la densité n'influence plus la lubrification du BB sur la surface. Concernant le squelette des BBs, l'augmentation de sa longueur peut relativement améliorer sa capacité de protection en raison de son léger accroissement de l'épaisseur du film greffé à la surface.

En répondant au deuxième objectif (défini dans la section **2.2**), le deuxième article de la thèse a déterminé l'avantage extraordinaire de l'addition du groupe d'ancrage à la structure des BBs zwitterions sur leurs propriétés tribologiques. En particulier, nous avons prouvé que les BBs peuvent adsorber rapidement sur différents types de surfaces molles comme le cartilage, l'œil et les lentilles de contact. Bien que le groupe d'ancrage adhésif n'accélère pas significativement la vitesse d'attachement des molécules BBs aux surfaces, il a considérablement renforcé sa lubrification et sa stabilité sous les pressions énormes et la répétition de cisaillement. De plus, le polymère BB possédant le groupe d'ancrage positif a montré une bonne interaction avec le HA pour devenir un super biolubrifiant qui prévient les dommages entre deux cartilages arthritiques et qui rafraîchit et régénère les yeux secs sans endommager les cellules. En simulant les conditions pathologiques d'arthrose et de la sécheresse des yeux, les résultats décrits dans le second article

ont démontré les propriétés prometteuses de ces BBs dans la viscosupplémentation, en association au HA, pour le traitement des pathologies dégénératives à cause de friction et d'usure. A côté des applications tissulaires, les résultats sur les lentilles de contact ont montré que ces BBs peuvent également leur fournir des propriétés lubrifiantes et antisalissures. Ces résultats remarquables nous persuadent que les BBs peuvent être appliqués comme revêtement polymère pour assurer la sécurité et prolonger la durée de vie des dispositifs médicaux implantables comme les prothèses, les orthèses et les organes artificielles.

Dans les études précédentes, les chercheurs ont découvert des effets de la densité de greffage et du squelette sur la conformation, la flexibilité et l'arrangement du BB à la surface [152-154]. En caractérisant la lubrification des BBs en fonction de leur architecture, la première partie du projet a apporté des informations utiles aux futurs designs de polymères dans l'ingénierie des matériaux et des surfaces. Toutefois, en raison du temps restreint du projet comparé au temps de synthèse et de caractérisation des BB, le nombre de BBs testés reste limité et insuffisant pour que l'on puisse avoir une conclusion globale sur l'impact de leur architecture. Dans la deuxième partie du projet, bien que l'interaction des BBs possédant le groupe d'ancrage avec le HA ait été démontrée pour fournir un coefficient de friction extrêmement bas sur les tissus, ce mécanisme d'interaction doit nécessairement être étudié, expliqué et approfondi. L'association des techniques comme SFA, AFM ou TEM (microscopie électronique en transmission) pourrait être nécessaire pour répondre à cette question. Finalement, après ces études in vitro, des tests in vivo sont indispensables pour assurer l'utilisation des BBs dans de vraies applications cliniques.

En termes techniques, à côté du protocole classique de SFA utilisé sur le mica dans la première partie du projet, un nouveau protocole a été créé, testé et manipulé dans la deuxième partie pour étudier les surfaces molles dans le système tribologique de SFA. Pour chaque type de surface

testée, un support spécifique dont la structure s'adapte simultanément au contour de la surface et aux critères exigés par SFA a été dessiné et imprimé par l'imprimante 3D. Bien que cette technique nous ait permis de bien mesurer le frottement des surfaces molles autres que mica, elle reste encore un désavantage. En effet, en appliquer les vrais tissus non-transparent au système de SFA, nous sommes obligés de ne pas tenir compte le principe MBI (Interférométrie à multiple faisceaux), ce qui nous permet de suivre la distance et la déformation de 2 surfaces pendant l'expérience. Ce problème pourrait être résolue dans le futur par le développement des surfaces artificielles qui mimer simultanément les propriétés physicochimiques des surfaces cibles et la transparence du mica. Etape par étape, le développement de la technique de SFA nous permettra de contribuer à la science de la tribologie qui reste encore plusieurs questions à répondre.

CHAPITRE 6 : CONCLUSION GENERALE

Dans ce projet, nous avons traité de l'importance et des effets de la conception de la structure chimique des polymères en brosse pour obtenir d'excellentes propriétés de lubrification et de résistance à l'usure. La densité de greffage, la longueur du squelette et l'effet du groupe d'ancrage sont les trois variables principales qui peuvent influencer la capacité des BBs dans la protection et la lubrification des interfaces. Nous avons également prouvé que les BBs peuvent adsorber rapidement sur différents types de surfaces pour les lubrifier et les protéger contre l'usure ou les attaques des bactéries. Ce projet nous a permis d'élargir notre librairie de polymères en brosse dont les propriétés lubrifiantes peuvent être optimisées suivant la surface d'intérêt. En formant des films lubrifiants avec des coefficients de frottement extrêmement bas et une protection élevée contre l'usure des tissus, nous sommes persuadés que les BBs deviendront un des éléments cruciaux contre la friction dans le traitement des maladies dégénératives dans les articulations humaines et dans la protection des dispositifs médicaux.

REFERENCES

(1) Ludema, K. History of tribology and its industrial significance. In *Fundamentals of Tribology and Bridging the Gap Between the Macro-and Micro/Nanoscales*, Springer, 2001; pp 1-11.

(2) Jin, Z.; Dowson, D. Bio-friction. *Friction* **2013**, *1*, 100-113.

(3) Ruggiero, A. Milestones in natural lubrication of synovial joints. *Frontiers in Mechanical Engineering* **2020**, *6*, 52.

(4) Arden, N.; Nevitt, M. C. Osteoarthritis: epidemiology. *Best practice & research Clinical rheumatology* **2006**, *20* (1), 3-25.

(5) Mobasheri, A.; Saarakkala, S.; Finnilä, M.; Karsdal, M. A.; Bay-Jensen, A.-C.; van Spil, W. E. Recent advances in understanding the phenotypes of osteoarthritis. *F1000Research* **2019**, *8*.

(6) Johnson, V. L.; Hunter, D. J. The epidemiology of osteoarthritis. *Best practice & research Clinical rheumatology* **2014**, *28* (1), 5-15.

(7) O'Neill, T. W.; McCabe, P. S.; McBeth, J. Update on the epidemiology, risk factors and disease outcomes of osteoarthritis. *Best practice & research Clinical rheumatology* **2018**, *32* (2), 312-326.

(8) Liu, R.; Kwok, W.; Vliet Vlieland, T.; Kroon, H.; Meulenbelt, I.; Houwing-Duistermaat, J.; Rosendaal, F.; Huizinga, T.; Kloppenburg, M. Mortality in osteoarthritis patients. *Scandinavian journal of rheumatology* **2015**, *44* (1), 70-73.

(9) Long, H.; Liu, Q.; Yin, H.; Wang, K.; Diao, N.; Zhang, Y.; Lin, J.; Guo, A. Prevalence trends of site-specific osteoarthritis from 1990 to 2019: findings from the Global Burden of Disease Study 2019. *Arthritis & Rheumatology* **2022**, *74* (7), 1172-1183.

(10) Forrester, J. V.; Dick, A. D.; McMenamin, P.; Roberts, F.; Pearlman, E. *The eye*; Elsevier, 2021.

(11) Mannis, M. J.; Holland, E. J. *Cornea*; Elsevier Health Sciences, 2021.

(12) Pflugfelder, S. C.; Stern, M. E. Biological functions of tear film. *Experimental eye research* **2020**, *197*, 108115.

(13) Clayton, J. A. Dry eye. *New England Journal of Medicine* **2018**, *378* (23), 2212-2223.

(14) Galor, A.; Moein, H.-R.; Lee, C.; Rodriguez, A.; Felix, E. R.; Sarantopoulos, K. D.; Levitt, R. C. Neuropathic pain and dry eye. *The ocular surface* **2018**, *16* (1), 31-44.

(15) Friedman, N. J. Impact of dry eye disease and treatment on quality of life. *Current opinion in ophthalmology* **2010**, *21* (4), 310-316.

(16) Markoulli, M.; Kolanu, S. Contact lens wear and dry eyes: challenges and solutions. *Clinical optometry* **2017**, 41-48.
(17) Wolffsohn, J. S.; Drew, T.; Dhallu, S.; Sheppard, A.; Hofmann, G. J.; Prince, M. Impact of soft contact lens edge design and midperipheral lens shape on the epithelium and its indentation with lens mobility. *Investigative Ophthalmology & Visual Science* **2013**, *54* (9), 6190-6196.
(18) Hantera, M. M. Trends in dry eye disease management worldwide. *Clinical Ophthalmology* **2021**, 165-173.
(19) Nelson, A. E. Osteoarthritis year in review 2017: clinical. *Osteoarthritis and cartilage* **2018**, *26* (3), 319-325.
(20) Kloppenburg, M.; Berenbaum, F. Osteoarthritis year in review 2019: epidemiology and therapy. *Osteoarthritis and cartilage* **2020**, *28* (3), 242-248.
(21) Nelson, A. E.; Allen, K. D.; Golightly, Y. M.; Goode, A. P.; Jordan, J. M. A systematic review of recommendations and guidelines for the management of osteoarthritis: the chronic osteoarthritis management initiative of the US bone and joint initiative. In *Seminars in arthritis and rheumatism*, 2014; Elsevier: Vol. 43, pp 701-712.
(22) D'Arcy, Y.; Mantyh, P.; Yaksh, T.; Donevan, S.; Hall, J.; Sadrarhami, M.; Viktrup, L. Treating osteoarthritis pain: mechanisms of action of acetaminophen, nonsteroidal anti-inflammatory drugs, opioids, and nerve growth factor antibodies. *Postgraduate Medicine* **2021**, *133* (8), 879-894.
(23) Xing, D.; Wang, Q.; Yang, Z.; Hou, Y.; Zhang, W.; Chen, Y.; Lin, J. Mesenchymal stem cells injections for knee osteoarthritis: a systematic overview. *Rheumatology international* **2018**, *38* (8), 1399-1411.
(24) Benke, M.; Shaffer, B. Viscosupplementation treatment of arthritis pain. *Current pain and headache reports* **2009**, *13*, 440-446.
(25) Peck, J.; Slovek, A.; Miro, P.; Vij, N.; Traube, B.; Lee, C.; Berger, A. A.; Kassem, H.; Kaye, A. D.; Sherman, W. F. A comprehensive review of viscosupplementation in osteoarthritis of the knee. *Orthopedic Reviews* **2021**, *13* (2).
(26) Richardson, C.; Plaas, A.; Block, J. A. Intra-articular hyaluronan therapy for symptomatic knee osteoarthritis. *Rheumatic Disease Clinics* **2019**, *45* (3), 439-451.
(27) Machado, R. C.; Capela, S.; Rocha, F. A. Polysaccharides as viscosupplementation agents: structural molecular characteristics but not rheology appear crucial to the therapeutic response. *Frontiers in Medicine* **2017**, *4*, 82.

(28) Kapadia, B. H.; Berg, R. A.; Daley, J. A.; Fritz, J.; Bhave, A.; Mont, M. A. Periprosthetic joint infection. *The Lancet* **2016**, *387* (10016), 386-394.
(29) Evans, J. T.; Walker, R. W.; Evans, J. P.; Blom, A. W.; Sayers, A.; Whitehouse, M. R. How long does a knee replacement last? A systematic review and meta-analysis of case series and national registry reports with more than 15 years of follow-up. *The Lancet* **2019**, *393* (10172), 655-663.
(30) Deere, K.; Whitehouse, M. R.; Kunutsor, S. K.; Sayers, A.; Price, A. J.; Mason, J.; Blom, A. W. How long do revised and multiply revised knee replacements last? A retrospective observational study of the National Joint Registry. *The Lancet Rheumatology* **2021**, *3* (6), e438-e446.
(31) Kojima, T.; Dogru, M.; Kawashima, M.; Nakamura, S.; Tsubota, K. Advances in the diagnosis and treatment of dry eye. *Progress in retinal and eye research* **2020**, *78*, 100842.
(32) Tuan, H.-I.; Chi, S.-C.; Kang, Y.-N. An updated systematic review with meta-analysis of randomized trials on topical cyclosporin A for dry-eye disease. *Drug design, development and therapy* **2020**, 265-274.
(33) Levy, O.; Labbé, A.; Borderie, V.; Laroche, L.; Bouheraoua, N. La ciclosporine topique en ophtalmologie: pharmacologie et indications thérapeutiques. *Journal Français d'Ophtalmologie* **2016**, *39* (3), 292-307.
(34) Liang, H.; Baudouin, C.; Daull, P.; Garrigue, J.-S.; Brignole-Baudouin, F. Ocular safety of cationic emulsion of cyclosporine in an in vitro corneal wound-healing model and an acute in vivo rabbit model. *Molecular Vision* **2012**, *18*, 2195.
(35) Prabhasawat, P.; Tesavibul, N.; Karnchanachetanee, C.; Kasemson, S. Efficacy of cyclosporine 0.05% eye drops in Stevens Johnson syndrome with chronic dry eye. *Journal of ocular pharmacology and therapeutics* **2013**, *29* (3), 372-377.
(36) Wirta, D. L.; Torkildsen, G. L.; Moreira, H. R.; Lonsdale, J. D.; Ciolino, J. B.; Jentsch, G.; Beckert, M.; Ousler, G. W.; Steven, P.; Krösser, S. A clinical phase II study to assess efficacy, safety, and tolerability of waterfree cyclosporine formulation for treatment of dry eye disease. *Ophthalmology* **2019**, *126* (6), 792-800.
(37) Donnenfeld, E. D.; Perry, H. D.; Nattis, A. S.; Rosenberg, E. D. Lifitegrast for the treatment of dry eye disease in adults. *Expert Opinion on Pharmacotherapy* **2017**, *18* (14), 1517-1524.

(38) Perez, V. L.; Pflugfelder, S. C.; Zhang, S.; Shojaei, A.; Haque, R. Lifitegrast, a novel integrin antagonist for treatment of dry eye disease. *The ocular surface* **2016**, *14* (2), 207-215.
(39) Holland, E. J.; Luchs, J.; Karpecki, P. M.; Nichols, K. K.; Jackson, M. A.; Sall, K.; Tauber, J.; Roy, M.; Raychaudhuri, A.; Shojaei, A. Lifitegrast for the treatment of dry eye disease: results of a phase III, randomized, double-masked, placebo-controlled trial (OPUS-3). *Ophthalmology* **2017**, *124* (1), 53-60.
(40) Donnenfeld, E. D.; Karpecki, P. M.; Majmudar, P. A.; Nichols, K. K.; Raychaudhuri, A.; Roy, M.; Semba, C. P. Safety of lifitegrast ophthalmic solution 5.0% in patients with dry eye disease: a 1-year, multicenter, randomized, placebo-controlled study. *Cornea* **2016**, *35* (6), 741.
(41) Findlay, Q.; Reid, K. Dry eye disease: when to treat and when to refer. *Australian prescriber* **2018**, *41* (5), 160.
(42) Laffleur, F.; Dachs, S. Development of novel mucoadhesive hyaluronic acid derivate as lubricant for the treatment of dry eye syndrome. *Therapeutic Delivery* **2015**, *6* (10), 1211-1219.
(43) Wegener, A. R.; Meyer, L. M.; Schönfeld, C.-L. Effect of viscous agents on corneal density in dry eye disease. *Journal of Ocular Pharmacology and Therapeutics* **2015**, *31* (8), 504-508.
(44) Walsh, K.; Jones, L. The use of preservatives in dry eye drops. *Clinical Ophthalmology* **2019**, 1409-1425.
(45) Farkouh, A.; Frigo, P.; Czejka, M. Systemic side effects of eye drops: a pharmacokinetic perspective. *Clinical ophthalmology* **2016**, 2433-2441.
(46) Pradal, C.; Yakubov, G. E.; Williams, M. A.; McGuckin, M. A.; Stokes, J. R. Lubrication by biomacromolecules: mechanisms and biomimetic strategies. *Bioinspiration & Biomimetics* **2019**, *14* (5), 051001.
(47) Coles, J. M.; Chang, D. P.; Zauscher, S. Molecular mechanisms of aqueous boundary lubrication by mucinous glycoproteins. *Current Opinion in Colloid & Interface Science* **2010**, *15* (6), 406-416.
(48) Wierzcholski, K. Joint cartilage lubrication with phospholipid bilayer. *Tribologia* **2016**, (2), 145--157.
(49) Lin, W.; Liu, Z.; Kampf, N.; Klein, J. The role of hyaluronic acid in cartilage boundary lubrication. *Cells* **2020**, *9* (7), 1606.
(50) Cone, R. A. Barrier properties of mucus. *Advanced drug delivery reviews* **2009**, *61* (2), 75-85.

(51) Jay, G.; Torres, J.; Warman, M.; Laderer, M.; Breuer, K. The role of lubricin in the mechanical behavior of synovial fluid. *Proceedings of the National Academy of Sciences* **2007**, *104* (15), 6194-6199.
(52) Jay, G. D.; Waller, K. A. The biology of lubricin: near frictionless joint motion. *Matrix Biology* **2014**, *39*, 17-24.
(53) Das, S.; Banquy, X.; Zappone, B.; Greene, G. W.; Jay, G. D.; Israelachvili, J. N. Synergistic interactions between grafted hyaluronic acid and lubricin provide enhanced wear protection and lubrication. *Biomacromolecules* **2013**, *14* (5), 1669-1677.
(54) Wang, M.; Liu, C.; Thormann, E.; Dedinaite, A. Hyaluronan and phospholipid association in biolubrication. *Biomacromolecules* **2013**, *14* (12), 4198-4206.
(55) Davidson, H. J.; Kuonen, V. J. The tear film and ocular mucins. *Veterinary ophthalmology* **2004**, *7* (2), 71-77.
(56) Wang, Y.; Toor, S. S.; Gautam, R.; Henson, D. B. Blink frequency and duration during perimetry and their relationship to test–retest threshold variability. *Investigative ophthalmology & visual science* **2011**, *52* (7), 4546-4550.
(57) Emami, A.; Namdari, H.; Parvizpour, F.; Arabpour, Z. Challenges in osteoarthritis treatment. *Tissue and cell* **2022**, 101992.
(58) Araújo-Neto, I.; Rêgo, A. C. M.; Araújo-Filho, I. Dry eye syndrome: Therapeutic challenges and future trends. *International Journal of Clinical and Experimental Ophthalmology* **2019**, *3* (2), 030-034.
(59) Banquy, X.; Faivre, J.; Shrestha, B. R.; Matyjaszewski, K.; Burdynska, J.; Moldovan, F. Bottlebrush polymer compositions, lubricating fluid, porous materials comprising said compositions, and surface bearing said compositions. Google Patents: 2021.
(60) Li, Z.; Tang, M.; Liang, S.; Zhang, M.; Biesold, G. M.; He, Y.; Hao, S.-M.; Choi, W.; Liu, Y.; Peng, J. Bottlebrush polymers: From controlled synthesis, self-assembly, properties to applications. *Progress in Polymer Science* **2021**, *116*, 101387.
(61) Xie, G.; Martinez, M. R.; Olszewski, M.; Sheiko, S. S.; Matyjaszewski, K. Molecular bottlebrushes as novel materials. *Biomacromolecules* **2018**, *20* (1), 27-54.
(62) Xia, Y.; Adibnia, V.; Huang, R.; Murschel, F.; Faivre, J.; Xie, G.; Olszewski, M.; De Crescenzo, G.; Qi, W.; He, Z. Biomimetic bottlebrush polymer coatings for fabrication of ultralow fouling surfaces. *Angewandte Chemie* **2019**, *131* (5), 1322-1328.

(63) Rahimi, M.; Charmi, G.; Matyjaszewski, K.; Banquy, X.; Pietrasik, J. Recent developments in natural and synthetic polymeric drug delivery systems used for the treatment of osteoarthritis. *Acta biomaterialia* **2021**, *123*, 31-50.
(64) Rzayev, J. Molecular bottlebrushes: new opportunities in nanomaterials fabrication. ACS Publications: 2012.
(65) Banquy, X.; Burdynska, J.; Lee, D. W.; Matyjaszewski, K.; Israelachvili, J. Bioinspired bottle-brush polymer exhibits low friction and Amontons-like behavior. *Journal of the American Chemical Society* **2014**, *136* (17), 6199-6202.
(66) Adibnia, V.; Mirbagheri, M.; Faivre, J.; Robert, J.; Lee, J.; Matyjaszewski, K.; Lee, D. W.; Banquy, X. Bioinspired polymers for lubrication and wear resistance. *Progress in Polymer Science* **2020**, *110*, 101298.
(67) Adibnia, V.; Olszewski, M.; De Crescenzo, G.; Matyjaszewski, K.; Banquy, X. Superlubricity of zwitterionic bottlebrush polymers in the presence of multivalent ions. *Journal of the American Chemical Society* **2020**, *142* (35), 14843-14847.
(68) Pettersson, T.; Naderi, A.; Makuška, R.; Claesson, P. M. Lubrication properties of bottle-brush polyelectrolytes: An AFM study on the effect of side chain and charge density. *Langmuir* **2008**, *24* (7), 3336-3347.
(69) Yan, W.; Ramakrishna, S. N.; Spencer, N. D.; Benetti, E. M. Brushes, graft copolymers, or bottlebrushes? the effect of polymer architecture on the nanotribological properties of grafted-from assemblies. *Langmuir* **2019**, *35* (35), 11255-11264.
(70) Faivre, J.; Shrestha, B. R.; Xie, G.; Delair, T.; David, L.; Matyjaszewski, K.; Banquy, X. Unraveling the correlations between conformation, lubrication, and chemical stability of bottlebrush polymers at interfaces. *Biomacromolecules* **2017**, *18* (12), 4002-4010.
(71) Linse, P.; Claesson, P. M. Modeling of bottle-brush polymer adsorption onto mica and silica surfaces. *Macromolecules* **2009**, *42* (16), 6310-6318.
(72) Olszewski, M.; Pham, D. A.; González Bolívar, S.; Rabanel, J.-M.; Martinez, M.; Matyjaszewski, K.; Banquy, X. Synthesis and Characterization of Biocompatible Sulfoxide-Containing Molecular Bottlebrushes. *ACS Applied Polymer Materials* **2022**, *4* (11), 8564-8573.
(73) Lee, H.-i.; Pietrasik, J.; Sheiko, S. S.; Matyjaszewski, K. Stimuli-responsive molecular brushes. *Progress in polymer science* **2010**, *35* (1-2), 24-44.

(74) Sheiko, S. S.; Sumerlin, B. S.; Matyjaszewski, K. Cylindrical molecular brushes: Synthesis, characterization, and properties. *Progress in Polymer Science* **2008**, *33* (7), 759-785.
(75) Müllner, M. Molecular polymer bottlebrushes in nanomedicine: therapeutic and diagnostic applications. *Chemical Communications* **2022**, *58* (38), 5683-5716.
(76) Zhao, K.; Gao, Z.; Song, D.; Zhang, P.; Cui, J. Assembly of catechol-modified polymer brushes for drug delivery. *Polymer Chemistry* **2022**, *13* (3), 373-378.
(77) Raj, W.; Jerczynski, K.; Rahimi, M.; Przekora, A.; Matyjaszewski, K.; Pietrasik, J. Molecular bottlebrush with pH-responsive cleavable bonds as a unimolecular vehicle for anticancer drug delivery. *Materials Science and Engineering: C* **2021**, *130*, 112439.
(78) Liu, F.; Zhao, X.; Zhang, X.; Zhang, X.; Peng, J.; Yang, H.; Deng, K.; Ma, L.; Chang, C.; Wei, H. Fabrication of theranostic amphiphilic conjugated bottlebrush copolymers with alternating heterografts for cell imaging and anticancer drug delivery. *Polymer Chemistry* **2018**, *9* (39), 4866-4874.
(79) Gao, J.; Wen, J.; Hu, D.; Liu, K.; Zhang, Y.; Zhao, X.; Wang, K. Bottlebrush inspired injectable hydrogel for rapid prevention of postoperative and recurrent adhesion. *Bioactive Materials* **2022**, *16*, 27-46.
(80) Vashahi, F.; Martinez, M. R.; Dashtimoghadam, E.; Fahimipour, F.; Keith, A. N.; Bersenev, E. A.; Ivanov, D. A.; Zhulina, E. B.; Popryadukhin, P.; Matyjaszewski, K. Injectable bottlebrush hydrogels with tissue-mimetic mechanical properties. *Science Advances* **2022**, *8* (3), eabm2469.
(81) Shukla, A.; Singh, A. P.; Maiti, P. Injectable hydrogels of newly designed brush biopolymers as sustained drug-delivery vehicle for melanoma treatment. *Signal Transduction and Targeted Therapy* **2021**, *6* (1), 63.
(82) Yoshikawa, C.; Sakakibara, K.; Nonsuwan, P.; Yamazaki, T.; Tsujii, Y. Nonbiofouling coatings using bottlebrushes with concentrated polymer brush architecture. *Biomacromolecules* **2021**, *22* (6), 2505-2514.
(83) Chowdhury, A. U.; Chang, D.; Xu, Y.; Hong, K.; Sumpter, B. G.; Carrillo, J.-M. Y.; Doughty, B. Mapping the Interfacial Chemistry and Structure of Partially Fluorinated Bottlebrush Polymers and Their Linear Analogues. *Langmuir* **2020**, *37* (1), 211-218.
(84) Joh, D. Y.; Zimmers, Z.; Avlani, M.; Heggestad, J. T.; Aydin, H. B.; Ganson, N.; Kumar, S.; Fontes, C. M.; Achar, R. K.; Hershfield, M. S. Architectural modification of conformal PEG-

bottlebrush coatings minimizes anti-PEG antigenicity while preserving stealth properties. *Advanced healthcare materials* **2019**, *8* (8), 1801177.
(85) Hoang Thi, T. T.; Pilkington, E. H.; Nguyen, D. H.; Lee, J. S.; Park, K. D.; Truong, N. P. The importance of poly (ethylene glycol) alternatives for overcoming PEG immunogenicity in drug delivery and bioconjugation. *Polymers* **2020**, *12* (2), 298.
(86) Liu, J.; Xu, Y.; Yang, Q.; Li, C.; Hennink, W. E.; Zhuo, R.; Jiang, X. Reduction biodegradable brushed PDMAEMA derivatives synthesized by atom transfer radical polymerization and click chemistry for gene delivery. *Acta biomaterialia* **2013**, *9* (8), 7758-7766.
(87) Dalal, R. J.; Kumar, R.; Ohnsorg, M.; Brown, M.; Reineke, T. M. Cationic Bottlebrush Polymers Outperform Linear Polycation Analogues for PDNA Delivery and Gene Expression. *ACS Macro Letters* **2021**, *10* (7), 886-893.
(88) Faivre, J.; Shrestha, B. R.; Burdynska, J.; Xie, G.; Moldovan, F.; Delair, T.; Benayoun, S.; David, L.; Matyjaszewski, K.; Banquy, X. Wear protection without surface modification using a synergistic mixture of molecular brushes and linear polymers. *ACS nano* **2017**, *11* (2), 1762-1769.
(89) Xia, Y.; Adibnia, V.; Shan, C.; Huang, R.; Qi, W.; He, Z.; Xie, G.; Olszewski, M.; De Crescenzo, G.; Matyjaszewski, K. Synergy between zwitterionic polymers and hyaluronic acid enhances antifouling performance. *Langmuir* **2019**, *35* (48), 15535-15542.
(90) Oh, K.-I.; Baiz, C. R. Crowding stabilizes DMSO–water hydrogen-bonding interactions. *The Journal of Physical Chemistry B* **2018**, *122* (22), 5984-5990.
(91) Xu, X.; Huang, X.; Chang, Y.; Yu, Y.; Zhao, J.; Isahak, N.; Teng, J.; Qiao, R.; Peng, H.; Zhao, C.-X. Antifouling surfaces enabled by surface grafting of highly hydrophilic sulfoxide polymer brushes. *Biomacromolecules* **2020**, *22* (2), 330-339.
(92) Mackenzie, M. C.; Shrivats, A. R.; Konkolewicz, D.; Averick, S. E.; McDermott, M. C.; Hollinger, J. O.; Matyjaszewski, K. Synthesis of poly (meth) acrylates with thioether and tertiary sulfonium groups by ARGET ATRP and their use as siRNA delivery agents. *Biomacromolecules* **2015**, *16* (1), 236-245.
(93) Işık, D.; Joshi, A. A.; Guo, X.; Rancan, F.; Klossek, A.; Vogt, A.; Rühl, E.; Hedtrich, S.; Klinger, D. Sulfoxide-functionalized nanogels inspired by the skin penetration properties of DMSO. *Biomaterials science* **2021**, *9* (3), 712-725.
(94) Hofmann, V.; Ringsdorf, H.; Muacevic, G. Pharmakologisch aktive polymere, 8. Poly [2-(methylsulfinyl) äthylacrylat] e und ihre vermittelnde wirkung auf die transkutane resorption von

pharmaka. *Die Makromolekulare Chemie: Macromolecular Chemistry and Physics* **1975**, *176* (7), 1929-1943.

(95) Garnier, S.; Laschewsky, A. Synthesis of new amphiphilic diblock copolymers and their self-assembly in aqueous solution. *Macromolecules* **2005**, *38* (18), 7580-7592.

(96) Li, S.; Chung, H. S.; Simakova, A.; Wang, Z.; Park, S.; Fu, L.; Cohen-Karni, D.; Averick, S.; Matyjaszewski, K. Biocompatible polymeric analogues of DMSO prepared by atom transfer radical polymerization. *Biomacromolecules* **2017**, *18* (2), 475-482.

(97) Işık, D.; Quaas, E.; Klinger, D. Thermo-and oxidation-sensitive poly (meth) acrylates based on alkyl sulfoxides: dual-responsive homopolymers from one functional group. *Polymer Chemistry* **2020**, *11* (48), 7662-7676.

(98) Yu, Y.; Xu, W.; Huang, X.; Xu, X.; Qiao, R.; Li, Y.; Han, F.; Peng, H.; Davis, T. P.; Fu, C. Proteins conjugated with sulfoxide-containing polymers show reduced macrophage cellular uptake and improved pharmacokinetics. *ACS Macro Letters* **2020**, *9* (6), 799-805.

(99) Israelachvili, J. Thin film studies using multiple-beam interferometry. *Journal of Colloid and Interface Science* **1973**, *44* (2), 259-272.

(100) Israelachvili, J.; Min, Y.; Akbulut, M.; Alig, A.; Carver, G.; Greene, W.; Kristiansen, K.; Meyer, E.; Pesika, N.; Rosenberg, K. Recent advances in the surface forces apparatus (SFA) technique. *Reports on Progress in Physics* **2010**, *73* (3), 036601.

(101) Martinez, M. R.; Sobieski, J.; Lorandi, F.; Fantin, M.; Dadashi-Silab, S.; Xie, G.; Olszewski, M.; Pan, X.; Ribelli, T. G.; Matyjaszewski, K. Understanding the relationship between catalytic activity and termination in photoATRP: Synthesis of linear and bottlebrush polyacrylates. *Macromolecules* **2019**, *53* (1), 59-67.

(102) Ribelli, T. G.; Konkolewicz, D.; Bernhard, S.; Matyjaszewski, K. How are radicals (re) generated in photochemical ATRP? *Journal of the American Chemical Society* **2014**, *136* (38), 13303-13312.

(103) Erdemir, A.; Erck, R. A.; Robles, J. Relationship of hertzian contact pressure to friction behavior of self-lubricating boric acid films. *Surface and coatings Technology* **1991**, *49* (1-3), 435-438.

(104) Drummond, C.; Marinov, G.; Richetti, P. Reinforcement of a Surfactant Boundary Lubricant Film by a Hydrophilic− Hydrophilic Diblock Copolymer. *Langmuir* **2008**, *24* (4), 1560-1565.

(105) Luengo, G.; Israelachvili, J.; Granick, S. Generalized effects in confined fluids: new friction map for boundary lubrication. *Wear* **1996**, *200* (1-2), 328-335.
(106) Nomura, A.; Ohno, K.; Fukuda, T.; Sato, T.; Tsujii, Y. Lubrication mechanism of concentrated polymer brushes in solvents: effect of solvent viscosity. *Polymer Chemistry* **2012**, *3* (1), 148-153.
(107) Subbotin, A.; Semenov, A.; Manias, E.; Hadziioannou, G.; Ten Brinke, G. Nonlinear rheology of polymer melts under shear flow. *Macromolecules* **1995**, *28* (11), 3898-3900.
(108) Luengo, G.; Schmitt, F.-J.; Hill, R.; Israelachvili, J. Thin film rheology and tribology of confined polymer melts: contrasts with bulk properties. *Macromolecules* **1997**, *30* (8), 2482-2494.
(109) Raviv, U.; Frey, J.; Sak, R.; Laurat, P.; Tadmor, R.; Klein, J. Properties and interactions of physigrafted end-functionalized poly (ethylene glycol) layers. *Langmuir* **2002**, *18* (20), 7482-7495.
(110) Daniel, W. F.; Burdyńska, J.; Vatankhah-Varnoosfaderani, M.; Matyjaszewski, K.; Paturej, J.; Rubinstein, M.; Dobrynin, A. V.; Sheiko, S. S. Solvent-free, supersoft and superelastic bottlebrush melts and networks. *Nature materials* **2016**, *15* (2), 183-189.
(111) Czichos, H. *Tribology: a systems approach to the science and technology of friction, lubrication, and wear*; Elsevier, 2009.
(112) Gebeshuber, I. C.; Van Aken, G. Friction and Lubricants Related to Human Bodies. MDPI: 2017; Vol. 5, p 4.
(113) Khan, F. A. Current Updates on Arthroplasty in Developing Countries.
(114) Walsh, D. J.; Dutta, S.; Sing, C. E.; Guironnet, D. Engineering of molecular geometry in bottlebrush polymers. *Macromolecules* **2019**, *52* (13), 4847-4857.
(115) Kim, K. H.; Nam, J.; Choi, J.; Seo, M.; Bang, J. From macromonomers to bottlebrush copolymers with sequence control: synthesis, properties, and applications. *Polymer Chemistry* **2022**, *13* (16), 2224-2261.
(116) *10X Phosphate-Buffered Saline (PBS) for Western Blotting*. https://www.sigmaaldrich.com/CA/en/support/calculators-and-apps/10x-phosphate-buffered-saline (accessed.
(117) Alexeev, V. L.; DAs, S.; Finegold, D. N.; AsHER, S. A. Photonic crystal glucose-sensing material for noninvasive monitoring of glucose in tear fluid. *Clinical chemistry* **2004**, *50* (12), 2353-2360.

(118) Shaner, S. PDMS (Silicone) Protocol. **2016**.
(119) Olfert, E. D.; Cross, B. M.; McWilliam, A. A. *Guide to the care and use of experimental animals*; Citeseer, 1993.
(120) Hayes, W.; Keer, L. M.; Herrmann, G.; Mockros, L. A mathematical analysis for indentation tests of articular cartilage. *Journal of biomechanics* **1972**, *5* (5), 541-551.
(121) IWANAGA, T.; Shikichi, M.; KITAMURA, H.; YANASE, H.; NOZAWA-INOUE, K. Morphology and functional roles of synoviocytes in the joint. *Archives of histology and cytology* **2000**, *63* (1), 17-31.
(122) FitzGerald, O.; Bresnihan, B. Synovial membrane cellularity and vascularity. *Annals of the rheumatic diseases* **1995**, *54* (6), 511.
(123) Nahian, A.; Sapra, A. Histology, Chondrocytes. **2020**.
(124) Henry, J. P.; Bordoni, B. Histology, osteoblasts. **2020**.
(125) Chen, H.; Tan, X.-N.; Hu, S.; Liu, R.-Q.; Peng, L.-H.; Li, Y.-M.; Wu, P. Molecular mechanisms of chondrocyte proliferation and differentiation. *Frontiers in Cell and Developmental Biology* **2021**, *9*, 664168.
(126) Bishnoi, M.; Jain, A.; Hurkat, P.; Jain, S. K. Chondroitin sulphate: a focus on osteoarthritis. *Glycoconjugate journal* **2016**, *33* (5), 693-705.
(127) Ren, K.; Reina Mahecha, M. A.; Hübner, M.; Cui, Z.; Kaper, H. J.; Van Der Veen, H. C.; Sharma, P. K. Tribology of enzymatically degraded cartilage mimicking early osteoarthritis. *Friction* **2023**, 1-17.
(128) Murphy, G.; Lee, M. What are the roles of metalloproteinases in cartilage and bone damage? *Annals of the rheumatic diseases* **2005**, *64* (suppl 4), iv44-iv47.
(129) Yamamoto, K.; Okano, H.; Miyagawa, W.; Visse, R.; Shitomi, Y.; Santamaria, S.; Dudhia, J.; Troeberg, L.; Strickland, D. K.; Hirohata, S. MMP-13 is constitutively produced in human chondrocytes and co-endocytosed with ADAMTS-5 and TIMP-3 by the endocytic receptor LRP1. *Matrix Biology* **2016**, *56*, 57-73.
(130) Mixon, A.; Bahar-Moni, A. S.; Faisal, T. R. Mechanical characterization of articular cartilage degraded combinedly with MMP-1 and MMP-9. *Journal of the Mechanical Behavior of Biomedical Materials* **2022**, *129*, 105131.
(131) Cabral-Pacheco, G. A.; Garza-Veloz, I.; Castruita-De la Rosa, C.; Ramirez-Acuna, J. M.; Perez-Romero, B. A.; Guerrero-Rodriguez, J. F.; Martinez-Avila, N.; Martinez-Fierro, M. L. The

roles of matrix metalloproteinases and their inhibitors in human diseases. *International journal of molecular sciences* **2020**, *21* (24), 9739.
(132) Leong, D. J.; Gu, X. I.; Li, Y.; Lee, J. Y.; Laudier, D. M.; Majeska, R. J.; Schaffler, M. B.; Cardoso, L.; Sun, H. B. Matrix metalloproteinase-3 in articular cartilage is upregulated by joint immobilization and suppressed by passive joint motion. *Matrix Biology* **2010**, *29* (5), 420-426.
(133) Hu, Q.; Ecker, M. Overview of MMP-13 as a Promising Target for the Treatment of Osteoarthritis. *International journal of molecular sciences* **2021**, *22* (4), 1742.
(134) Mustonen, A.-M.; Käkelä, R.; Finnilä, M. A.; Sawatsky, A.; Korhonen, R. K.; Saarakkala, S.; Herzog, W.; Paakkonen, T.; Nieminen, P. Anterior cruciate ligament transection alters the n-3/n-6 fatty acid balance in the lapine infrapatellar fat pad. *Lipids in Health and Disease* **2019**, *18*, 1-9.
(135) Mittelstaedt, D.; Kahn, D.; Xia, Y. Topographical and depth-dependent glycosaminoglycan concentration in canine medial tibial cartilage 3 weeks after anterior cruciate ligament transection surgery—a microscopic imaging study. *Quantitative Imaging in Medicine and Surgery* **2016**, *6* (6), 648.
(136) Pollard, T. D. A guide to simple and informative binding assays. *Molecular biology of the cell* **2010**, *21* (23), 4061-4067.
(137) Erfani, A.; Seaberg, J.; Aichele, C. P.; Ramsey, J. D. Interactions between biomolecules and zwitterionic moieties.
(138) Liu, X.; Dedinaite, A.; Rutland, M.; Thormann, E.; Visnevskij, C.; Makuska, R.; Claesson, P. M. Electrostatically anchored branched brush layers. *Langmuir* **2012**, *28* (44), 15537-15547.
(139) Li, D.; Wei, Q.; Wu, C.; Zhang, X.; Xue, Q.; Zheng, T.; Cao, M. Superhydrophilicity and strong salt-affinity: Zwitterionic polymer grafted surfaces with significant potentials particularly in biological systems. *Advances in Colloid and Interface Science* **2020**, *278*, 102141.
(140) Aragona, P.; Simmons, P. A.; Wang, H.; Wang, T. Physicochemical properties of hyaluronic acid–based lubricant eye drops. *Translational Vision Science & Technology* **2019**, *8* (6), 2-2.
(141) Huynh, A.; Priefer, R. Hyaluronic acid applications in ophthalmology, rheumatology, and dermatology. *Carbohydrate research* **2020**, *489*, 107950.
(142) Blau, P. J. *Friction science and technology: from concepts to applications*; CRC press, 2008.
(143) Maeda, N.; Chen, N.; Tirrell, M.; Israelachvili, J. N. Adhesion and friction mechanisms of polymer-on-polymer surfaces. *Science* **2002**, *297* (5580), 379-382.

(144) Van der Post, J.; De Waal, P.; De Kam, M.; Cohen, A.; Van Gerven, J. No evidence of the usefulness of eye blinking as a marker for central dopaminergic activity. *Journal of Psychopharmacology* **2004**, *18* (1), 109-114.
(145) Dutta, D.; Cole, N.; Willcox, M. Factors influencing bacterial adhesion to contact lenses. *Molecular vision* **2012**, *18*, 14.
(146) Jain, N.; Bhosale, P.; Tale, V. Biofilm formation on contact lenses by bacterial pathogens. *J. Pharm. Res* **2016**, *10* (1), 50-53.
(147) Spadafora, A.; Korogiannaki, M.; Sheardown, H. Antifouling silicone hydrogel contact lenses via densely grafted phosphorylcholine polymers. *Biointerphases* **2020**, *15* (4).
(148) Yang, J.; Chen, H.; Xiao, S.; Shen, M.; Chen, F.; Fan, P.; Zhong, M.; Zheng, J. Salt-responsive zwitterionic polymer brushes with tunable friction and antifouling properties. *Langmuir* **2015**, *31* (33), 9125-9133.
(149) Fleiszig, S. M.; Kroken, A. R.; Nieto, V.; Grosser, M. R.; Wan, S. J.; Metruccio, M. M.; Evans, D. J. Contact lens-related corneal infection: Intrinsic resistance and its compromise. *Progress in retinal and eye research* **2020**, *76*, 100804.
(150) Cong, Y.; Vatankhah-Varnosfaderani, M.; Karimkhani, V.; Keith, A. N.; Leibfarth, F. A.; Martinez, M. R.; Matyjaszewski, K.; Sheiko, S. S. Understanding the synthesis of linear–bottlebrush–linear block copolymers: toward plastomers with well-defined mechanical properties. *Macromolecules* **2020**, *53* (19), 8324-8332.
(151) Simula, A.; Nikolaou, V.; Anastasaki, A.; Alsubaie, F.; Nurumbetov, G.; Wilson, P.; Kempe, K.; Haddleton, D. M. Synthesis of well-defined α, ω-telechelic multiblock copolymers in aqueous medium: in situ generation of α, ω-diols. *Polymer Chemistry* **2015**, *6* (12), 2226-2233.
(152) Lin, T.-P.; Chang, A. B.; Luo, S.-X. L.; Chen, H.-Y.; Lee, B.; Grubbs, R. H. Effects of grafting density on block polymer self-assembly: From linear to bottlebrush. *ACS nano* **2017**, *11* (11), 11632-11641.
(153) Xiao, L.; Li, J.; Peng, G.; Huang, G. The effect of grafting density and side chain length on the conformation of PEG grafted bottlebrush polymers. *Reactive and Functional Polymers* **2020**, *156*, 104736.
(154) Aviv, Y.; Altay, E.; Fink, L.; Raviv, U.; Rzayev, J.; Shenhar, R. Quasi-two-dimensional assembly of bottlebrush block copolymers with nanoparticles in ultrathin films: combined effect of graft asymmetry and nanoparticle size. *Macromolecules* **2018**, *52* (1), 196-207.